CONNECTIVITY AND PERFORMANCE EVALUATIONS FOR FRACTURED AND CLOSED LOOP GEOTHERMAL SYSTEMS

A Thesis

Presented to the Faculty of the Graduate School

of Cornell University

in Partial Fulfillment of the Requirements for the Degree of

Master of Science

by

Harish Chandrasekar

December 2021

ABSTRACT

The thermal energy stored in the Earth's interior to depths of 10 km is vast compared to the annual global consumption of primary energy. Despite these large resource estimates, the installed worldwide geothermal production capacity is limited to 16 GW electric and 30 GW thermal. The reason for the limited capacity primarily lies in the fact that profitable high enthalpy geothermal systems also called Hydrothermal systems are geographically rare. Two technologies are being proposed to expand deep geothermal development and to make it globally accessible, namely-Enhanced Geothermal Systems (EGS) and Closed Loop Geothermal Systems (CLG). The primary difference between the two systems being the circulation of fluid takes place through hydraulically stimulated fractures in the rock for the former and the circulation of fluid takes place in a closed pipe for the latter. This thesis aims at dealing with the connectivity and thermal hydraulic performance of both these systems through analytical and numerical modeling techniques. The connectivity and thermal hydraulic performance in the context of EGS/CLG refers to the flow and thermal profile evaluation of a working fluid as it advances through the fractures in the subsurface between an injection and production well or through a closed pipe in the subsurface.

A characterization technique for evaluating the hydraulic connectivity of a fractured bedrock is developed using periodic pumping tests. Traditional pumping tests performed to characterize the subsurface are often not suitable for fractured EGS systems since the diffusion length or radius of penetration quickly expands beyond the inter-well distance. Periodic pumping tests allow us to

control the diffusion length by varying the period or frequency of the oscillation. Therefore, testing at multiple frequencies help probe different distances in the system. Analytical models and signal processing techniques are developed and employed to analyze the data generated from the periodic pumping tests conducted at a meso scale field site known to exhibit extreme flow channeling. The width of the channel formed was computed for various periods or frequency of oscillations and were found to decrease with period. Besides, the storage of fluid in the medium was compared with that of the storage in the monitoring wells and the former was found to be the dominating storage mechanism at the meso scale field site.

Numerical Simulations are performed using a developed Finite Element Method (FEM) technique to evaluate CLG technologies. Sensitivity analysis is performed and their thermal performance is evaluated for various operating conditions. The developed models are also validated with Slender Body Theory (SBT) based approaches. In all scenarios, the results exhibit a large rapid drop in production temperature immediately after initiation of operations that levels off to a lower near steady state value. CLG is also compared with EGS using analytical techniques. In summary, it is found that CLG may be more appropriate when traditional hydrothermal systems and EGS are off the table, in situations with existing wells and for direct-use heat applications.

BIOGRAPHICAL SKETCH

Harish Chandrasekar was born on the 4th of August,1997 in the city of Chennai, India. His nascent interest in science and physics was encouraged by his mother and developed through the conducive environment at PSBB Senior Secondary School in Chennai. He graduated in 2015 and then moved on to Anna University, Chennai for undergraduate studies where he majored in Chemical Engineering. His interactions with professors and mentors in undergraduate internships along with background reading led to an increased interest in reservoir engineering and computational modeling. Right after obtaining his Bachelors of Technology in Chemical Engineering in 2019 he pursued a Master of Science in Chemical Engineering at Cornell University.

At Cornell he resonated well with the research carried out by Professor Jefferson Tester and Professor Donald Koch and joined their group. He has since spent the last two years working on problems that cover areas such as geothermal reservoir engineering, analytical/computational/data driven modeling, effective deployment and management of both the Cornell Earth Source Heat(ESH) initiative and advanced or closed loop geothermal systems to achieve and accelerate innovation in the sustainable energy systems space.

Besides academics, Harish was actively involved in several student body organizations at Cornell and held key leadership roles. He served as the Vice President of the Geothermal Rising Student Chapter at Cornell, Treasurer of the Cornell India Association, Social Chairperson of ASHA Cornell and an Executive Board Member of the Graduate and Professional Student Financial Assembly. He was a nominee of the Global Citizen Award at Cornell for the year 2021.

To my Parents, my grandmother and my maternal uncles without whose constant support this work could not have been possible

ACKNOWLEDGEMENTS

There are so many people that have helped and guided me to this point in life, that it is hard to know where to start, or rather where to stop.

I would first like to first thank my principal advisor, professor Jefferson Tester. He has always been extremely supportive and has stood by my side even during very difficult and challenging times over the past few years. I'm truly grateful to call him a close friend of mine with whom I was comfortable talking about both work and personal life. Jeff appreciates the value of hard work, while also realizing the importance of relaxing occasionally to enjoy the other extracurricular activities. I would also like to sincerely thank my committee member professor Donald Koch for helping me immensely throughout my graduate study.

I was truly amazed at the amount of time both Jeff and Don had put into getting me to the point of defending my research. Thank you for all the time you devoted towards my professional development. You both have taught me to tackle technical and research problems at the highest level. I have a greater confidence in my technical and modeling abilities now along with having a much broader and deeper problem solving skill set. On the writing and presentation side, your honest criticism and positive feedback have immensely helped.

I would also like to extend my gratitude to Dr. Adam Hawkins and Dr. Koenraad Beckers for the numerous technical discussions we have had over the past few years. I have learnt a tremendous amount of modeling from the both of you and my research couldn't have progressed without your timely support and help. The Tester group, in specific, Nicolas, Nazih and Hanif, have also helped

me a lot and supported me through thick and thin. Dr. Don Fox has also been an extremely useful source for my technical questions. You have truly inspired me through your ingenious coding and modeling abilities. In addition, I would like to thank Polly Marion, Jeff's assistant, who has been a great resource for answering my questions and helping me with administrative matters.

I cannot fully express the many ways my friends have had an influence on me. I am ever in debt to Venktesh and Shikhar for introducing me to the Tester group. You both have turned out to be very close friends of mine with whom I could express myself freely. Anirudh my roommate at Cornell has also served as a close friend of mine right since my undergraduate days. Thanks for tolerating me for all these years and helping in uncountable instances. Thank you Siddarth and Simon for your deep friendship. Besides being such amazing friends, I could also discuss highly technical topics with the both of you, which in turn has helped me develop my technical skills and problem solving abilities. Thank you Arvind for being a trustworthy friend and teaching me the beautiful art of cooking. Thank you Rewa for always being supportive of me and for showing immense hospitality. My fellow clean energy buddies Akshay and Samay, thanks for the all the intellectual conversations and for being extremely kind and friendly.

Thank you Anthea, Shamika, Sahana, Abha, Akhila and Nidhi for your hospitality and friendship. We have truly spent memorable time together which I can never forget. I must also sincerely thank you for listening to me and always being there for me. I appreciate your friendship Harman, thanks a ton for organizing the multiple road trips and my best birthday party in a cruise on the

cayuga lake.

I would be remiss not to mention my best buddies from the Cornell India Association, Sourbh, Chaitanya, Vikram, Swatah. We have organized several great events together as well as fund raised on a large scale during the time of the pandemic. Thanks for all the effort and help. You all continue to inspire me through your simplicity and modesty.

CONTENTS

LIST OF TABLES

LIST OF FIGURES

CHAPTER 1

INTRODUCTION

Geothermal energy is the stored thermal energy within the earth. It can provide a constant base load power and therefore has a great advantage over intermittent renewable energy sources such as solar and wind. Although the geothermal resource base is vast with the thermal energy stored in the upper continental crust being several orders of magnitude larger than the annual global primary energy demand (Armstead and Tester, 1987; Rybach et al., 2000), the current installed geothermal electric and thermal capacity is relatively small. As of 2019, installed worldwide capacity is limited to roughly 16 GW_e in electricity production (Huttrer, 2020) and 30 GW_{th} in direct-use heat systems (excluding ground-source or "geothermal" heat pumps) (Lund and Toth, 2020). Most systems today produce from highly-permeable, high-temperature reservoirs, also referred to as hydrothermal systems, which are geographically limited. Much more common are formations where heat is present, but in-situ fluids are lacking or natural permeability is low, hindering profitable production. Two techniques are currently being proposed to utilize these unconventional geothermal systems namely - Enhanced geothermal systems (EGS) and Closed loop geothermal systems (CLG).

EGS involves the stimulation of fluid flow pathways within the bulk rock using hydraulic, chemical and thermal techniques that create, or re-open existing fracture networks. The working fluid (usually water) is then introduced into this fracture network through an injection well and the heated fluids are removed through a production well. Although technical feasibility has been demonstrated in certain sites, challenges remain for EGS to become a reliable and fi-

nancially appealing approach to harness geothermal energy on a global scale. Induced seismicity, short circuiting of the reservoir leading to flow through narrow channels or pathways that offer the least resistance to flow are a couple of major challenges that need to be mitigated for the success of an EGS project.

On the other hand, in CLG, the heat transfer or working fluid (e.g., water or supercritical CO_2) does not permeate the reservoir. Instead, fluids circulate through a closed loop wellbore system that exchanges heat with the surrounding bulk rock. Proponents of CLG indicate that no reservoir stimulation is required, lowering the risk of induced seismicity and avoiding the technical challenge of creating a set of fractures with sufficient area and without short circuits. Other benefits are that CLG can be applied to repurpose abandoned or ill-producing wells, or extract heat from a reservoir without producing reservoir fluids to avoid challenging fluid chemistry or insufficient subsurface fluid pressures. However, CLG introduces new challenges such as obtaining sufficient contact area with the rock for sustained and acceptable rates of heat extraction, as well as the need in certain designs to drill and connect multiple loops of horizontal wells at acceptable costs.

There are several areas of ongoing research that promise to mature both EGS and CLG to realize their full potential such as, drilling technologies, geophysical surveying, stimulation techniques, connectivity and thermal hydraulic performance modeling. This study aims at dealing with the connectivity and thermal hydraulic performance of both EGS and CLG through analytical and numerical modeling techniques. The connectivity and thermal hydraulic performance in the context of EGS/CLG refers to the flow and thermal profile evaluation of a

working fluid as it advances through the fractures in the subsurface between an injection and production well or through a closed pipe in the subsurface.

1.1 Objectives and Organization

This thesis seeks at developing and implementing analytical and numerical frameworks to analyze both EGS as well as CLG. Therefore, the thesis is divided into four sections. The first section (Chapter 2) deals with developing a characterization tool to better understand the phenomenon of flow channeling at a meso scale field site through periodic pumping tests.

Traditional pumping tests performed to characterize the subsurface are often not suitable for fractured systems since the diffusion length or the radius of penetration quickly expands beyond the inter-well distance. Periodic pumping tests allows to control the diffusion length by varying the period or frequency of oscillation of the pressure or head signal created at the source well. The primary objective of this study is to compute the width of the formed channel between two wells at the field site for the different periods of testing using the analytical characterization tool created as a part of the work. This analysis is particularly useful in EGS applications since flow channeling in fractures can be evaluated by providing a pathway to calculate the geometric properties of the fracture (i.e. fracture channel width or hydraulic aperture) either before or during geothermal operations. Since there is no need to extract water or shut down pumps to conduct these tests, they are likely to be much more cost effective than shut-in hydraulic or cross-hole tracer tests.

A secondary objective of the work is to explore the fluid storage mechanism at the same meso scale site. The fluid can either be stored in the fractured formation or in the monitoring wellbores as a result of the periodic pumping tests. A quantitative study is performed to analyze both these mechanisms and separate their influence on the results. The most dominant out of the two mechanisms is then chosen to represent the field site.

The second section of this thesis (Chapter 3) deals with evaluating the thermal performance of CLG systems. A numerical finite element based approach is developed and used to evaluate the thermal drawdown of a specific CLG configuration (co-axial systems). Different operating conditions, reservoir conditions and designs are simulated and a thorough sensitivity analysis is performed for the system. The finite element method developed is also validated with a semi-analytical approach using Slender body theory (SBT) and an analytical technique (Ramey, 1962). The model developed in this section can help in planning and modeling closed loop coaxial systems in a commercial scale.

The third section of this thesis (Chapter 4) deals with comparing the performance of CLG with EGS. The long term performance of a U-Loop CLG (with insulated injection and production wells) is compared with an idealized parallel fracture system and a discretely fractured system. Analytical and semi-analytical techniques (Ramey, 1962; Murphy et al., 1981; Fox et al., 2016) are used to evaluate both these systems for a set of design conditions.

The fourth section of this thesis (Chapter 5) encompasses the conclusions and recommendations for future work.

CHAPTER 2

PERIODIC PUMPING TESTS IN FRACTURED BED ROCK FORMATIONS

2.1 Introduction and Theoretical Background

The commercial success of Enhanced/Engineered Geothermal Systems (EGS) is highly dependent on developing a deep subsurface heat exchanger that doesn't experience the phenomenon of "short-circuiting" (Hawkins et al., 2018), which leads to a decrease in the effective heat transfer area swept by the fluid in the subsurface, which in turn results in "premature thermal drawdown" in the reservoir (Brown et al., 1999; Horne et al., 1985; Robinson and Tester, 1984).

Premature thermal drawdown may arise due to an increase in fracture roughness (i.e., fracture aperture variations), the result of which causes changes in the fluid flow. Paths or channels that offer the least resistance to flow are preferred over larger sections that may offer a larger fracture area for heat exchange with the fluid. Therefore, the majority of the fluid flow in such natural fractures takes place in channels and the rest of the fracture surface conducts only a small portion of the total flow (Liu, 2005) resulting in decreased overall reservoir lifetime, which is not preferred. Hence, it's important to study the hydraulic connectivity of the fractured media as it helps in understanding flow channelization (Tsang and Neretneiks., 1998) and is critical in the development and operational stages of EGS.

Theoretically speaking, hydraulic connectivity can be understood by solving the Navier-Stokes equations under a set of complicated fracture surfaces to pro-

vide details on pressure and flow velocity distributions in fractures. However, a great number of practical constraints limit the direct application of the Navier-Stokes equation. Three coupled, nonlinear partial differential equations have to be solved in a three-dimensional domain, making the process computationally cumbersome. Analytical models to describe the hydraulic connectivity of the media on the other hand can provide a computationally fast approach as compared to numerical codes which may rely on finite element, finite volume, or finite difference methods. If one is content with the simplifications that come along with deriving analytical equations, the models can be handy in predicting and understanding the consequences of flow channelization.

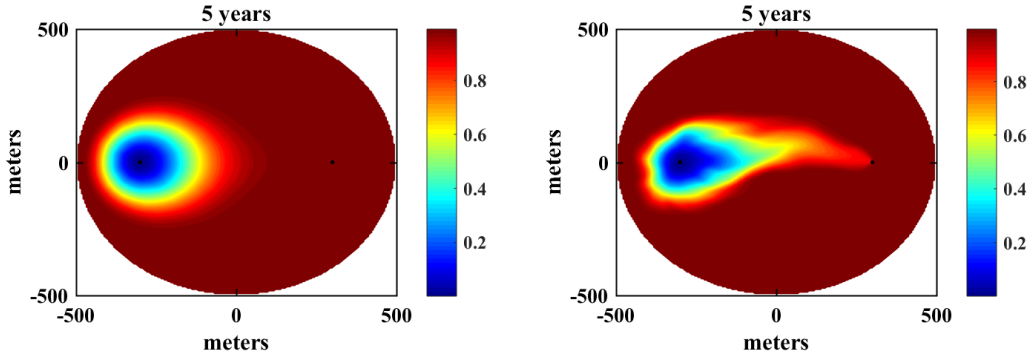

(a) (b)

Figure 2.1: (a) Thermal Drawdown plot after 5 years for Ideal Dipole Flow conditions in a Circular Fracture with a uniform aperture. It can be seen that for the doublet system (one injector and producer) the drawdown is negligible. (b) Thermal Drawdown plot after 5 years for a rough fracture with non uniform aperture (short-circuit conditions). It can be observed that the cold front has traversed a larger distance and is much farther away from the injector signifying a significant drawdown in the reservoir. The simulations were conducted using a hybrid Finite Element Method (FEM) and Boundary Element Method (BEM) based on the technique illustrated in Fox et al., 2016. The legend shows the dimensionless temperatures $\theta = (T(t) - T_w)/(T_r - T_w)$. $T(t)$ refers to the reservoir temperature at a particular time, T_w refers to the water injection temperature and T_r refers to the initial reservoir temperature. θ can be viewed as the fraction of thermal drawdown with 1 being no drawdown and 0 being complete drawdown.

Several experimental and theoretical studies conducted by researchers (Iwai, 1976; Neuzil and Tracy, 1981; Tsang and Witherspoon, 1981; 1983) have led to the conclusion that laminar flow of a viscous incompressible fluid can be used to successfully evaluate fracture flows. One can then adopt the analogy of parallel planar plates to represent fracture surfaces, and the volumetric flow rate per unit fracture width normal to the direction of flow can be expressed through the Boussinesq equation (Boussinesq, 1868) for steady and isothermal flows.

$$q = -\frac{b_h^3 \rho g}{12\mu} \nabla h \tag{2.1}$$

where q is the volumetric flow rate of fluid per unit width of the fracture in m^2/s, ρ is the density of the fluid in kg/m^3, μ is the dynamic viscosity of the fluid in kg/m.s, h is the hydraulic head in m and b_h refers to the hydraulic fracture aperture which is the aperture available for advective fluid flow through the fracture in m.

Equation 2.1 is also the basis for what is often called the "cubic law" in fractured rock hydrogeology. It is important to note that the equation is derived by assuming the fractures are "open" (i.e., the planar surfaces remain parallel, and thus are not in contact at any point). Besides, for the cubic law to hold true in a heterogenous system such as fractures with increased roughness, a hydraulic fracture aperture term needs to be introduced (b_h) in its formulation (Zhang, 2017). The hydraulic aperture can be defined as the aperture required in a smooth fracture to produce the same flow rate under a given pressure gradient as the real rough-walled fracture.

Several modifications have been proposed to the cubic law such as the quadratic law (Uchida, 1994) and quintic law (Klimczak et al., 2010). However, these

methods lack theoretical and experimental rigor. Therefore, this study will only focus on employing the cubic law to describe fracture flows and channelization since its validity has been established by several researchers over a wide range of subsurface hydrological conditions with apertures ranging down to a minimum of 0.2 µm both experimentally as well as through theoretical analysis (Witherspoon et al., 1980).

From equation 2.1, Transmissivity T can be defined as the flow of fluid through a unit width of the fracture over its entire aperture with units m^2/s. Therefore, mathematically T can be represented as -

$$T = \frac{b_h^3 \rho g}{12\mu} \tag{2.2}$$

Transmissivity of a fracture can physically be viewed as its ability to transmit water. In groundwater hydrology, analyzing T helps in understanding the amount of water that a fracture can deliver to a pumping well and therefore plays a vital role in analyzing the hydraulic connectivity of fractured bedrocks.

Another important term required to evaluate the hydraulic connectivity of fractures is Storativity (S), which can be mathematically understood through the application of mass conservation in fractured media. The resultant governing equation is expressed below-

$$S_s \frac{\partial h}{\partial t} - \nabla.(k \nabla h) = 0 \tag{2.3}$$

where S_s is the specific storage and is defined as the volume of fluid released from a unit volume of the media for a unit decrease in hydraulic head. This equation is non linear in nature due to the fact that specific storage is related to the change in the hydraulic head. However, the nonlinearity is weak in nature

(Pinder and Celia, 2006), which implies that there is very little change in S_s for changes made in the hydraulic head with time. Besides, the above expression neglects the spatial gradient of density of the fluid, ρ. Storativity (S) can then be expressed as the specific storage through a unit fracture aperture. Physically speaking, Storativity can be viewed as the volume of water released or taken into storage per unit surface area of the fracture for a unit change in hydraulic head.

$$S = S_s b \tag{2.4}$$

Traditionally, T and S are used to evaluate the hydraulic connectivity in fractured bedrock environments. A high T and a low S would imply that the fractures can transmit large quantities of water with minimal storage of water in the fractured media thereby increasing the chance of flow channeling which is undesirable in EGS applications. Therefore, to establish a good reservoir performance between two wells (injection and production wells) it is pivotal to establish flow connectivity through T but also ensure that the fluid is being stored within the fracture that is in contact with a large surface area of the rock through S.

Another quantity that can be used to quantify flow through fractures is the hydraulic conductivity represented by the symbol k. It describes the flow through a unit area of the fracture (unlike T which represents flow through a unit width of the fracture) and can therefore be mathematically expressed by dividing equation 1.1 by b_h which would give the following expression-

$$q' = -\frac{b_h^2 \rho g}{12\mu} \nabla h \tag{2.5}$$

where q' refers to the specific flow or the flow rate per unit area of the fracture. and $k = b_h^2 \rho g / 12\mu$. k is therefore dependent on both the geometric property of

the fracture (i.e. $b_h^2/12$) also called the intrinsic permeability which has units of m^2 and the fluid properties (i.e. $\rho g/\mu$).

Core sampling can be done to analyze the hydraulic conductivity of the fractures in the subsurface. However, local variations in aperture aren't taken into consideration for this form of analysis since sampling is only done at particular points in the subsurface. Slug and constant rate pumping tests on the other hand help capture such regional fluctuations and aid in understanding the inter well connectivity (Pinder and Celia, 2006) and provide averaged hydraulic parameters over a wide area. However, it was found that these techniques are only ideal for heterogenous porous media or soil and not for fractured or bedrock environments (Guiltinan and Becker, 2015).

The difficulty in analyzing fractured bedrock environments through traditional pumping tests arises due to their low effective porosity resulting in a large area or radius of influence (Renner and Messar, 2006; Becker and Guiltinan, 2010; Sayler et al., 2017). This would mean that local formation information is only captured during early drawdown leading to averaging of hydraulic properties across the wide heterogeneous network. Spatial averaging leads to errors in transport models where highly conductive pathways are missed. Additionally, this channeling, or short-circuiting, among fractures may lead to the testing of only a few preferred pathways that do not represent the flow of groundwater or transport of contaminants in their natural state. Besides, pumping and slug tests are also sensitive to borehole influences and hence may provide inaccurate results (Rasmussen et al., 2003; Rabinovich et al., 2015).

Periodic pumping or harmonic tests overcome many of these limitations by creating a head oscillation at one well (source well) and the corresponding oscillatory head response is studied in one or more monitoring wells. Since the head signal is in the state of constant transience, the change in fluid release from storage for a change in head can be estimated accurately. In addition, the head response to local storativity during a traditional pumping test can be overwhelmed with wellbore storage effects and pump flow transients. Periodic tests reduce this noise, producing a better measurement of formation storage and, therefore, connectivity (Knudby and Carrera, 2006).

Therefore, the primary objectives of this part of the study is to create a characterization technique for computing T and S through periodic pumping tests between two wells in a single bedding plane fracture at a meso scale field site. The tests are operated at different periods and the fracture channel width is evaluated for each of these periods. Varying the period of oscillation can have an influence on the head oscillations created at the source and monitoring wells. This might change the driving pressure and time for fluid storage in the void spaces along the fracture, leading to changes in the fluid channel properties.

This analysis is particularly useful in EGS applications since flow channeling in fractures can be evaluated by providing a pathway to calculate the geometric properties of the fracture (i.e. fracture channel width or hydraulic aperture) either before or during geothermal operations. Since there is no need to extract water or shut down pumps to conduct these tests, they are likely to be much more cost effective than shut-in hydraulic or cross-hole tracer tests.

A secondary objective of this study is to explore the fluid storage mechanism at the meso scale site. When pumping tests are conducted in a medium where the storativity is high, the volume of water released to the well from storage in the formation is significantly larger than the volume of water stored in the wells. Thus the error produced from the results of pumping tests are low in such high storativity media such as sand and gravel. However, when storativity (S) of the media is low such as in fractured formations, the effects of storage of fluid in the wellbore could be significant. Storage in the monitoring wells can reflect a rise in volume and height of the fluid as the fluid enters the interior of the pipe in the well. To reduce wellbore storage, packer systems are introduced to isolate the target fracture zone. However, these effects can still be significant (Cole, 2018). Therefore, this study will also focus on quantitatively estimating the effect of monitoring well storage effects and comparing it to the effects of storage in the formation (i.e. fracture).

2.2 Site Description

Periodic pumping tests were conducted in the Altona flat rock site which is located in Clinton County, New York, approximately 15 miles northwest of Plattsburgh, New York and around 266 miles from the Cornell University, Ithaca Campus.

Figure 2.2: Altona Flat Rock Site in Clinton County, New York

The site has shallow water levels and doesn't have a soil cover which makes it an attractive option for conducting hydraulic testing. Reconnaissance Ground Penetrating Radar (GPR) imaging located a reflection at 7.6 m from the ground surface that was interpreted as an open bedding plane fracture (Hawkins et al., 2017). A well field was installed at the site with 4 four wells (104, 204, 304 and 504) forming the corners of a 10 m by 10 m square with an additional well in the middle (well 404) which was equidistant to the others.

Multiple tests have been carried out at the site to investigate transport and connectivity (Becker and Tsoflias, 2010, Castagna et al., 2011, Guiltinan and Becker, 2015, Talley et al., 2005, Tsoflias and Becker, 2008). In general, the results of these field experiments have indicated that there is poor connectivity between wells 504 and 104 and good connectivity between wells 204 and 304.

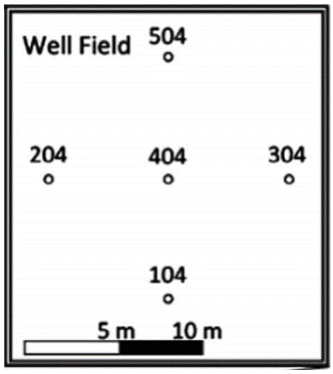

Figure 2.3: Layout of the different wells (104-504) at the Altona Field Site

Hydraulic testing indicates that the wells communicate through a shallow fracture with a transmissivity of 5 m^2/day which suggest a mean aperture of 0.45 mm (Talley et al., 2005) for the entire 5 spot well framework.

In July of 2011, all five wells were deepened with percussion air rotary drilling

with a 14 cm drill bit. The new well depths range from 18.3 m to 21.3 m. Bentonite clay was used to seal the casing to the formation. The periodic harmonic tests were conducted with a 1.9 cm diameter water tight cylindrical slug in the source well. This slug was lifted and lowered in the annulus of the well using a winch operated by a computer controlled stepper motor. A straddle packer system was placed in the wellbore to isolate the hydraulic disturbance to the target fracture. The packer was also installed in such a way that its diameter was equal to the wellbore diameter of 14 cm.

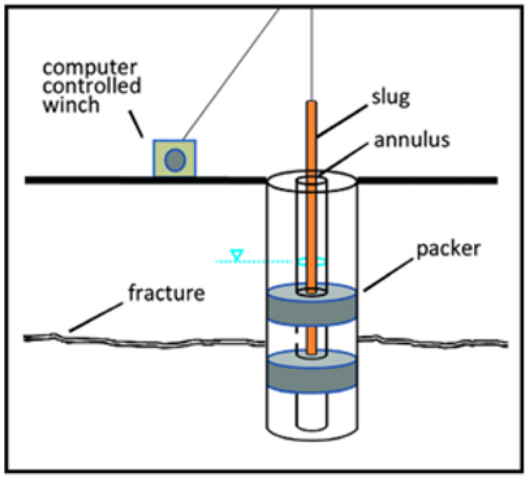

Figure 2.4: Setup of the hydraulic source well for the periodic pumping test. Adapted from Guiltinan and Becker (2015)

Three distinct frequencies were created and examined at each well and all wells were monitored for head changes using pressure transducers. The tests were conducted at a temperature of 10°C. Besides, the volumetric flow rate of fluid entering/leaving the source well was also monitored to aid in the evaluation of hydraulic connectivity of the formation.

2.3 Previous Characterization Studies of Fracture Flow at The Altona Field Site

Baker (2014) conducted 3-D imaging of flows in the subhorizontal fractures using GPR tests at the Altona Field Site which builds on the results from Beyrle (2005) and Talley (2005). The multi component surface based GPR system allowed to monitor saline tracer flow through the same water saturated fracture.

The multi component system approach proved advantageous over a previous single component system since the former allowed for simultaneous acquisition of orthogonal polarizations. Summing up the multiple orthogonal polarizations can help simulate a circular wavefront similar to seismic wavefields, thus allowing for more accurate processing utilizing standard seismic methods. The effects of polarization caused by fracture channeling and roughness can therefore be reduced and isolation of individual channels within the field site can be achieved along with imaging channels with great accuracy.

GPR surveys can be grouped into three categories namely background survey, full dipole and natural gradient. The background survey at Altona was conducted under ambient subsurface conditions and there was no imposed hydraulic effects. Three full dipole tests were performed between wells 204-304 (E-W) with water electrical conductivity increasing for each test. These tests were also conducted between wells 104-504 (N-S) with equal injection and production flow rates under forced fluid flow conditions.

It was found that for the E-W dipoles the flow rate could be maintained at ap-

proximately 8 liters per minute and for the N-S dipole approximately 5 liters per minute. The N-S dipole could not sustain the higher pumping rate attained in the E-W dipole tests. This might be due to the fact that there is no direct path that connects wells 504 and 104 unlike that observed between wells 204 and 304 (Perll, 2011) . Steady state electrical conductivities for the three dipole tests were ~ 180 mS/m, ~ 400 – 500 mS/m and ~700 mS/m.

The natural gradient tests were conducted by continuous injection of saline solution into well 204 at a low flow rate for the entire duration of the GPR survey. During the tracer tests inflatable rubber packers were placed below the fracture of interest in each well to isolate the fracture from deeper, hydraulically conductive fractures. The saline tracer was used to increase the electrical conductivity of the water in the fracture, which causes changes in the amplitude and phase of the reflected GPR signal, and can be used to highlight fracture channels (Tsoflias and Becker, 2008). Table salt behaves predictably in a system and the formation water quickly returns to normal background electrical conductivity after pumping (Talley et al., 2005). The amplitude of the reflected GPR electromagnetic signal is a function of fracture aperture and salinity of the fluid (Tsoflias and Becker, 2008). The borehole conductivities in the natural gradient test were between ~4500 – 5000 mS/m. The occurrence of flow channeling between wells 204 and 304 were indicated through the natural gradient test as well.

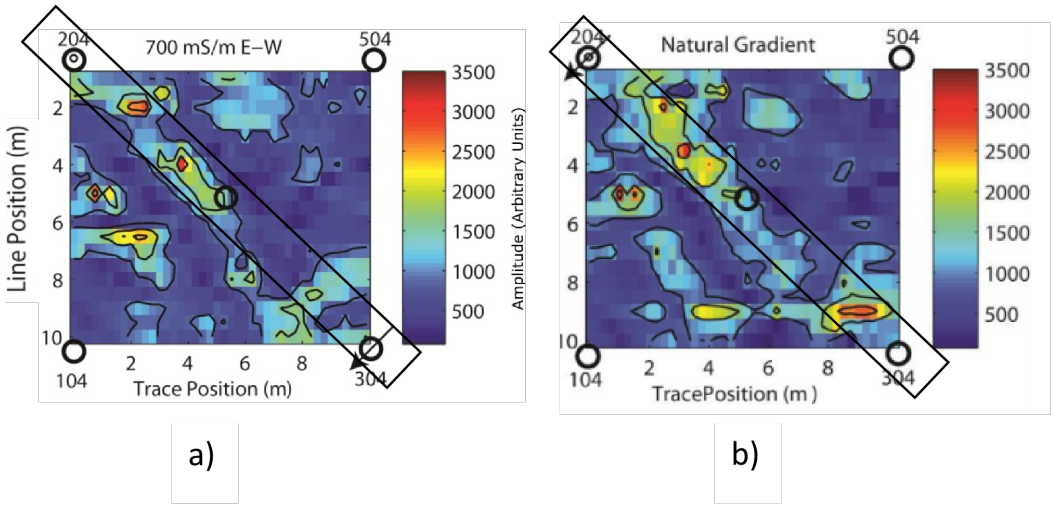

Figure 2.5: Reflected amplitude information at the depth of 7.6 m during a) Third dipole GPR test after subracting the background signal and b) Natural Gradient GPR test. The dipole test achieved a steady state electrical conductivity of 700 mS/m with the water being injected at Well 304 and pumped out of Well 204. For both the tests the regions with higher measured amplitudes are expected to have a larger fracture aperture. The tests reveals the possibility of a narrow channel between wells 204-304 with a width of 1-2 m and a length of 14.1 m. Adapted from Hawkins et al., 2018 and Perll, 2011.

More recent work by Hawkins et al., 2018 further strengthens the channeling claims in the Altona Field Site using an advection dispersion reaction model employed in one dimension using the data generated from a inert/adsorbing tracer test at the field site to identify the channeling effects. The presence of two flow channels between the injector and producer is assumed with one being the dominant flow channel having a lower effective surface area. The results from the analysis was roughly consistent with independent measurements of fluid flow paths. For a reservoir volume of 82.4 L and a surface area of 28.3 m^2, the fracture aperture for the dominant channel was found to be close to 5.8 mm. Following a similar analysis the aperture for the other channel was found to be 5 mm.

Hawkins et al., 2018 also evaluated the heating of the reservoir by injecting hot water into well 204. The ambient formation temperature was 11°C and water was being injected at a temperature of 74°C and flow rate of 5.7 L/min. The temperature at different points on the field site were recorded using Fiber Optic Distributed Temperature Sensing(FO-DTS) techniques. It was found that the sensors that were arranged in between wells 204 and 304 (b8, b6, b5) recorded the highest temperatures and the ones that were arranged away exhibited lower temperatures suggesting the channeling between the wells leads to the increase in reservoir temperature between the two wells.

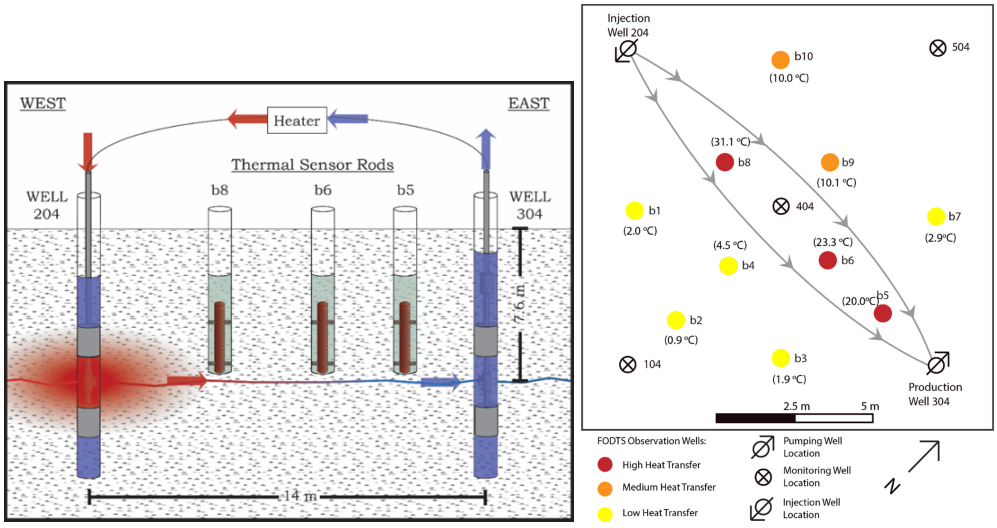

(a) (b)

Figure 2.6: (a) Schematic of the FODTS setup which is in between the injection and pumping wells. Hot Fluids flow from Well 204 and get cooled towards Well 304. Adapted from Hawkins Dissertation 2017. (b) Temperature measurements in all the 10 FODTS wells adapted from Hawkins et al., 2018.

Hawkins et al., 2020 computed the non uniform aperture distribution between wells 204 and 304 by discretizing the fractured bedrock using Finite Element Method (FEM) with 7100 elements (7196 nodes) and using a Genetic Algorithm (GA) - Principal Component Analysis (PCA) approach of self affine and

rough walled fractures to obtain the large/small scale aperture fluctuations determined by the number of PCA modes or scores.

The first PCA mode would therefore represent large scale variations in aperture and would capture most of the variance in the data. As the number of PCA modes increases, small scale variations are captured as well. This helps in representing the total system more accurately. The tracer Breakthrough Curve (BTC) data along with the frictional pressure drop between the two wells is used in a two stage optimization procedure to predict the aperture field. Inverse problems such as these do not have a unique solution and therefore the Genetic algorithm is useful due to its stochastic nature. This aperture field is then used to forecast the temperature at each finite element node through Fox et al., 2015.

The approach clearly indicated the channeling between wells 204 and 304, with a mean aperture close to 5 mm between the injection and production wells. The mean aperture of the entire field was computed to be equivalent to 2.2 mm with an L^2 norm of 0.06.

Although all the above listed techniques (GPR, inert/adsorbing tracers, FO-DTS and PCA-GA approaches) have been successful in determining the hydraulic aperture of the fracture, they can only give rough estimates of the expected width of the fracture. Characterizing channeling in a fracture requires knowledge of both the aperture as well as the fracture channel width. The analysis of periodic pumping tests through fractured bed rock formations known to exhibit channeling can help in quantifying the unknown width (which has usually been ignored in the previously tested approaches) for a predetermined or known hy-

draulic aperture of the channeled section between wells 204 and 304.

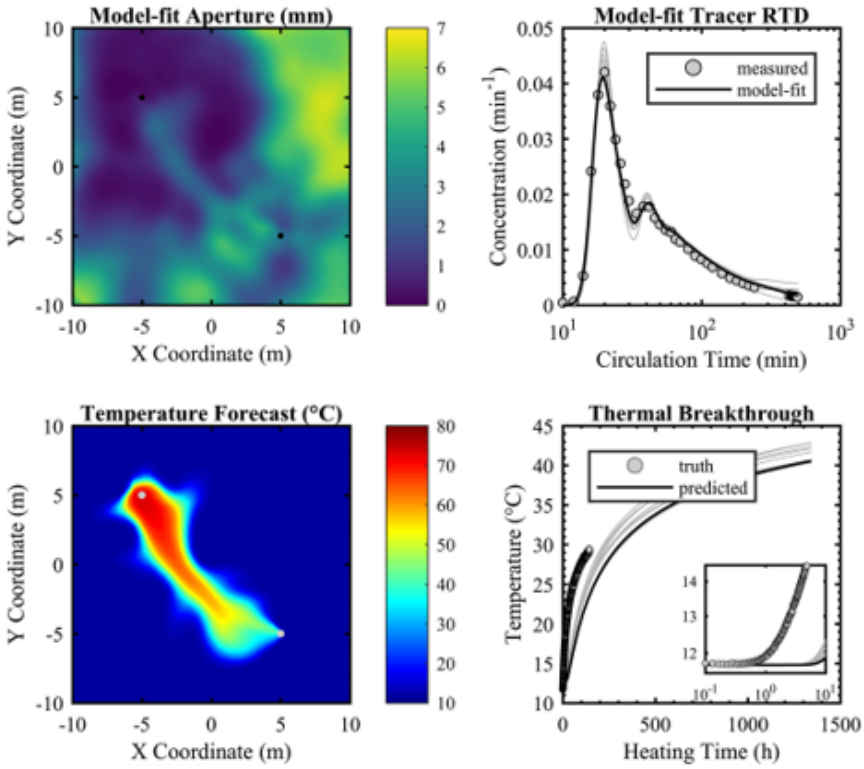

Figure 2.7: Results using 200 PCA Modes from the two stage optimization showing a good fit with the tracer residence time distribution or BTC data (top right) and the thermal breakthrough or advective heat transport in the fracture (bottom right). The lighter gray lines that are present in the top right and bottom right plots refer to the results obtained through the 9 realizations of the Genetic Algorithm which occurs due to the stochastic nature of the process. The dark lines represent the lowest L^2 norm. Adapted from Hawkins et al., 2020.

2.4 Theoretical Analysis of Periodic Pumping Tests

The hydraulic connectivity of the field site through periodic pumping tests is analyzed by solving an inverse problem using two approaches. The first approach assumes the storage of the fluid to entirely take place in the monitoring wells and the second approach assumes the storage of fluid to entirely take place in

the fractured formation. In the former approach, inversion is performed using the set of experimentally measured head oscillations at the source and monitoring wells (between wells 204 and 304) as the known quantities to obtain the channel properties such as the width of the channel for a predetermined hydraulic aperture. In the latter approach, the hydraulic parameters namely T and S are computed through inversion using the same measured head oscillations at the source and monitoring wells as the former, along with the volumetric flow rate at the source well as the known quantities. The channel properties such as the width of the channel are then determined using the computed hydraulic parameters for a known hydraulic aperture of the fracture. This section provides the theoretical basis and methods on which this work relies upon.

2.4.1 Methods

Hydraulics of Flow Channeling with Storage in the Wells:- Since there is sufficient evidence to prove the extreme flow channeling effects between wells 204 and 304, it is hypothesized that the exact connectivity between them can be evaluated through channel hydraulics. Storage in a monitoring well can then be easily taken into account by performing a volume balance around it. The performed volume balance can then be used to solve for the width of the channel formed (W) and L_∞ for a known hydraulic aperture b_h of the channel. Here, L_∞ is defined as the distance probed by the source signal beyond the boundaries of the field site during a particular period of oscillation. In other words, at a distance of L_∞ from the last monitoring well in the channelized section, the hydraulic head reduces to 0 ($h_\infty = 0$).

The presence of water bodies can also affect L_∞ as the injected fluids may tend to percolate through the fracture towards the closest water body. Therefore, L_∞ can be viewed as the distance between the last monitoring well and the water body (lake, river, dam etc). It can also be viewed as the distance to a void space within the fracture where new water can be stored.

When wells 204 or 304 were used as source wells it was noted that hydraulic signals could also be monitored at wells 504 and 104. These wells (i.e. wells 504 and 104) do not lie in the section which is known to exhibit flow channeling, suggesting the existence of unknown channels or paths that connect wells 104 and 504 with 204 or 304. By not writing the volume balance around the source well, it is assumed that the fluid could be flowing into other unknown flow paths such as these.

When well 304 is used as a source well the head oscillations created at the well vary with time as $h_{304}(t) = h_{304a}\exp(i\omega t)$, where h_{304a} refers to the amplitude of the source signal. In a similar fashion, the head oscillations at the monitoring wells 404 and 204 can be expressed as $h_{404}(t) = \hat{h}_{404}\exp(i\omega t)$ and $h_{204}(t) = \hat{h}_{204}\exp(i\omega t)$, where $\hat{h}_{404} = h_{404a}\exp(i\phi_{404})$ and $\hat{h}_{204} = h_{204a}\exp(i\phi_{204})$. Both $\hat{h}_{404}$ and $\hat{h}_{204}$ are the head signals measured at wells 404 and 204. ϕ_{404} and ϕ_{204} are the phase shifts of the monitoring signal at wells 404 and 204 respectively.

At first, a simple case is considered by neglecting the storage in well 404 and only considering the storage in well 204. The volume balance around well 204 can then be expressed as follows-

$$\frac{dV_{204}}{dt} = \frac{\rho g W b_h^3}{12\mu \times 2L}(h_{304a} - \hat{h}_{204}) - \frac{\rho g W b_h^3}{12\mu L_\infty}(\hat{h}_{204}) \tag{2.6}$$

where L is the distance between wells 304 and 404 and $2L$ is the distance between wells 304 and 204. The change in the volume of water in the monitoring well can be expressed in terms of the area of the monitoring wellbore (A_m) and the change in head with time as follows-

$$\frac{dV_{204}}{dt} = A_m \frac{d(\hat{h_{204}} \exp(i\omega t))}{dt} = A_m i\omega \hat{h_{204}} \tag{2.7}$$

Substituting equation 2.7 in equation 2.6, the following equation is obtained-

$$i\omega \hat{h}_{204} = \frac{\rho g W b_h^3}{12\mu \times 2LA_m}(1 - \hat{h}_{204}) - \frac{\rho g W b_h^3}{12\mu L_\infty A_m}(\hat{h}_{204}) \tag{2.8}$$

A dimensionless number (B) can then be defined. B can be viewed as a dimensionless resistance to flow at a particular period or frequency since it is directly proportional to fractured channel properties namely the channel width (W) and the hydraulic aperture of the fracture (b_h^3).

$$B = \frac{\rho g W b_h^3}{12\mu A_m L\omega} \tag{2.9}$$

Since the distance between well 204 and the skeleton dam on chasm lake (which is the nearest water body to Altona field site) is known to be roughly 50 m (Hawkins, 2017), it is hypothesized that L_∞= 50 m. This would mean that the plane bedding fracture at the field site is connected to the chasm lake, and the periodic signals that are being tested at the field site propagate through to the lake without any storage of fluid in the fracture. Therefore, the only region where fluid storage is assumed to occur is in the monitoring well 204 when well 304 is used as a source well. As it is known that the field site is extensively fractured it is reasonable to hypothesize that the flow of the fluid would be skewed towards the direction of the lake.

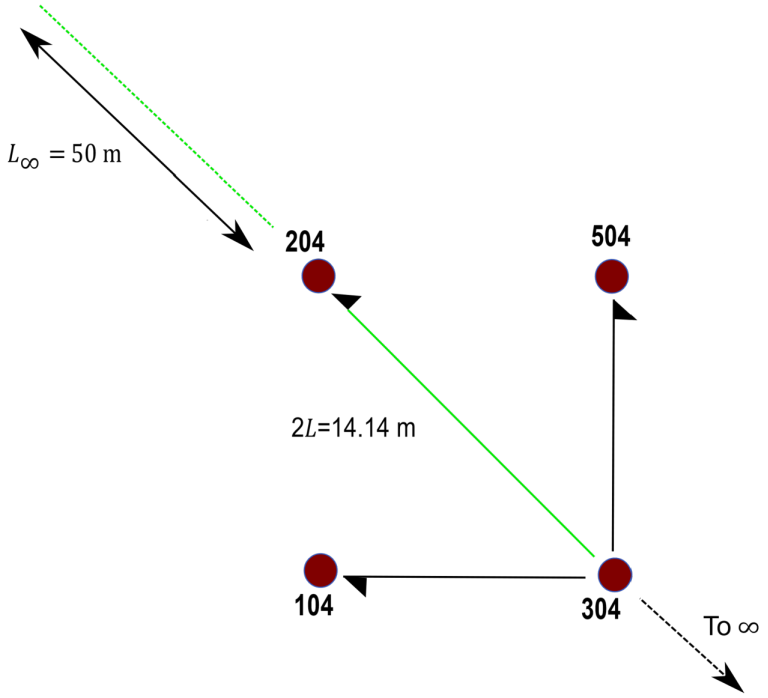

Figure 2.8: Using well 304 as the source well to model the storage effects in the monitoring well 204. The geometric properties of the fracture i.e. the width and the aperture are held a constant in the sections denoted by the green color. The sections in black are the possible flow channels that may exist from well 304 and are not considered for the analysis. Since L_∞ is defined before hand the only unknown solved for is the channel width for a given hydraulic fracture aperture.

The amplitude of the periodic head signal at the monitoring well 204 (h_{204a}) is then extracted through Fast Fourier Transformation (FFT) algorithms (Frigo and Johnson, 1998) and used to solve for the dimensionless parameter B, from which W is extracted for the different periods of testing for a given b_h (The complete derivation is shown in Appendix A.1).

Besides, it can be observed that the method is very sensitive to the measured head amplitudes at the monitoring wells, incorrect measurements could lead to inaccurate or imaginary results due to solving non linear polynomial expressions.

To incorporate the fluid storage effects in all the monitoring wells (including well 404), volume balances are performed around all the monitoring wells. For the case where well 204 is used as a source well, the following equations can be derived from the volume balances around wells 404 and 304.

$$i\omega\hat{h}_{404} = \frac{\rho g W b_h^3}{12\mu L A_m}(h_{204a} - \hat{h}_{404}) - \frac{\rho g W b_h^3}{12\mu L A_m}(\hat{h}_{404} - \hat{h}_{304}) \tag{2.10}$$

$$i\omega\hat{h}_{304} = \frac{\rho g W b_h^3}{12\mu L A_m}(\hat{h}_{404} - \hat{h}_{304}) - \frac{\rho g W b_h^3}{12\mu L_{\infty\,204-304} A_m}(\hat{h}_{304}) \tag{2.11}$$

B^* [units s^{-1}] and ℓ [dimensionless] can then be mathematically expressed as follows-

$$B^* = \frac{\rho g W b_h^3}{12\mu L A_m} \tag{2.12}$$

$$\ell = \frac{L}{L_{\infty\,204-304}} \tag{2.13}$$

Similarly, when well 304 is used as a source well, the following equations can be derived from the volumetric balances around wells 404 and 204.

$$i\omega\hat{h}_{404} = \frac{\rho g W b_h^3}{12\mu L A_m}(h_{304} - \hat{h}_{404}) - \frac{\rho g W b_h^3}{12\mu L A_m}(\hat{h}_{404} - \hat{h}_{204}) \tag{2.14}$$

$$i\omega\hat{h}_{204} = \frac{\rho g W b_h^3}{12\mu L A_m}(\hat{h}_{404} - \hat{h}_{204}) - \frac{\rho g W b_h^3}{12\mu L_{\infty\,204-304} A_m}(\hat{h}_{204}) \tag{2.15}$$

B^* and ℓ' (dimensionless) can then be expressed. B^* has already been mathematically expressed in equation 2.12. ℓ' is given below-

$$\ell' = \frac{L}{L_{\infty\,304-204}} \tag{2.16}$$

To obtain B^*, ℓ and ℓ' that satisfy the data from different wells (204,404 and 304), all periods of operation and two different flow directions (from 304 to 204 and vice versa), a minimization of least squares sum of errors for head amplitudes is performed (Complete derivation in Appendix A.1).

Given the limited amount of data available from the three wells and the fact that the period of oscillation was different when 204 was used as a source well as compared to using 304 as a source well, the period of oscillation in the optimization was treated as causing random variations as opposed to treating it as a systematic variable as presented in the previous case (304 used as a source well with L_∞ predefined).

The best fit ℓ, ℓ' and B^* can then be used to obtain the optimal fracture channel width (W_{opt}), $L_{\infty\,304-204\,opt}$ and $L_{\infty\,204-304\,opt}$ for a given hydraulic fracture aperture (b_h). The objective function used is the l^2-norm error of the computed monitoring wellhead amplitudes and the measured monitoring well head amplitudes. The l^2-norm error for a variable is defined mathematically as follows-

$$l^2 = ||h_{mc} - h_m||_2 \tag{2.17}$$

where h_{mc} is the vector of computed monitoring well amplitudes and h_m is the vector of measured monitoring well amplitudes. The l^2-norm error is a standard objective function used in minimization problems and is an adequate choice for this study.

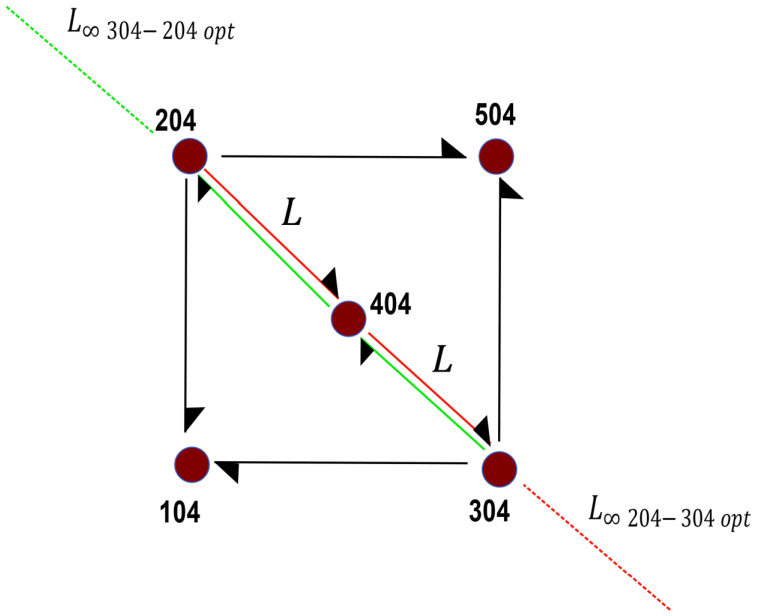

Figure 2.9: Constrained optimization problem to model the storage in the monitoring wells by using data across the three different periods for both well 204 and 304 as the source well. The geometric properties of the fracture i.e. the optimal width and the aperture are held a constant in the sections denoted by the red and green color. The sections in black are the possible flow channels that may exist from well 204 and 304 and are not considered for the analysis. The three unknowns in the optimization framework include $L_{\infty\,204-304\,opt}$, $L_{\infty\,304-204\,opt}$ and the optimal width of the fractured channel (W_{opt}) for a given hydraulic fracture aperture (b_h).

The methods assume the existence of the channel beyond wells 304 and 204. This assumption is reasonable since the generated periodic signals at the field site have been found to probe distances that are beyond the 5 spot well framework by assuming radial flow in the fractured system (Guiltinan and Becker, 2015).

Besides, the approach requires predetermining the hydraulic aperture (b_h). Hydraulic apertures can traditionally be obtained by solving inverse problems which usually do not have a unique solution. A PCA-GA approach (Hawkins et al., 2020) is used to predict the hydraulic aperture at the meso scale field site

and two realizations (b_h=2.5 mm and b_h=5 mm) are employed in the analysis to compute the fracture channel width.

Hydraulics of Flow Channeling with Storage in the Fractures:- Assuming storage effects are only in the fracture, the governing equation along with the appropriate boundary conditions can be represented as follows (The complete derivation can be found in Appendix A.2)-

$$\frac{\partial h}{\partial t} - D\frac{\partial^2 h}{\partial x^2} = 0 \tag{2.18}$$

where h is the head signal oscillation with respect to the reference steady state signal. $h = 0$ at $t = 0$, $h = 0$ at $x \to \infty$, $x \to -\infty$ and h=$h_a \exp(i\omega t)$ at $x = 0$. h_a is the amplitude of the head signal at the source well(slug oscillation). On solving, the following expression is obtained-

$$h(x,t) = h_a \exp\left(\frac{-x}{\sqrt{2}l_d}\right)\exp\left[i\left(\omega t - \frac{x}{\sqrt{2}l_d}\right)\right] \tag{2.19}$$

where l_d refers to the diffusion length and the amplitude of the head signal at a distance x from the source is $h_a \exp(-x/\sqrt{2}l_d)$. The diffusion length is defined using the frequency of operation and the diffusivity as follows-

$$l_d = \sqrt{\frac{D}{\omega}} \tag{2.20}$$

The diffusion length scale can also be called the radius of investigation for radial flows in the subsurface. It can be tuned on the basis of the region of the bedrock being investigated and allows the hydraulic parameters to be evaluated with respect to a variable distance from the source well. When these tests are performed at multiple frequencies more information about the region can be obtained when compared to a constant rate or single frequency test (Cole, 2018).

From equation 2.19 it is also noted that the monitoring well signal has a phase shift component associated with it. Therefore as the periodic signal propagates through the fracture, the signal is attenuated and shifted. One can solve equation 2.19 to obtain the diffusion length consistent with measured head oscillations in the monitoring well.

$$l_d = -\frac{x}{\sqrt{2}} \ln\left[\frac{h_m}{h_s}\right]^{-1} \tag{2.21}$$

where h_m refers to the amplitude of the monitoring well signal and h_s refers to the amplitude of the source well signal. h_m can vary for different periods since the fluid storage in the void spaces along the fracture can change. This can therefore lead to a variation in the diffusion length with period. The ratio h_m/h_s is called the amplitude attenuation. In terms of phase shift, the diffusion length can be expressed in terms of the normalized delay between the monitoring and injection well head signals i.e. $\Delta t/T_0$. Here, Δt is the delay between the two signals and T_0 is the period of the signal.

$$l_d = \frac{x}{\sqrt{2}} \left[\frac{\Delta t}{T_0}\right]^{-1} \tag{2.22}$$

The phase shift provides another way to estimate diffusion length. Rennar and Messar (2006) attributed the difference between the two diffusion lengths to the heterogeneity of the reservoir considered. The diffusion length obtained through the phase shift information is inversely proportional to the delay Δt. Therefore, for obtaining diffusion lengths that are within the formation of investigation Δt should be large.

At the Altona field site, it is noticed that the 204-304 section shows minimal time lag (Guiltinan and Becker, 2015). This implies the diffusion lengths investigated tend to go well beyond (100's of meters) the boundary of the 5 spot well

network and hence the information from the phase shift would not be useful to understand the local heterogeneity. On the other hand, the poorly connected 104-504 section exhibits a significant phase shift as seen in Figure 2.10 (a). In such cases the phase shift may also be able to probe distances that are within the boundaries of the prescribed formation and hence the information from the phase shift cannot be neglected.

Rasmussen et al., 2003 illustrated a technique that incorporates both the amplitude attenuation and the phase shift into the analysis to give a single solution for diffusivity assuming radial flow in the formation. Flow channeling cannot be analyzed using this method and hence calls for separate amplitude attenuation and phase shift analysis. The focus of this study is restricted to flow channeling that is observed in the section between the wells 204 and 304 (including well 404) where the information from the amplitude attenuation alone is sufficient to understand the connectivity between the wells.

The amplitude of the periodic head signals at the source and monitoring wells are extracted through Fast Fourier Transformation algorithms. Fourier transforms help in revealing the strength of the periodic components by reducing the digitally recorded signal into amplitude and phase components at distinct frequencies whose values are determined by the sampling rate and the record length.

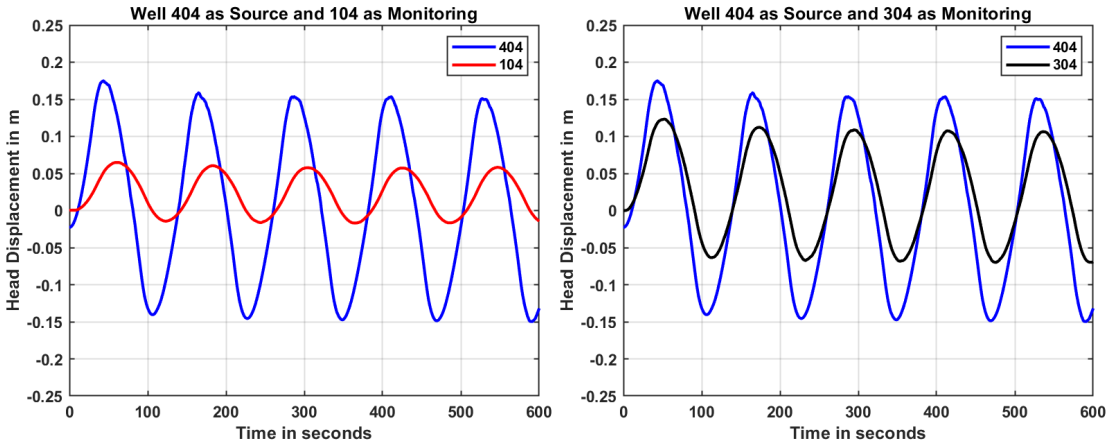

(a) (b)

Figure 2.10: (a) Variation of head with time with Well 404 being the source and 104 being the monitoring well. The signal of the monitoring exhibits a significant phase shift with respect to the source signal and therefore information from the phase shift must also be used for the analysis. (b) Variation of head with time with Well 404 being the source and 304 being the monitoring well. The signal of the monitoring exhibits a negligible phase shift with respect to the source signal and therefore information from amplitude attenuation alone can be used for the analysis. Both the tests were done at a constant period of 121.4 seconds.

Since for fractures, the flow rate per unit width of the fracture is expressed as-

$$q = -T\nabla h \tag{2.23}$$

The flow rate through the fracture in m^3/s can therefore be expressed as-

$$Q(x,t) = -TW\frac{\partial h(x,t)}{\partial x} \tag{2.24}$$

where W refers to the width of the channel formed in the fracture. This can then be simplified into the following form and the amplitude attenuation between the source well flow rate and the source well head signal is used to predict W for a known l_d and T.

$$Q(x,t) = \frac{TW}{\sqrt{2}l_d}(1+i)\exp\left[-(1+i)\frac{x}{\sqrt{2}l_d}\right]h_0\exp(i\omega t) \tag{2.25}$$

$$\left|\frac{Q(0,t)}{h(0,t)}\right| = \frac{TW}{l_d} \tag{2.26}$$

Here, $|Q(0,t)/h(0,t)|$ refers to the amplitude ratio of the source well volumetric flow rate to the source well head oscillation. To compute T it is necessary to have information about the hydraulic aperture (b_h) of the fracture.

Similar to the previous analysis which assumed the storage to entirely occur in the monitoring wellbores, the PCA-GA approach (Hawkins et al., 2020) is used to predict the hydraulic aperture and two realizations (b_h=2.5 mm and b_h=5 mm) are employed in the analysis. Therefore, b_h is predetermined in this analysis as well to compute the width of the fracture. Storativity can also be computed using the computed T and D as $S = T/D$.

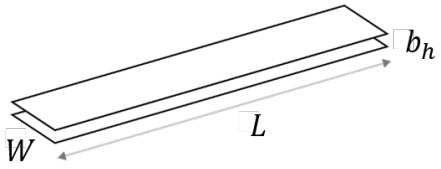

Figure 2.11: Schematic of the three parameters involved in characterizing a channel. L corresponds to the length of the channel(distance between wells 204 and 304), b_h is the hydraulic aperture of the fracture and W is the width of channel formed between the two wells.

Storage in Fracture Vs Storage in Monitoring Wellbores:- When pumping tests are conducted in low storativity media such as in fractured formations, the effects of wellbore storage could be significant. Storage in the monitoring wells can reflect a rise in volume and height of the fluid as the fluid enters the interior of the pipe in the well. To reduce the effect of wellbore storage in the monitoring wells, double packer systems were employed at the Altona Field Site to isolate the target fracture zone. However, it is to be noted that the effects of wellbore storage can be significant in spite of the insertion of such packer systems (Cole,

2018).

The significance of wellbore storage can be understood by calculating the storativity term assuming all fluid storage occurs only at the monitoring wellbores. This storativity is symbolized as S_{pseudo} and is defined as the volume of water released from storage in the wellbore per unit decrease in hydraulic head per unit area of the fracture. Mathematically it can be expressed as follows-

$$S_{\text{pseudo}} = \frac{V_m}{A_F \times h_s} \tag{2.27}$$

where V_m refers to the volume of water in the monitoring well. For a known hydraulic head at the monitoring well $V_m = \pi r_m^2 h_m$ with r_m being the radius of the monitoring wellbore, h_m being the magnitude of head oscillation at the monitoring well and h_s being the magnitude of head oscillation at the source well. A_F refers to the estimated fracture surface area exposed to the monitoring well which is the product of the estimated width of the fracture ($W_{estimated}$) and the fracture length between the source and the monitoring wellbore (L_F).

Several studies (Hawkins et al., 2018; Perll, 2011; Hawkins et al., 2017 and Hawkins et al., 2020) strongly indicate that the width of the channel is close to 1.5 m through rigorous inert/adsorptive tracer testing, GPR testing and PCA-GA optimization. Therefore, S_{pseudo} reports the fluid volume stored in a dimensionless fashion that is not influenced by the width determinations of this study (i.e. $W_{estimated}$ is taken to be equal to 1.5 m to compute S_{pseudo}).

The computed S_{pseudo} is compared with S which refers to the storativity of fracture assuming all storage is occurring in the fracture. The latter is computed by $S = T/D$ for a given hydraulic aperture as described earlier. This comparison of

dimensionless fluid volume helps in understanding the dominant mode of fluid storage in the system.

2.5 Results and Discussions

A characterization technique for evaluating the hydraulic connectivity of the single bedding plane fracture at the Altona field site is developed in this study. The technique relies on the results from periodic pumping tests (conducted at three distinct periods) at the field site between wells 204 and 304. The section between these wells is known to exhibit extreme flow channeling.

By varying the period of oscillation or testing, head oscillations created at the source and the monitoring wells are influenced significantly, which in turn brings about changes in flow channeling. The technique developed in this study provides a pathway to calculate and understand the variation of fracture channel width with oscillation period for a given hydraulic aperture (b_h).

Besides, when the fluid storage capacity of the media is very low such as in fractured systems, the bulk of fluid storage may occur in the monitoring wellbores as compared to the media. This hypothesis hasn't been verified in published literature pertaining to the field site. Hence, quantitative estimates pertaining to the effect of monitoring wellbore storage are also provided in this study. Storage of fluid in the media is then compared to the effect of wellbore storage and the dominant storage mechanism in the fractured system is analyzed.

The connectivity of the channeled section between wells 204 and 304 is esti-

mated using two mechanisms-

1. Fluid storage entirely occurring in the monitoring wellbores.
2. Fluid storage entirely occurring in the fractured formation.

For the first mechanism which assumes the fluid storage to entirely occur in the monitoring wellbores, the average channel width for the 304-204 section (well 304 as source well and well 204 as monitoring well) with b_h = 2.5 mm and b_h = 5 mm is found to be 15.53 m and 1.94 m respectively for a given L_∞ = 50 m and a period of oscillation of 224.6 seconds (It is however important to keep in mind that these results assume that wellbore storage occurs only in well 204 and neglects the storage in well 404). The width estimates however were found to reduce with period. For a period of 112.4 seconds with b_h = 2.5 mm and b_h = 5 mm, the width was found to be 7.31 m and 0.91 m respectively (Figure 2.12).

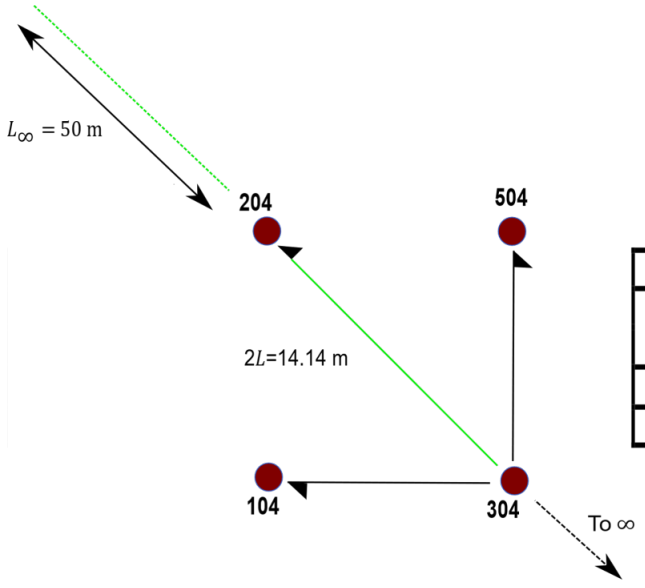

304 — 204		
Period In seconds	b_h = 2.5 mm	b_h = 5 mm
	W in m	W in m
112.4	7.31	0.91
224.6	15.53	1.94

Figure 2.12: Computed fractured channel width (W) for the section between the wells 304 and 204 at the Altona Field Site, NY for different frequencies and two sets of hydraulic apertures (b_h). The results portrayed assume the storage of the fluid to entirely occur in the monitoring well 204.

In order to incorporate the storage effect in all monitoring wells including well 404, data from all the wells in the channel along with different flow directions and different periods of operation are used for a constrained optimization formulation. Given the limited amount of data available from the three wells, the period of oscillation in the optimization was treated as causing random variations as opposed to treating it as a systematic variable as presented in the previous case (304 used as a source well with L_∞ predefined).

The constrained optimization problem is solved for three variables which include the optimal width (W_{opt}), $L_{\infty 204-304 opt}$ and $L_{\infty 304-204 opt}$ for a given set of hydraulic apertures with a l^2 norm of 0.05.

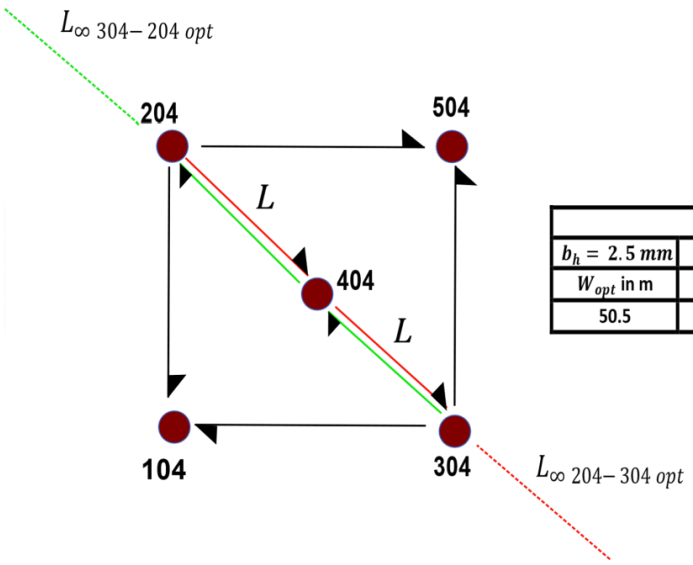

Results of Optimization			
$b_h = 2.5\ mm$	$b_h = 5\ mm$	L_{∞} 204– 304 opt	L_{∞} 304– 204 opt
W_{opt} in m	W_{opt} in m	in m	in m
50.5	6.31	14.14 m	59.82

Figure 2.13: Constrained optimization problem to model the storage in the monitoring wells by using data across the three different periods for both well 204 and 304 as the source well. The geometric properties of the fracture i.e. the optimal fractured channel width and the hydraulic aperture are held a constant in the sections denoted by the red and green color. The sections in black are the possible flow channels that may exist from well 204 and 304 and are not considered for the analysis. The three unknowns in the optimization framework include the optimal width of the channel W_{opt}, $L_{\infty 204-304 opt}$ and $L_{\infty 304-204 opt}$ for a set of hydraulic apertures (b_h)

To satisfy the experimental data collected during periodic pumping tests at the field site, it is observed that the optimal width of the fracture should be close to 50.5 m and 6.31 m for a hydraulic aperture of 2.5 mm and 5 mm respectively. The optimal L_∞ for the 304-204 section is found to be around 60 m which is higher than the optimal L_∞ for the 204-304 section (204 is the source well and 304 is the monitoring well) which was found to be close to 14 m.

For the second mechanism of connectivity evaluation which assumes the fluid storage to entirely occur in the fractured formation, the width of the formed channel in the fracture is on an average equal to 1.31 m for the 204-304 section when the hydraulic aperture is 2.5 mm. For a larger aperture of 5mm, the average width is close to 0.17 m. On the other hand, for the 304-204 section, the average width is 6.07 m and 0.76 m when the hydraulic aperture is 2.5 mm and 5 mm respectively.

Similar trends are observed for the 204-404 and 404-304 sections and vice versa as summarized in Figure 2.14 (b). The channel widths are found to decrease with periods for all cases similar to the trend observed when wellbore storage is assumed. The decrease in widths with period when storage is occurring in the fracture can be explained by studying the period dependence of fracture conductivity using a single inhomogeneous inclusion as performed by Rabinovich et al. (2015).

A square box was defined by Rabinovich et al. (2015) which enclosed a spherical inclusion of radius R and was subject to oscillatory flow. Hydraulic diffusivity which is related to both the storage component (storativity represented by S)

and the hydraulic flow component (transmissivity represented by T) has proven to be a good estimator of connectivity (Knudby and Carrera 2006). Therefore, applying two different diffusivities for the outside (D_{out}) and inside (D_{in}) of the sphere results in defining an inhomogeneous system.

For such an inhomogenous system experiencing oscillatory flow, it was found that with decreasing period, there was a greater increase in the hydraulic gradient outside of the inclusion as compared to the inside which proved to be the contributing factor towards the increase of the equivalent conductivity (k_{eq}) of the entire square region. In other words, at shorter periods, flow occurs through highly conductive pathways (or outside of the spherical inclusion leading to increased swept surface area) leading to larger channel widths for fixed b_h. The same argument can apply for our case of the channeled section at Altona by considering a circular inclusion instead of a spherical one. Therefore, heterogeneity of the channel properties can lead to changes in widths.

It is also observed that the 304-204 section showed greater widths as compared to the 204-304 section. This indicates the influence of source wells on flow channeling. Using a different source well can alter the nature of the fluid channel which in turn influences the channel width for a fixed hydraulic aperture. A hydraulic aperture of 5 mm with 304 as the source well is seen to give widths that are in line with the rough estimates of the channel width provided by experimental GPR techniques (Perll, 2011). However, when 204 is used as a source well, a hydraulic aperture of 2.5 mm is found to match the experimental observations.

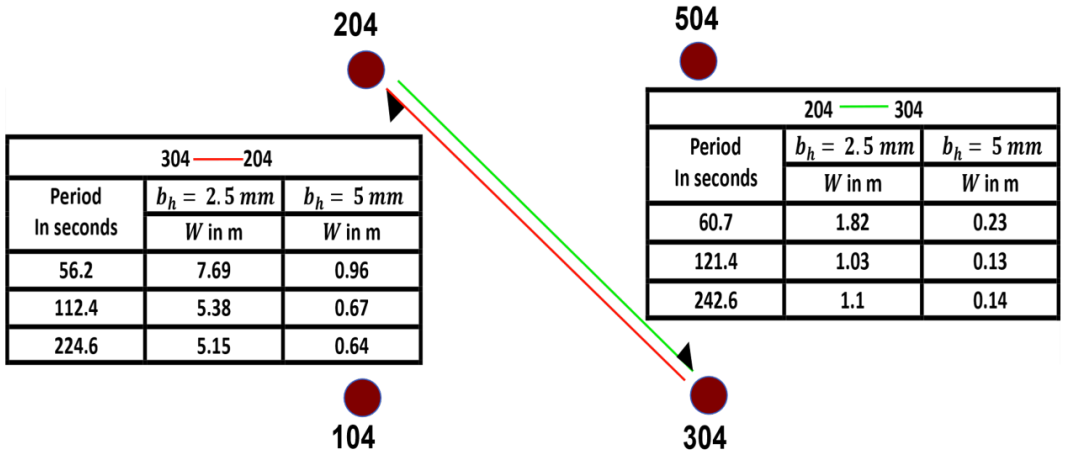

304 — 204

Period In seconds	$b_h = 2.5\ mm$	$b_h = 5\ mm$
	W in m	W in m
56.2	7.69	0.96
112.4	5.38	0.67
224.6	5.15	0.64

204 — 304

Period In seconds	$b_h = 2.5\ mm$	$b_h = 5\ mm$
	W in m	W in m
60.7	1.82	0.23
121.4	1.03	0.13
242.6	1.1	0.14

(a)

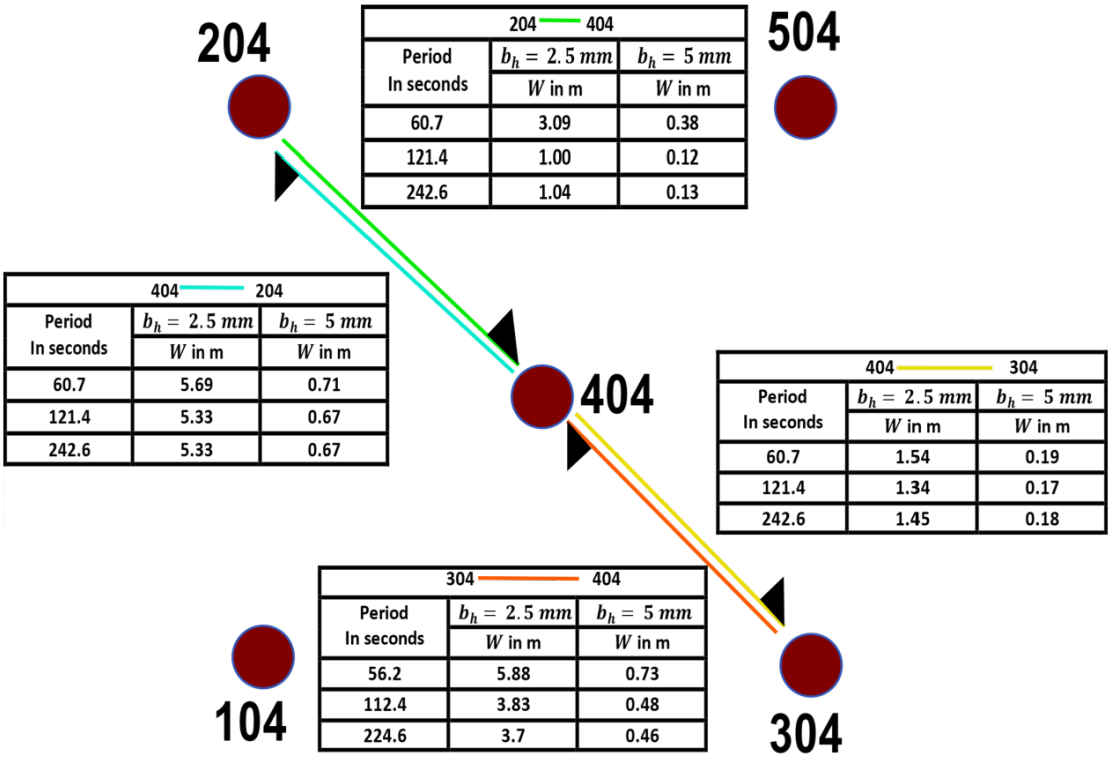

204 — 404

Period In seconds	$b_h = 2.5\ mm$	$b_h = 5\ mm$
	W in m	W in m
60.7	3.09	0.38
121.4	1.00	0.12
242.6	1.04	0.13

404 — 204

Period In seconds	$b_h = 2.5\ mm$	$b_h = 5\ mm$
	W in m	W in m
60.7	5.69	0.71
121.4	5.33	0.67
242.6	5.33	0.67

404 — 304

Period In seconds	$b_h = 2.5\ mm$	$b_h = 5\ mm$
	W in m	W in m
60.7	1.54	0.19
121.4	1.34	0.17
242.6	1.45	0.18

304 — 404

Period In seconds	$b_h = 2.5\ mm$	$b_h = 5\ mm$
	W in m	W in m
56.2	5.88	0.73
112.4	3.83	0.48
224.6	3.7	0.46

(b)

Figure 2.14: Computed Fracture Channel Width for the section between wells 204 and 304 at the Altona Field Site, NY for different frequencies and two sets of hydraulic apertures. Each periodic pumping test is represented by a distinct color. For example- The red color corresponds to the case where Well 204 is used as a source well and Well 304 is used as the monitoring well (represented as 204 - 304 in the table). The results portrayed assume the storage of the fluid to completely take place in the fracture.

Besides analyzing the widths of the different sections with varying period of oscillation, hydraulic diffusivity is computed for the channelized region between wells 204 and 304. The range of diffusivities (Figure 2.15) obtained through the multi frequency analysis confirms the fact that the periodic pumping tests are sensitive to inter well connectivity.

Using 304 as the source well yields the highest estimates of diffusivity suggesting the existence of stronger channeling effects when using 304 as the source well. It is also observed that when well 404 is used as the source well the diffusivity for the 404-204 section is higher than the 404-304 section. This reiterates the possibility of stronger channeling effects towards well 204.

It is also observed that the diffusivity reduces with increasing period of oscillation, similar to the findings reported by Guiltinan and Becker (2015) using the radial flow assumption at the field site. Mathematically this would mean that either the transmissivity is decreasing or the storativity is increasing or both are occurring at the same time with an increase in the period of oscillation. However, it is noted that in most cases the reason for the change is due to increased storativity in the fracture at higher periods.

Several researchers have attempted to rigorously investigate the consistent trend in estimates of D with period (Cardiff et al., 2013; Rennar and Messar, 2006). It is likely that for the region between wells 204 and 304, which has been observed to show no wellbore skin effects (wellbore skin refers to a zone of reduced or enhanced transmissivity around the wellbores), the interpretation of Rennar and Messar (2006) may be the most suitable to explain the trend of

decreasing D with period. They reason that the trend of a nearly constant transmissivity may be controlled by a "backbone" of conduits insensitive to period variations. The greater the period, the more is the time given for pressure equilibration, which in turn results in more conduits being used for storage that do not contribute to transport. Therefore, although S increases with period, T remains fairly constant.

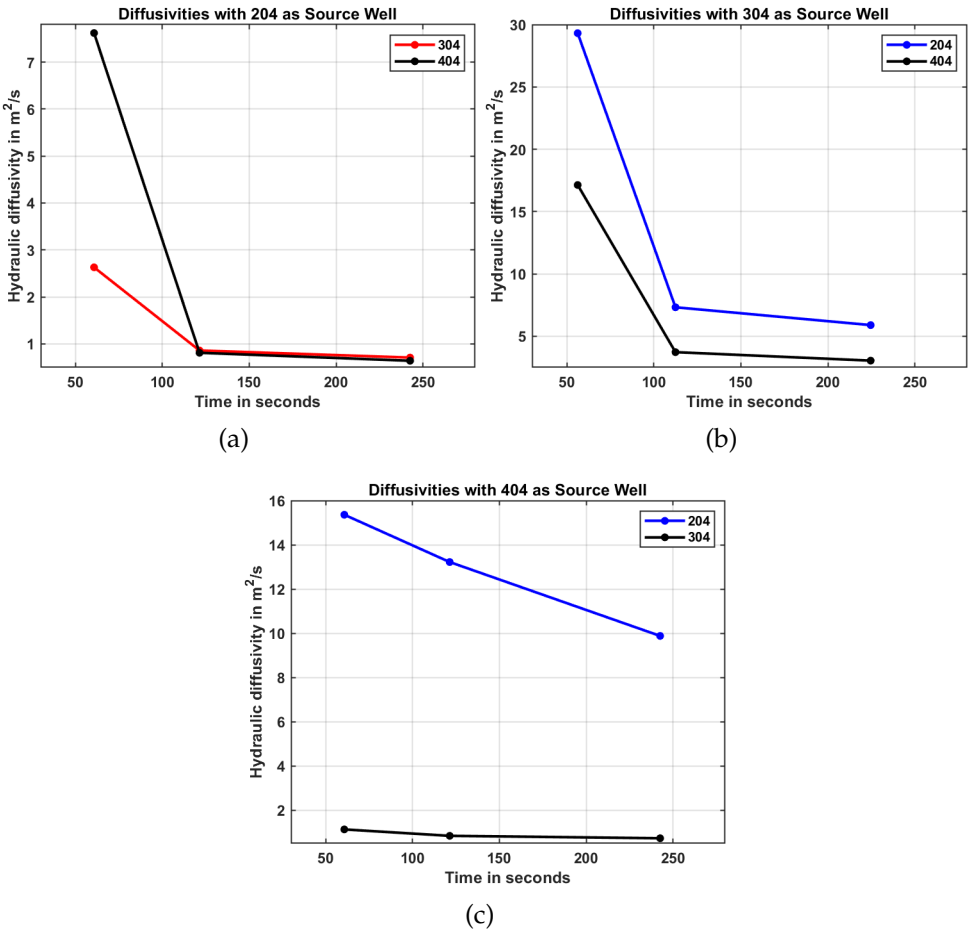

Figure 2.15: (a) Variation of Hydraulic Diffusivity with Time or Period of operation in seconds using 204 as Source Well. (b) 304 as Source Well. (c) 404 as Source Well. It is to be noted that the diffusivity values potrayed here are by assuming storage is taking place entirely in the fracture.

The diffusion length or radius of investigation is directly proportional to the

period of oscillation. Therefore, higher periods tend to probe larger distances in the fractured bedrock system as demonstrated by Rosa (1991). The average diffusion length across the periods for the 204-304 section is close to 12 m. This would mean that the distances probed through the periodic pumping tests using 204 as the source well are within the boundaries of the field site, therefore, the local heterogeneity of the field site is characterized. On the other hand, the diffusion lengths probed by the 304-204 test were much greater (average of 35.21 m) than that probed for the 204-304 section. Therefore, distances beyond the boundaries of the field site were investigated when well 304 was used as a source well.

The overall computed diffusion lengths for the periodic pumping tests at the field site ranged from 8.27 m to around 48.96 m with a total average diffusion length of 23 m. In contrast, Guiltinan and Becker (2015) reported diffusion lengths in the range of 4 m to 161 m with an average diffusion length of 61 m. The primary reason for this large difference in diffusion lengths between the two approaches is due to the assumption of radial flow in the latter rather than linear or channel flow hydraulics assumed in this study to model a section which is known to exhibit flow channeling.

Having evaluated the width of the fracture channel in the field site over different periods using two storage mechanisms, it is important to verify and evaluate the dominant storage mechanism in the system. This would aid in choosing one of the two approaches that would best describe the fractured bedrock system at the field site. Hence, S which assumes storage to entirely occur in the fracture is compared with S_{pseudo} which assumes the storage to entirely occur in the moni-

toring wellbores.

S is found to be much higher than S_{pseudo} (Figure 2.16) in most cases. This implies, storage of fluid in the fracture predominates over storage in the monitoring wells at the Altona field site. S for b_h = 2.5 mm and 5 mm is found to uniformly increase with period, however, the trend with S_{pseudo} is found to be opposite with S_{pseudo} decreasing with increasing period of oscillation.

The increase in S_{pseudo} for decreasing period of oscillation may be due to the fact that at lower periods, the rise in volume and height of the fluid in the wellbore increases leading to increased storage of fluid in the wellbores. It is also observed that S_{pseudo} for well 404 is higher than well 304 or 204 when they are used as source wells. This indicates that as the distance of fluid propagation increases, the effects of wellbore storage decreases. In other words, monitoring wells that are positioned near the source well are expected to show greater wellbore storage effects as compared to monitoring wells that are further away.

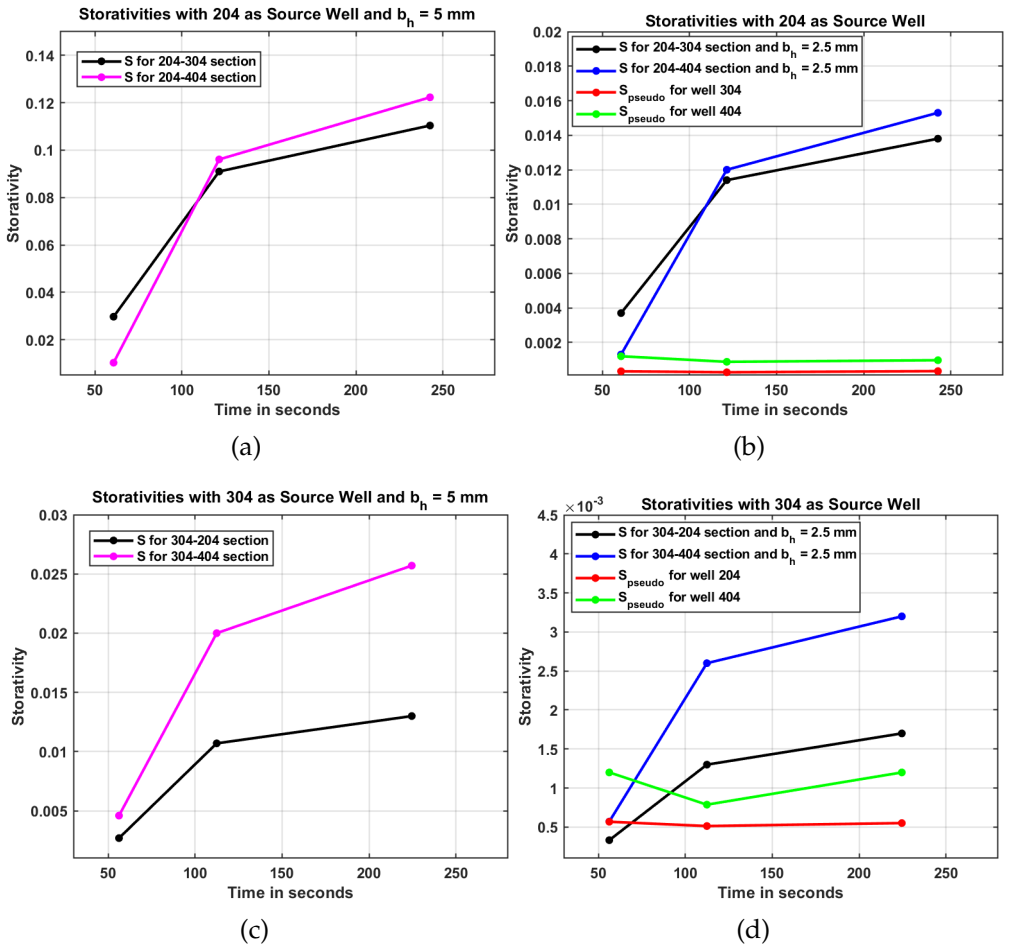

Figure 2.16: (a) Variation of Storativity with time or period of operation in seconds using well 204 as the source well and b_h = 5 mm. (b) Storativity with well 204 as the source well and b_h = 2.5 mm. S_{pseudo} for wells 304 and 404 is also computed. (c) Storativity with well 304 as the source well and b_h = 5 mm. (d) Storativity with well 304 as the source well and b_h = 2.5 mm. S_{pseudo} for wells 204 and 404 is also computed.

Since the mechanism involving fluid storage in the fracture dominates over the monitoring well storage effects, the model without well storage may be the most representative of the Altona field site. Therefore, reducing the period of testing can help reduce the diffusion length, which in turn leads to better understanding of the connectivity closer to the wellbore (Cardiff et al., 2013). Accurate predictions of channel widths between the wells can be obtained only when the

diffusion length is close to the actual distance between the wells. In hindsight, conducting the periodic pumping tests at periods that ranged between 0.5 min to 2 min could have helped predict the inter well connectivity of the field site more accurately as opposed to the 1 to 4 min periods.

Besides, while choosing the period of the signal, additional care must be taken to ensure that the amplitude attenuation and phase shift lie in the range (0,1). The period of oscillations should be determined based on preliminary diffusivity estimates of the medium. Simultaneous multi frequency tests could also help in this regard (Cardiff et al., 2013). The amplitude attenuation and phase lag should be treated independently while dealing with flow channeling by assuming storage in the fractures, unlike in radial flow models where both the phase shift and the attenuation are used together to understand the connectivity of the system. It is undesirable to have an observed signal that is highly attenuated with almost zero magnitude or a phase shift which is delayed over a cycle. If that happens, lowering the periodicity is recommended to obtain a clear observation head or pressure signal. Wellbore storage may play a significant role when the packers at the monitoring wells aren't installed accurately or functioning properly to isolate flow in specific regeions. In addition, uncertainty increases in fractured systems where the storativity is very low. Reduced period of oscillation can also increase monitoring wellbore storage effects.

Greater storage in the fracture as well as in the wellbores combined with skin effects attenuates and delays the head signal in the time space such as observed in section between the wells 104 to 504 (which weren't investigated as a part of this study). Ahn and Horne (2011) observed that as storage and skin effects

increased, the deviation from their steady state radial flow ring model also increased. Therefore, their sinusoidal model was unable to capture such trends. Although an analytical model was derived considering storage in the monitoring wells in this study, factors such as skin or well damage aren't considered in the model framework. These effects are also known to be highly localized. Besides, the combined effect of storage in the wellbores and storage in the fracture was also not considered in this study. Numerical finite element method based approaches as described by Cardiff et al. (2013), Fokker et al. (2013) and Vinci et al. (2014) might be better suited to explain such effects. Recent analytical techniques developed by Borello et al. (2019) for computing the connectivity of an EGS system in Pohang, Korea may also be well suited to explain such trends.

2.6 Conclusions

Periodic pumping tests conducted at the Altona field site, NY, for the channelized section between wells 204 and 304 are used to estimate an effective width for the channeled flow path. At first, analytical expressions were derived by considering storage of the fluid to entirely occur in the monitoring wellbores. A constrained optimization framework is then developed using data from all the monitoring wells, different directions of flow and different periods to compute the channel width for a known hydraulic aperture of the fracture. Fast Fourier transformation (FFT) analysis was performed to extract the amplitude of the head oscillations at different periods of pumping.

Analytical expressions for the steady state channeling behavior at the site considering storage of fluid to occur entirely in the fractured formation were also

derived as a part of the study to compute the width of the channel for a given hydraulic aperture. It was observed that the width of the channel decreased with increasing period of oscillation for a given hydraulic aperture of the fracture. This behavior could be due to the fact that highly conductive pathways that offer the least resistance to flow are preferred at shorter periods leading to increased width estimates. Besides, phase shifts for the section between the wells 204 and 304 were very low when compared to the amplitude attenuation in the signals indicating low skin or storage in the fracture.

In order to separate the influence of fluid storage in the fracture and the storage in the monitoring wells from the results, the effect of monitoring wellbore storage was quantitatively analyzed by expressing the fluid volume stored in the monitoring wells in a non dimensional fashion. This was then compared with fracture storativity to understand the dominant storage mechanism. It was found that storage in the fracture predominated over storage in the monitoring wells at the Altona field site suggesting the use of the former mechanism to characterize the channeling between wells 204 and 304.

The diffusion length of analysis can be changed by performing the tests at different periods. This resulted in a range of interrogated areas that were sensitive to different distances from the pumping well. Shorter periods can aid in understanding the local heterogeneity in greater detail as compared to larger periods. The period of oscillations considered for testing must be determined using preliminary diffusivity estimates to ensure distances that are well beyond the boundaries of a field site aren't investigated.

It is recommended that future periodic pumping tests at Altona be run at lower periods (0.5 - 2 mins) to understand the channeling and wellbore storage effects in greater detail. Theoretical models may also need to be developed such that the fracture opening behavior is incorporated in the modeling framework. Hence, an effective reservoir compressibility may be required as an input in the expressions. Geomechanical correlations that assess the effective stresses working on the fractures must then be developed for these tests. The combined effect of storage taking place simultaneously in both the fracture as well as the monitoring wells should be developed to help understand the inter well connectivity better.

CHAPTER 3

PERFORMANCE EVALUATIONS FOR CLOSED LOOP GEOTHERMAL SYSTEMS

3.1 Introduction and Background

The thermal energy stored in the Earth's interior to depths of 10 km is vast compared to the annual global consumption of primary energy (~ 10^8 EJ compared to ~ 600 EJ) (IEA, 2021; Rybach et al., 2000). For example, Armstead and Tester (1987) calculate that a 1°C decline in the top ten kilometers of Earth's crust corresponds to 2×10^6 EJ of thermal energy, or roughly 3300 years of global primary energy consumption at today's consumption rates. Despite these large resource estimates, the installed worldwide geothermal electricity production capacity is limited to 16 GW_e (Huttrer, 2020) and about 30 GW_{th} is used in direct-use heat systems (excluding ground-source heat pumps) (Lund and Toth, 2020).

The reason for the limited capacity primarily lies in the fact that profitable high-enthalpy geothermal systems are geographically rare. These systems are usually hot aquifers (up to 350°C) located at depths of 1 to 4 km in permeable and porous geological formations (Tester et al., 2012) where the effects of convection are significant. These systems can also be referred to as "Hydrothermal Systems" where the heat sources originate from magmatic intrusions or shear heating. Geysers and hot springs are surface manifestations of hydrothermal systems and were the first to be identified and developed. Without the rapid thermal recharge occurring in highly convective systems, one must rely on low-enthalpy, conduction-dominated geothermal systems. In these systems,

the thermal lifetime of the subsurface heat exchanger is determined mostly by two factors: heat transfer surface area and the mass flow rate.

There has recently been increased interest in researching and developing Closed-Loop Geothermal (CLG) systems, also called Advanced Geothermal Systems (AGS). Although CLG designs have been proposed for nearly a century (Hodgson.,1927), considerable attention and commercial investment has only recently been afforded to the potential for these systems. In these systems, the heat transfer fluid, e.g., water or supercritical CO_2 (sCO_2) does not flow through the rock pores and fractures but stays within the subsurface borehole system and follows a closed path from the injector to the reservoir and back to the surface through the production well. Various designs have been proposed and studied. Popular designs include a co-axial ("pipe-in-pipe") wellbore heat exchanger (Figure 3.1.a), a co-axial wellbore heat exchanger with a horizontal extension (Figure 3.1.b) and a U-loop piping configuration where one or several long horizontal heat exchangers connect the injection and production wells(Figure 3.1.c).

The main advantage of CLG is that reservoir permeability (either through matrix or fractures) or naturally–occurring reservoir fluids are not required for their operation. However, in conduction-dominated reservoirs, limited contact area between the boreholes and the host rock and slow heat transfer within the reservoir (due to low rock thermal conductivity and diffusivity to replenish heat extracted from the direct vicinity of the wellbore) may inhibit thermal performance. Some attempt to overcome this limitation by increasing the heat transfer area with the rock through multiple closed-loop heat exchangers in parallel, or

by targeting very deep and hot reservoirs, where high temperatures compensate for limited heat transfer area.

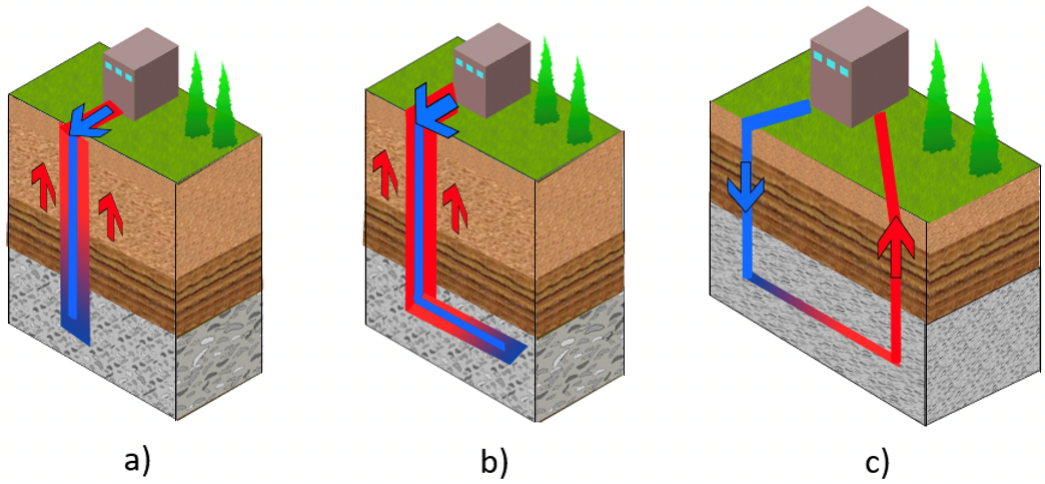

Figure 3.1: Common CLG designs with fluid color in wells representing arbitrary temperature (blue = cold; red = hot). a) Vertical co-axial or "pipe-in-pipe" system with insulation (e.g., vacuum insulated tubing) between annulus and center pipe. Diagram shows cold fluid injection in the center pipe and hot fluid production through the annulus; certain designs consider reverse flow; b) Co-axial system similar to a) but with horizontal extension; c) U-loop system with injection in one well, production through a second well through a single horizontal lateral; some designs consider multiple horizontal laterals connecting the two wells. Schematics are not to scale.

Certain designs propose developing CLG in hot and permeable sedimentary aquifers, where fluid flow–either gravity driven or forced may sufficiently replenish depleted heat surrounding the borehole. Other designs propose hybrid AGS/EGS (Enhanced Geothermal Systems) configurations, involving convective fluid flow in existing or created fractures in the rock. Some systems focus on power production and circulate the working fluid directly in the closed loop heat exchanger. AGS has also been proposed to repurpose idle or abandoned (but not plugged) geothermal, oil or gas wells and in areas where hydraulic stimulation is banned. In certain cases, idle wells in existing geothermal

fields may be unable to produce fluid due to reservoir hydraulic drawdown constraints, permit limitations, aggressive fluid chemistry or the presence of high levels of non–condensable gases. Besides, in ultra hot reservoirs the creation of a fracture network may be extremely challenging and circulation of fluids through the subsurface may lead to the accumulation of minerals in the production wells due to the solubility of such minerals in water at high temperatures. This may lead to very high disposal costs. AGS has been proposed for all such wells to deliver heat to the surface without fluid extraction from the reservoir.

Significant debate remains on feasibility and performance of CLG. Various claims have been made in literature and industry regarding their cost and output, but underlying assumptions are not always reported. In some circumstances, no clear distinction is made between heat and electricity. In others, reported performances appear to be unrealistically favorable. With various assumptions for subsurface and operating conditions, comparing designs and determining the ideal system for a certain resource is challenging.

With recent uptake in interest and investment in closed loop geothermal, a careful and independent evaluation of the technical performance of these systems is both timely and desirable. Here, the thermal performance of Co-Axial configurations is studied using a combination of numerical simulators and the Slender Body Theory (SBT). The variation of production temperatures with time is studied and the thermal output (in MW_{th}) is also evaluated. The influence of several parameters including depth, geothermal gradient, reinjection temperature, and mass flow rate for these systems are explored. In addition, the potential advantage of convective heat transfer from in–situ fluids surrounding the closed-loop

is quantitatively investigated.

3.2 Literature Review

Horne (1980) investigated design considerations for co-axial heat exchangers. The estimated heat production was found to lie in the range 5 to 60 kW_{th} for a 200 m deep well with a bottom hole temperature of 100°C and water as working fluid. Morita and Tago (1995) and Morita et al. (2005) investigated the performance of a 2 km deep co-axial AGS with bottom hole temperature on the order of 320°C and water as heat transfer fluid. They calculated heat output on the order of 1 MW_{th} and electricity production on the order of 100 kW_e assuming a 10% conversion efficiency. Bobok et al. (2007) simulated a 2 km deep co-axial well with a bottom-hole temperature of around 120°C with water as heat transfer fluid. For vacuum insulated tubing and flow rates ranging from 1 to 15 kg/s, the production temperature settled in the range of 25 to 65°C (higher temperature for lower flow rate) and the thermal power fell in the range of 200 to 350 kW_{th} (higher power for highest flow rate). Nalla et al. (2005) simulated a vertical co-axial heat exchanger of 5,600 m depth with bottom hole temperature of 350°C. They considered different flow rates, wellbore diameters, and rock types and found maximum power production of about 50 kW_e.

Riahi et al. (2017) investigated a co-axial configuration that is 2.5 km deep with a 1.1 km horizontal extension. Water was used as the heat transfer fluid with a flow rate of 60 kg/s and an injection temperature of 75°C. For a bottom-hole temperature of 240°C, heat production was on the order of 3 MW_{th}. Xu et al. (2020) modeled a vertical co-axial closed loop system of 2800 m depth with a

bottom hole temperature of 77°C, circulating water through the annulus and producing through the center pipe. Different injection temperatures, flow rates, reservoir thermal conductivity, porosity and permeability were considered, as well as both intermittent and continuous operation. Stable production temperature and heat production (excluding the initial peak following a shut-off period) were in the range of 35°C to 55°C and 300 kW_{th} to 700 kW_{th}, respectively. Porosity and permeability were found to have negligible impact on the performance.

Fox and Higgins (2016) estimate roughly 1 MW_e of power production over a 25 year lifetime using sCO_2 for a 5.5 km deep well with bottom-hole temperature of 680°C. They found that a well spacing of 75 m or more would limit the degradation due to thermal interference between the wellbores. Recently, a demonstration project at the Coso geothermal field in California was undertaken by GreenFire Energy of their co-axial ("tube-in-tube") downhole borehole heat exchanger (DBHX) system (Higgins et al., 2019; Amaya et al., 2020). The GreenFire DBHX system considers convection in the reservoir and brine flow in the well annulus. The selected well for the demonstration site had high concentrations of non-condensable gases, preventing direct power production with the brine. The DBHX system was installed down to 330 m in the well, and circulated a secondary heat transfer/working fluidwater or sCO_2 allowing to produce heat or power without the production of non-condensable gases. The local geothermal gradient is 120°C/km. Tests with water as heat transfer fluid flowing at 23-30 kg/s (Higgins et al., 2019) validated their model and indicated potential power production of up to 1.2 MW_e. A separate set of tests with sCO_2 (Amaya et al., 2020) at low flow rates, solely driven by the thermosiphon effect (1.5-5.5 kg/s), provided additional model validation and resulted in power production in the

range of 5-30 kW_e. Scherer et al. (2020) estimated that a 4 km deep closed loop system at Coso with a 4 km horizontal section using sCO_2 as the working fluid would produce close about 1 MW_e of electricity assuming thermal conduction-only in the reservoir.

3.3 Methodology

Wellbores that are entirely vertical to the target depth as well as wellbores with a horizontal section at the target depths are considered in this study. Cases are simulated to allow for the investigation of the thermal performance over a 20 year lifetime for a variety of subsurface temperatures ranging from 100 to 500°C, injection temperatures ranging from 10 to 40°C and mass flow rates ranging from 10 to 40 kg/s. In addition, different fluid types (water or sCO_2), and reservoirs with and without convection are considered.

Reservoir heat transfer simulations are carried out using three different model frameworks: (1) a hybrid numerical-analytical model using Slender-Body Theory (SBT) (Beckers et al., 2015); (2) a numerical finite element solver using the commercial COMSOL software. These models vary in ease-of-use, computational efficiency, and capabilities. COMSOL is a computationally-intensive simulator able to handle various AGS configurations and reservoir conditions, requiring more user experience. The SBT model represents an approach which provides accurate simulations in a computationally-efficient fashion. Both SBT and COMSOL are employed to simulate the co-axial AGS cases in conduction-only reservoirs. The natural convection cases are simulated with COMSOL.

3.3.1 Slender Body Theory

The SBT model is a hybrid model that discretizes the wellbore numerically but solves heat transfer between the wellbore and the rock using analytical equations based on Green's functions. The model was originally developed by Beckers et al. (2015) for transient heat transfer simulations with U-loop type heat exchangers with only heat conduction in the reservoir, and water with constant thermo-physical properties as heat transfer fluid.

The model was updated for the present work to account for pipe-in-pipe configurations, alternate working fluids and variable fluid properties as a function of pressure and temperature. The SBT model can simulate multiple, curved and thermally-interacting heat exchangers in reservoirs with conduction-only heat transfer or forced convection. The SBT model obtains fast computational times on the order of seconds as a result of (1) the use of a hybrid approach only requiring a one-dimensional discretization along the heat exchanger instead of a full three-dimensional discretization of the reservoir domain, (2) further simplification of the analytical reservoir heat transfer equations by taking advantage of the slenderness of the heat exchanger and the large spatial extent of the reservoir (e.g., in certain cases, a cylindrical source can become a line source, a point source, or can even be neglected), and (3) incorporating the fast multipole method (Greengard and Rokhlin, 1997) to combine point sources in space and time.

3.3.2 COMSOL Multiphysics

The software COMSOL Multiphysics v5.5 (COMSOL, 2019) is a commercial finite element numerical simulator and is used in this study to simulate vertical co-axial configurations in conduction dominated systems and provide validation for the SBT Model. It is also used to capture natural convection effects in the reservoir. Vertical co-axial CLG configurations are implemented using a two-dimensional axisymmetric model that solves for the coupled fluid flow and heat transport in the heat exchanger, within the rock formation, and in between. The element height (axially) is kept constant at 50 m; the element width varies radially and starts at 0.05 m close to the wellbore with a total of 2500 mesh elements. Computation time for simulations with this model is on the order of 1 to 2 minutes.

3.4 Results and Discussions

3.4.1 Overview of the simulated CLG cases

Around 14 cases were selected for simulation and most of them had fluid injection in the annulus (CXA). One co-axial case considers fluid injection in the center pipe (CXC) and one case assumes a CXA design with a horizontal extension.

All cases assume: (1) temperature at ground surface is 20°C; (2) rock thermal conductivity is uniformly 2.83 W/m.K; (3) the bulk rock density is 2875 kg/m^3;

and (4) the specific heat capacity of the bulk rock is 825 J/kg·K. For CXA and CXC, the inner radius of the center pipe is 0.0635 m (5-inch inner diameter), the thickness of the pipe is 0.0127 m (0.5 inch) and the thermal conductivity of the pipe material (assuming vacuum insulation) is 0.006 W/m·K. The well radius for the co-axial systems is 0.1143 m (9-inch diameter). The thermal influence of the casing material and the annulus-filling cement are assumed negligible. All cases assume continuous operation (i.e., with utilization factor of 100%) over a 20-year lifetime. sCO_2 instead of water is considered for a few cases and a high injection temperature of (40°C) is assumed along with a high injection pressure of (10^7 Pa) to ensure operation above the critical point of CO_2 (31°C; 74×10^5Pa). Cases with natural convection assume an isotropic porosity of 5% and pore compressibility of 7.25×10^{-12} Pa^{-1}.

For the cases with conduction-only in the reservoir, parameters such as reservoir temperature (150 to 500°C), injection temperature (10 to 40°C), flow rate (10 to 40 kg/s), and working fluid (water or sCO_2) are varied to determine their impact on thermal performance. Other parameters are kept constant in each simulation, however, others have shown they could have a significant impact on system performance. For example, bulk rock thermal conductivity ranges from roughly 1 to 7 W/m.K (Robertson, 1988); larger values tend to increase production temperatures and heat production (Xu et al., 2020; Esmaeilpour et al., 2021).

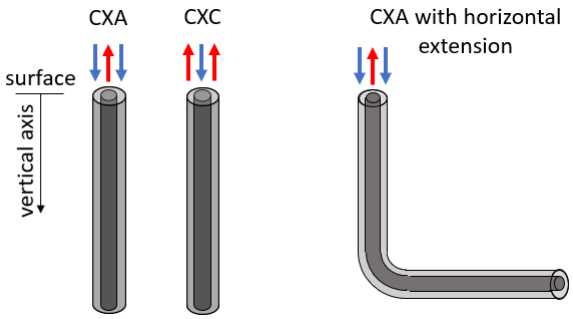

Figure 3.2: Common CLG designs with fluid color in wells representing arbitrary temperature (blue = cold; red = hot). a) Vertical co-axial or "pipe-in-pipe" system with insulation (e.g., vacuum insulated tubing) between annulus and center pipe. Diagram shows cold fluid injection in the annulus and hot fluid production through the center pipe; certain designs consider reverse flow; b) Co-axial system similar to a) but with horizontal extension; c) U-loop system with injection in one well, production through a second well, and one or multiple horizontal laterals connecting the two wells. Schematics are not to scale.

3.4.2 CLG thermal performance with heat conduction only

3.4.2.1 Base case and impact of reservoir temperature

Through the extensive literature review, a base case co-axial CLG design is considered with a 2 km vertical well and 200°C reservoir temperature, operating with water as the heat transfer fluid at an injection temperature of 20°C and flow rate of 20 kg/s. The solid blue curve in Figure 3.3 illustrates the results of production temperature and heat production over time. As observed in previous studies, production temperature and power are relatively high immediately after the start of operation, but then rapidly fall to much lower values. For this base case scenario, the average production temperature is 27°C (7°C above the injection temperature), corresponding to 0.57 MW_{th} of heat.

The solid green, red and pink curves in Figure 3.3 show the results from similar cases (2, 3 and 4) but with reservoir temperature of 150°C, 300°C and 500°C respectively.

The relationship between reservoir temperature and thermal output (production temperature and heat production) is linear. For a reservoir temperature of 150°C, the average heat production is on the order of 0.4 MW_{th} compared to 0.6 MW_{th} for 200°C, 0.9 MW_{th} for 300°C, and 1.5 MW_{th} for 500°C.

The "low-temperature" scenario with 150°C at 2 km depth (Case 2) corresponds to a medium-grade resource with geothermal gradient of 65°C/km. Scenarios with lower reservoir temperatures would result in even lower thermal performance and are not further considered in this study.

Case	AGS Type	Reservoir Temp	Reservoir Depth	Lateral Length	Inj Temp	Flow Rate	Fluid	Simulator
1	CXA	**200°C**	2 km	N/A	20°C	20 kg/s	Water	SBT/COM
2	CXA	**150°C**	2 km	N/A	20°C	20 kg/s	Water	SBT/COM
3	CXA	**300°C**	2 km	N/A	20°C	20 kg/s	Water	SBT/COM
4	CXA	**500°C**	2 km	N/A	20°C	20 kg/s	Water	SBT/COM

Table 3.1: Co-axial CLG cases simulated to investigate impact of reservoir temperature. Heat transfer within reservoir is through heat conduction only. Case 1 represents the co-axial AGS base case. The changes with respect to the base case are highlighted in bold. CXA = co-axial with injection in annulus; Inj Temp = Fluid Injection Temperature; SBT = Slender Body Theory Model; COM = COMSOL Model.

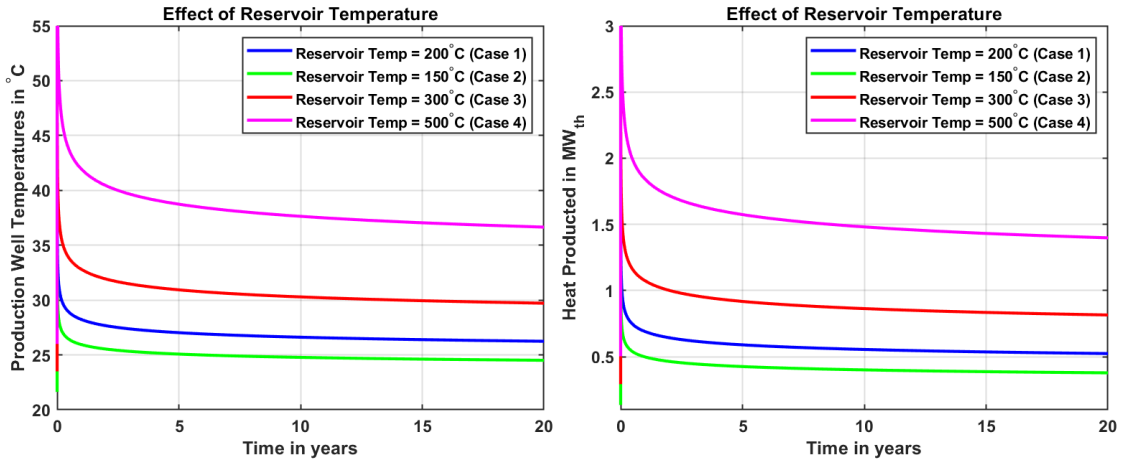

(a) (b)

Figure 3.3: (a)Co-axial CLG simulation results for production temperature (°C) and (b)Produced Heat (MW_{th}) for different reservoir temperature. Case 1 represents base case with reservoir temperature of 200°C. Cases 2 through 4 consider different reservoir temperature and depth. The base case yields long-term heat production of 0.57 MW_{th} with long-term production temperatures about 7°C above the injection temperature. All cases assume CXA configuration, reservoir depth of 2 km, and water as heat transfer fluid with flow rate of 20 kg/s and injection temperature of 20°C.

3.4.2.2 Impact of depth in coaxial systems

Higher reservoir temperatures can be obtained through deep drilling and hence the influence of depth on thermal performance is considered. The reservoir temperature is kept a constant at 200°C but the depth at which the temperature occurs (at 3 km in Case 5; at 4 km in Case 6) is varied. An approximate linear increase of long-term heat production with depth is assumed. For a 3 km deep co-axial CLG system (Case 5), the heat production increases to 0.85 MW_{th}; for a 4 km deep system (Case 6), the long-term heat production is 1.1 MW_{th}. Although the reservoir temperature is the same in these cases, increasing the heat exchanger area results in an increase in production temperature and heat production.

Case	AGS Type	Reservoir Temp	Reservoir Depth	Lateral Length	Inj Temp	Flow Rate	Fluid	Simulator
1	CXA	200°C	**2 km**	N/A	20°C	20 kg/s	Water	SBT/COM
5	CXA	200°C	**3 km**	N/A	20°C	20 kg/s	Water	SBT/COM
6	CXA	200°C	**4 km**	N/A	20°C	20 kg/s	Water	SBT/COM

Table 3.2: Co-axial AGS cases simulated to investigate impact of reservoir depth.

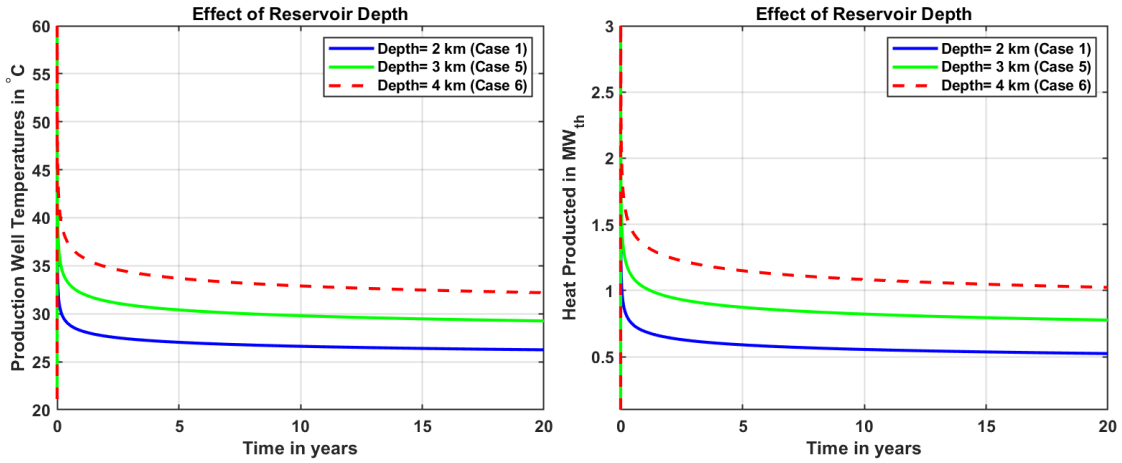

(a) (b)

Figure 3.4: (a)Co-axial CLG simulation results for production temperature (°C) and (b)Produced Heat (MW_{th}) for different reservoir depth. Case 1 represents base case with reservoir temperature of 200°C. Cases 5 through 6 consider different reservoir depth. All cases assume CXA configuration, reservoir temperature of 200°C, and water as heat transfer fluid with flow rate of 20 kg/s and injection temperature of 20°C.

3.4.2.3 Impact of injection temperature in co-axial systems

While 3.4.2.1 and 3.4.2.2 investigated the influence of reservoir conditions, operational considerations for co-axial systems are studied henceforth including injection temperature, flow rate and fluid type. Cases 7 and 8 have the same parameters as Case 1 but have injection temperatures of 10°C and 40°C rather than 20°C. Figure 3.5 (a) illustrates that a lower injection temperature results

in lower production temperatures but larger temperature gains (i.e., difference between injection and production temperature). The relationship between injection temperature and heat production is approximately linear: a decrease in injection temperature results in a linear increase in heat production. Injection temperatures are dependent on the surface application. For example, electricity generation typically results in a relatively high injection temperature while a heat pump can achieve a relatively low injection temperature.

Case	AGS Type	Reservoir Temp	Reservoir Depth	Lateral Length	Inj Temp	Flow Rate	Fluid	Simulator
1	CXA	200°C	2 km	N/A	**20°C**	20 kg/s	Water	SBT/COM
7	CXA	200°C	2 km	N/A	**10°C**	20 kg/s	Water	SBT/COM
8	CXA	200°C	2 km	N/A	**40°C**	20 kg/s	Water	SBT/COM

Table 3.3: Co-axial CLG cases simulated to investigate impact of injection temperature.

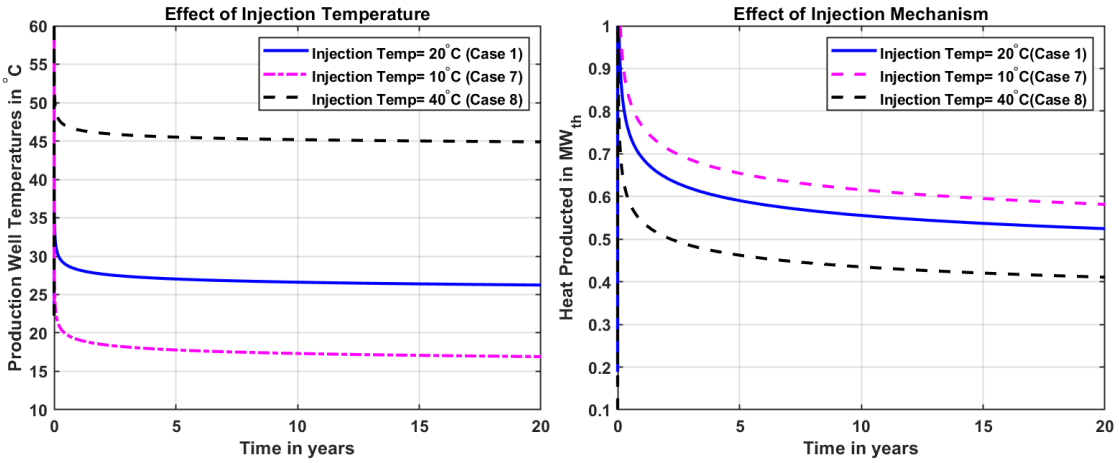

(a) (b)

Figure 3.5: (a)Co-axial CLG simulation results for production temperature (°C) and (b)Produced Heat (MW_{th}) for different injection temperature. Case 1 represents base case with injection temperature of 20°C. Case 7 and 8 consider injection temperature of 10°C and 40°C, respectively. Injection temperature has moderate impact on thermal performance with lower injection temperature resulting in lower production temperature but higher heat output. All cases assume CXA configuration, reservoir temperature of 200°C at 2 km depth, and water as heat transfer fluid with flow rate of 20 kg/s.

3.4.2.4 Impact of flow rate in co-axial systems

To assess the impact of mass flow rate, the base case (Case 1) is considered and compared with Cases 9 and 10 which have a mass flow rate of 10 and 40 kg/s respectively rather than 20 kg/s.

Amongst the model results, a lower flow rate (Case 9) results in a higher production temperature but a slightly lower heat output. Keeping everything else a constant, varying the flow rate allows to reach the target temperature as required for a certain surface application. However, operating at very low flow rates also results in low levels of heat production. For example, additional COMSOL simulations show that operating at 1 kg/s results in average production temperatures of around 100°C, but average heat production of only 0.23 MW_{th}. In comparison, the base case (Case 1; flow rate of 20 kg/s) results in average production temperatures of 27°C but average heat production of 0.57 MW_{th}.

Case	AGS Type	Reservoir Temp	Reservoir Depth	Lateral Length	Inj Temp	Flow Rate	Fluid	Simulator
1	CXA	200°C	2 km	N/A	20°C	**20 kg/s**	Water	SBT/COM
9	CXA	200°C	2 km	N/A	20°C	**10 kg/s**	Water	SBT/COM
10	CXA	200°C	2 km	N/A	20°C	**40 kg/s**	Water	SBT/COM

Table 3.4: Co-axial CLG cases simulated to investigate impact of injection temperature.

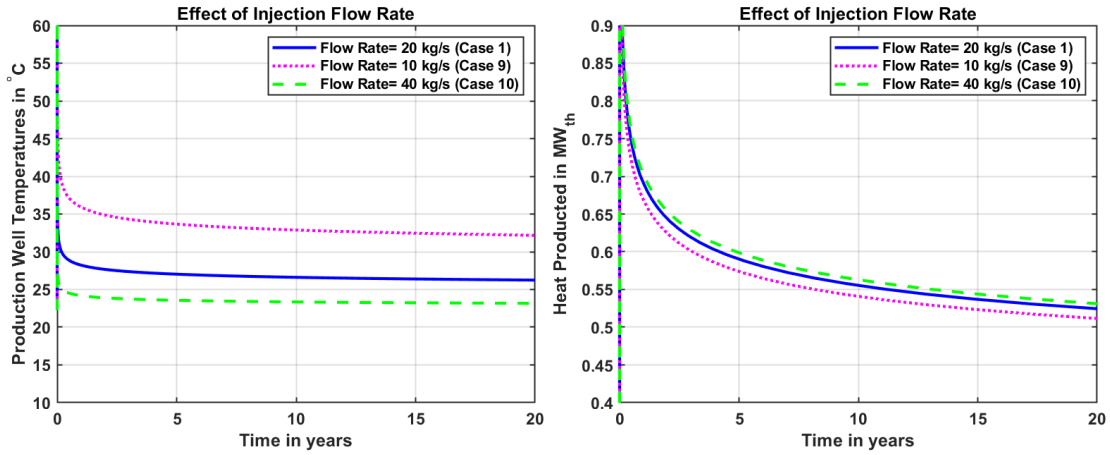

(a) (b)

Figure 3.6: (a)Co-axial CLG simulation results for production temperature (°C) and (b)Produced Heat (MW_{th}) for different injection mass flow rate. Case 1 represents base case with injection temperature of 20°C. Case 7 and 8 consider injection temperature of 10°C and 40°C, respectively. Injection temperature has moderate impact on thermal performance with lower injection temperature resulting in lower production temperature but higher heat output. All cases assume CXA configuration, reservoir temperature of 200°C at 2 km depth, and water as heat transfer fluid with an injection temperature of 20°C.

3.4.2.5 Impact of heat transfer fluid type in co-axial systems

Case 11 uses sCO_2 instead of water as heat transfer working fluid for the co-axial configuration resulting in an average production temperature of 42.3°C and an average heat production of 0.27 MW_{th}. The injection temperature and pressure are set at 40°C and 107 Pa respectively, to ensure CO_2 remains in the supercritical phase. In comparison, the equivalent case with water (Case 8) results in an average production temperature of 45.3°C and an average heat production of 0.45 MW_{th}. Hence, keeping everything else the same, utilizing sCO_2 instead of water results in 40% lower enthalpy gain. However, due to the thermosiphon effect, no pumping power is required when utilizing sCO_2 while the average

pumping power with water (Case 8) is 9.5 kW_e.

Case	AGS Type	Reservoir Temp	Reservoir Depth	Lateral Length	Inj Temp	Flow Rate	Fluid	Simulator
8	CXA	200°C	2 km	N/A	40°C	20 kg/s	**Water**	SBT/COM
11	CXA	200°C	2 km	N/A	40°C	20 kg/s	**sCO_2**	SBT/COM

Table 3.5: Co-axial CLG cases simulated to investigate impact of utilizing sCO_2 as heat transfer fluid instead of water.

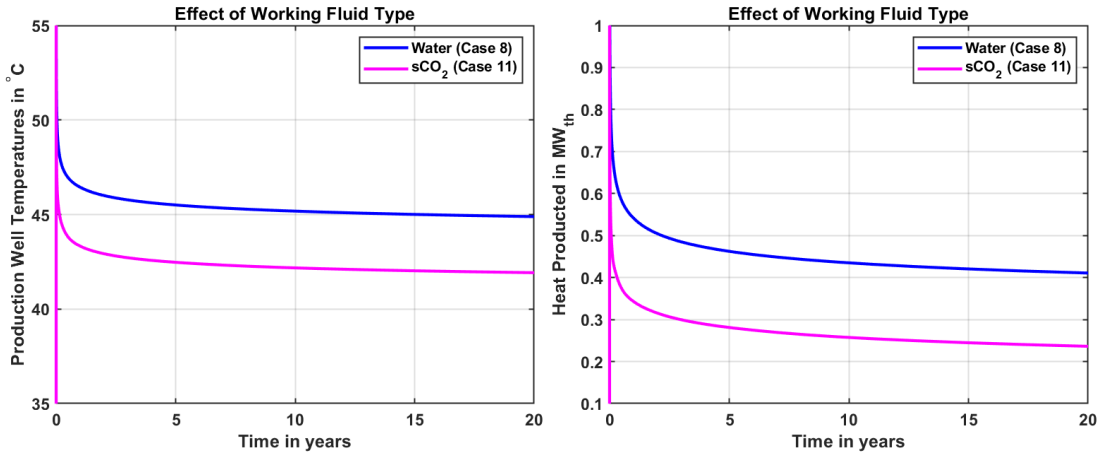

(a) (b)

Figure 3.7: (a)Co-axial CLG simulation results for production temperature (°C) and (b)produced enthalpy (MW_{th}) when using sCO_2 (Case 11) in comparison with the base case of 40°C injection temperature (Case 8). With all other conditions identical, utilizing sCO_2 instead of water results in 40% lower enthalpy gain. However, no pumping power is required with sCO_2 as heat transfer fluid (Case 11), while, when utilizing water (Case 8), average pumping power is 9.5 kW_e. All cases assume CXA configuration, reservoir temperature of 200°C at 2 km depth, fluid flow rate of 20 kg/s and fluid injection temperature of 40°C.

3.4.2.6 Impact of injection in annulus (CXA) vs. in center pipe (CXC)

Design choices in co-axial systems are considered and the effect of injection in the center pipe (CXC) versus in the annulus (CXA) as in our other co-axial sim-

ulations is studied. For the set of reservoir and operating conditions used in the co-axial base case (Case 1), it is seen that there is very little difference between CXA versus CXC which is in line with the conclusions drawn by Holmberg et al., (2016), with injection in the annulus (CXA) performing just slightly better than injection in the center pipe. However, it is possible that this finding may not apply for other geometries or reservoir and operating conditions (Fox et al., 2016).

Case	AGS Type	Reservoir Temp	Reservoir Depth	Lateral Length	Inj Temp	Flow Rate	Fluid	Simulator
1	**CXA**	200°C	2 km	N/A	20°C	20 kg/s	Water	SBT/COM
12	**CXC**	200°C	2 km	N/A	20°C	20 kg/s	Water	SBT/COM

Table 3.6: Co-axial CLG cases simulated to investigate impact of injection in the center pipe rather than the annulus.

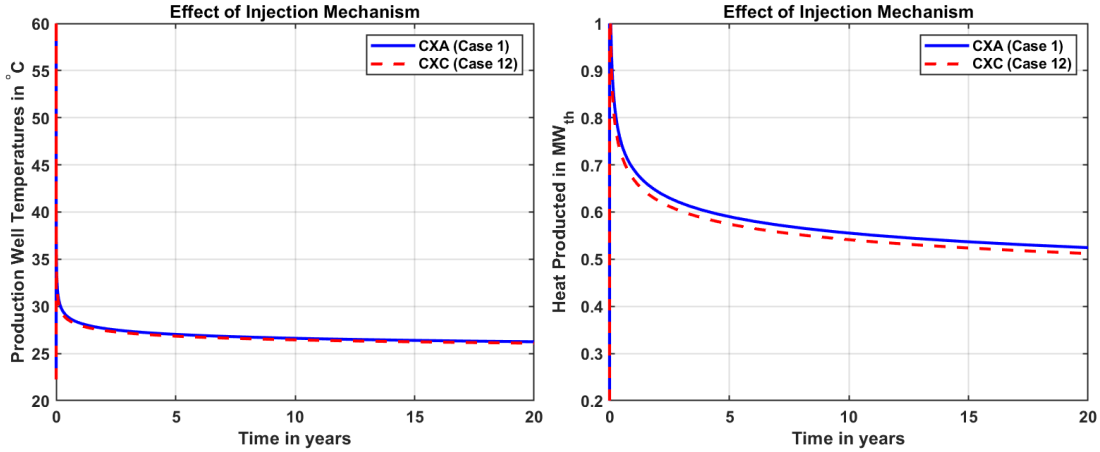

(a) (b)

Figure 3.8: (a)Co-axial CLG simulation results for production temperature (°C) and (b)produced enthalpy (MW_{th}) for injection in center pipe (CXC) vs. injection in the annulus (CXA), which is the base case (Case 1). The impact is negligible with a slightly higher performance of the CXA configuration. All cases assume reservoir temperature of 200°C at 2 km depth, and water as heat transfer fluid with flow rate of 20 kg/s and injection temperature of 20°C.

3.4.2.7 Impact of horizontal extension in co-axial systems

The influence of including a horizontal extension at the base of a co-axial system is studied. This type of design has been proposed as a way to increase the heat exchange area where formation temperatures are greatest. Comparing to the base case (Case 1), Case 13 simulates the effects of including a 2 km horizontal extension at 2 km depth.

The results illustrate that the horizontal extension increases the average production temperature from 27 to 40°C, and average heat production from ~0.6 MW_{th} to ~1.7 MW_{th}. Increasing the heat exchanger length within the reservoir significantly increases the surface area and boosts the system thermal performance.

Case	AGS Type	Reservoir Temp	Reservoir Depth	Lateral Length	Inj Temp	Flow Rate	Fluid	Simulator
1	CXA	200°C	2 km	**N/A**	20°C	20 kg/s	Water	SBT/COM
13	CXA	200°C	2 km	**2 km**	20°C	20 kg/s	Water	SBT

Table 3.7: Co-axial CLG cases simulated to investigate impact of a horizontal extension.

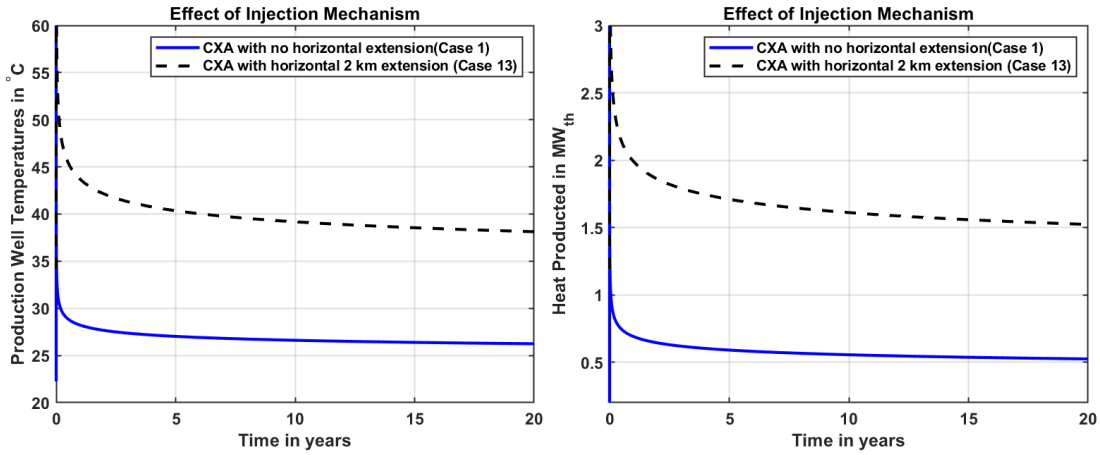

(a) (b)

Figure 3.9: (a)Co-axial CLG simulation results for production temperature (°C) and (b)produced heat (MW_{th}) when adding a 2 km long horizontal extension (Case 13) in comparison with the base case (Case 1). Increasing the subsurface heat exchanger length (and area) significantly increases the production temperature and heat output. All cases assume CXA configuration, reservoir temperature of 200°C at 2 km depth, and water as heat transfer fluid with flow rate of 20 kg/s and injection temperature of 20°C.

3.4.3 CLG Thermal Performance with natural convection in the reservoir

The impact of natural convection within the reservoir on the thermal performance of co-axial CLG is investigated through two cases 14 and 15 with different permeabilities. COMSOL is used for simulations to solve for the fluid flow and heat transport in both the pipe and formation. Due to convergence issues with the CXA configuration the CXC scenario is analyzed (injection in the center pipe and return flow in the annulus). Case 15 assumes a permeability of 10^{-15} m^2 (~1 mD), which represents a typical in-situ permeability in the continental crust at a depth of 2 km (Ingebritsen and Manning, 2010). Simulation results indicate that with a permeability of 10^{-15} m^2, (Case 15), average thermal out-

put increases by about 20% in comparison with the conduction-only scenario. The thermal output for Case 14 with very low permeability of 10^{-18} m^2 overlaps with the conduction-only case (Case 12). Even at moderate depths of 2 to 4 km, a low permeability of 10^{-18} m^2 is not uncommon, e.g., in granite or shale formations. This suggests that the conduction-only cases are representative in many scenarios.

Case	AGS Type	Reservoir Temp	Reservoir Depth	Lateral Length	Inj Temp	Flow Rate	Fluid	Reservoir Permeability	Simulator
12	CXC	200°C	2 km	N/A	20°C	20 kg/s	Water	**Conduction Only**	SBT/COM
14	CXC	200°C	2 km	N/A	20°C	20 kg/s	Water	**10^{-18} m^2**	COM
15	CXC	200°C	2 km	N/A	20°C	20 kg/s	Water	**10^{-15} m^2**	COM

Table 3.8: Co-axial CLG cases simulated with natural convection in the reservoir.

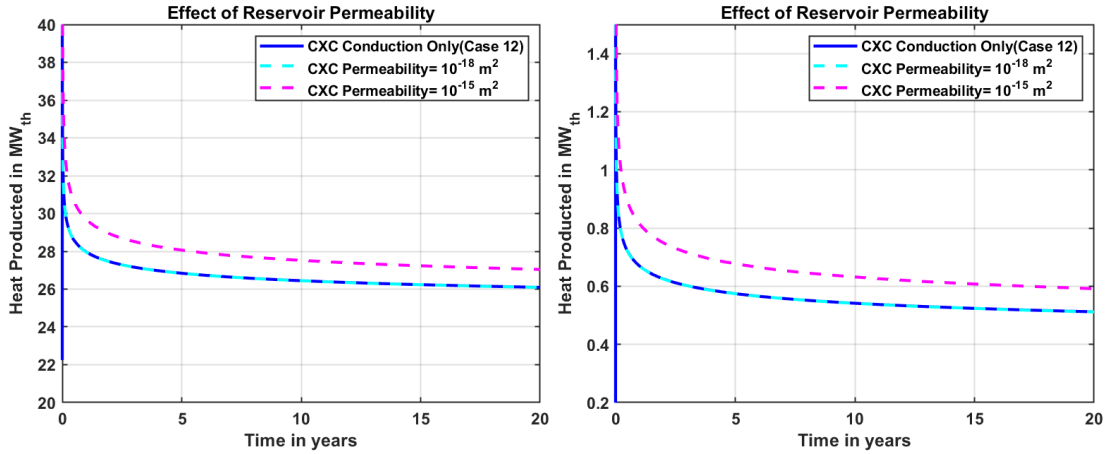

(a) (b)

Figure 3.10: (a)Simulation results of co-axial CLG production temperature with natural convection in the reservoir versus heat conduction-only (b)produced heat (MW_{th}) versus time. A typical reservoir permeability of ~1 mD results in 20% increase in heat production with respect to the heat conduction-only scenario. All cases assume a CXC configuration with reservoir temperature of 200°C at 2 km depth, and water as heat transfer fluid with flow rate of 20 kg/s and injection temperature of 20°C.

3.5 Conclusions

The analysis provides a systematic evaluation of the technical performance of co-axial CLG systems for heat production over a 20 year period. By considering a range of different CLG designs and geometries, reservoir characteristics, operating conditions, the results provide insight into the influence of these parameters and can help guide development decisions.

Based on the simulations, for reservoir temperatures ranging between 150 and 300°C at a 2km depth (which corresponds to relatively high average geothermal gradients, from 65 to 140°C/km), thermal outputs are expected to be in the range of 0.4 to 0.9 MW_{th} for the 2 km vertical co-axial system.

Heat extraction rates from closed loop systems in conduction-dominated reservoirs are limited because of two underlying reasons: 1) the inherently low thermal conductivity (~1–5 W/m·K) and diffusivity of the rock (~10^{-6} m^2/s of rock), which controls the heat flux through the rock zone surrounding the wellbore, and 2) the restricted contact area in between the fluid and the rock mass as a result of confining the fluid in sealed wells. Larger thermal outputs are obtainable with higher reservoir temperatures, or through more well contact area with the rock, e.g., with a long horizontal extension for a co-axial system (Figure 3.2 (b)). Natural or forced convection increases output but requires relatively high reservoir permeability to have a considerable impact. For in-situ reservoir permeability of $10^{-15}m^2$ (~1 mD), a common natural permeability found at depths of 2 to 4 km, there is only a moderate increase in thermal output (Figures 3.10 (a) and (b)).

For all the cases considered in this study, the thermal output and production temperature results reveal a characteristic behavior of reaching a peak during the first few hours of operation, but then quickly dropping and converging to a much lower long-term steady value. With initial rock temperatures ranging from 150 to 300°C and fluid mass flow rates ranging from 10 to 40 kg/s, production temperatures for most cases decline to values of 20 to 60°C after a few hours, which are suitable for some direct-use applications and, if necessary, could be boosted to higher utilization temperatures with heat pumps. Under the conditions considered, production temperatures are too low to efficiently produce electricity with a heat-to-power conversion cycle. Production temperatures can be increased when operating at very low flow rates, in very hot rock reservoirs, or in systems with extensive total lengths of the heat exchangers in the reservoir.

Future work can focus on simulating Co-Axial Systems with a horizontal extension using a series of 2-D sections wherein, the finite element method could be applied along with finite difference method being employed within each section. In this way the 3-D mesh that is required to simulate the geometry can be reduced to a computationally less expensive 2-D simulation with convection in the reservoir being captured as well.

CHAPTER 4

COMPARATIVE ANALYSIS BETWEEN CLOSED LOOP AND ENHANCED GEOTHERMAL SYSTEMS

4.1 Introduction and Background

The large majority of geothermal systems today produce heat from hydrothermal resources, where in-situ hot water in permeable reservoirs is delivered to the surface using production wells. The produced fluid generally gets reinjected into the reservoir, to discard the brine and sustain reservoir pressures. High-grade hydrothermal reservoirs tend to occur in limited areas in the world, often in tectonically or volcanically active regions, e.g., in Iceland, New Zealand, the Geysers in California, and Matsukawa field in Japan.

To expand geothermal development to other areas and make it globally accessible, significant research and development is ongoing in developing technologies to tap into the stored heat in hot but often dry and low-permeable rocks, also called Hot Dry Rock (HDR). One technology that shows promise in this domain is Enhanced or Engineered Geothermal Systems (EGS).

The standard EGS approach is to generate pathways in the rock by creating new or opening pre-existing fractures using hydraulic, chemical and thermal stimulation techniques. This allows injected water (or another heat transfer fluid) to absorb heat from the rock by flowing through the fractures before flowing back to the surface through production wells. In case the natural rock permeability is sufficiently high, but no or insufficient in-situ water is present, techniques simi-

lar to waterflooding or steam drive as used for oil recovery applications can be employed (Tester and Smith, 1977; Bodvarsson and Hanson, 1977).

Over the last 45 years, EGS technology has been tested, demonstrated, and applied in about two dozen projects, ranging from improving individual well performance to developing entire greenfields (Tester et al., 2006; Breede et al., 2013; Olasolo et al., 2016; Lu, 2018). Project results were mixed: in some cases, a fracture network was successfully established, reservoir permeability increased significantly and commercial flow rates could be obtained; in other cases, the improvement in well injectivity or productivity was insufficient, attainable flow rates were too low, or induced seismicity was too high.

The world's first EGS site was developed in the 1970's-1990's at the Fenton Hill site in New Mexico (Cummings and Morris, 1979; Tester et al., 1989), demonstrating creating a fracture network using hydraulic stimulation in the granite basement at about 3.5 km depth and circulating water for small-scale power production. At the Habanero (Cooper Basin) EGS project in Australia, six wells were drilled in ~250°C granite basement at about 4 km depth and multiple hydraulic stimulation campaigns were undertaken (Hogarth and Heinz-Gerd, 2017). Two multi-month closed-loop circulation tests with flow rates up to about 20 kg/s and production temperatures up to about 215°C were successfully conducted, with about 1 MW_e of electricity production with a pilot power plant during the second test. Although technically successful, the project did not meet economic criteria and was abandoned.

The first EGS project on a commercial-scale started generating electricity in 2016

at Soultz-Sous-Foret in France (Mouchot et al., 2018). The project started in 1987 and created a fracture network in the granite basement at about 5 km depth. Water at 150°C is produced at 30 kg/s, driving a 1.7 MW_e net binary cycle power plant. Other successful examples include at Rittershoffen, France, where hydraulic stimulation (in combination with thermal and chemical stimulation) created a 24 MW_{th} EGS reservoir for an industrial direct-use application, and at Desert Peak, Nevada where the injectivity of a poorly-performing injection well increased 175-fold after hydraulic stimulation.

At other sites, the results were less successful. For example, at Newberry, Oregon, the created reservoir using hydraulic stimulation was relatively small in volume, and at Brady Hot Springs, Nevada, hydraulic stimulation of a poorly-performing injection well did not result in a significant increase of injectivity. In a few cases, induced seismicity caused damage to surface infrastructure (e.g., Basel, Switzerland and Pohang, South-Korea) and led to suspension or termination of the project.

To avoid the technical challenges and risks associated with EGS development, interest in researching and developing Closed Loop Geothermal Systems (CLG) has increased. Over the last several decades, a number of studies have been conducted to analyze the performance of EGS and CLG separately (Horne 1980; Higgins et al., 2019; Malek et al., 2021; Van Oort et al., 2021; Okoroafor et al., 2021; Murphy et al., 1981; Fox et al., 2016).

To the best of our knowledge there has been no published work in literature that provides a comparative analysis between discretely fractured EGS, closed

loop systems and traditional hydrothermal systems for extracting heat.

4.2 Methodology

The U-Loop CLG configuration with a number of horizontal sections was considered for the comparison with an EGS reservoir containing a set of uniform, equal sized and spaced, non thermally interacting fractures. In addition, the CLG and EGS cases were compared with a reference case of a conventional hydrothermal system. All simulations were conducted for continuous operation of these systems over a 20-year lifetime and assuming water to be the working fluid.

The mass flow rate was kept a constant at 40 kg/s for the analysis. The cases assume constant rock temperatures that are representative of the basement rock conditions at Ithaca, New York. The reservoir block is at a depth of around 3.5 km beneath the ground surface (Tester et al., 2020). The thermal conductivity of the rock is 2.83 W/m.K (uniform throughout), the bulk density of the rock is 2875 kg/m^3 and the specific heat capacity of the rock is 825 J/kg.K (Gustafson et al., 2019).

The initial reservoir temperature was assumed to be 100°C at the considered depth. The specified dimensions of the reservoir block were 1000 m×1000 m×250 m ($H \times W \times H$) embedded with equally spaced, uniformly sized fractures as depicted in Figure 4.1.

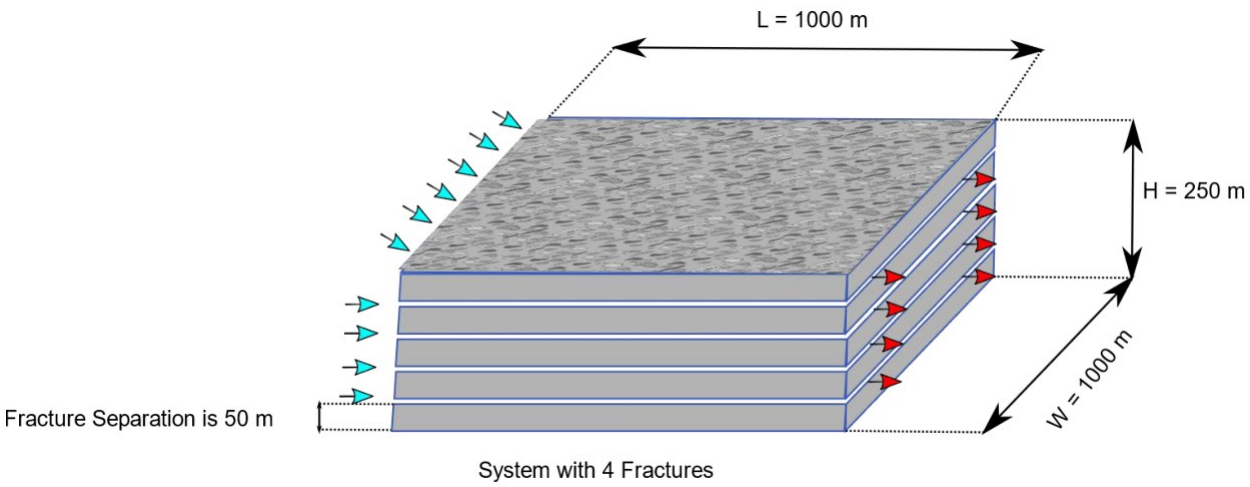

Figure 4.1: Schematic of the reservoir in the Precambrian basement. 4 horizontal fractures are considered in this domain with cold fluids entering represented by the blue arrows. The fluids exiting the reservoir are represented by the red arrows.

The flow in each fracture was assumed to be identical. Therefore, the mass flow rate in each fracture can be expressed as $m_f = m_t/n$. Where, m_f refers to the mass flow rate in each fracture, m_t refers to the total mass flow rate and n refers to the number of fractures in the reservoir considered. The injection and production wells are assumed to be completely insulated for simplicity for both the EGS and CLG setups and the injection temperature was kept a constant for all the cases studied (25°C).

The diameter of each horizontal section or loop is held a constant at 0.25m or 9.84 inches. It is however important to note that complete insulation of deep vertical wells is difficult to achieve and can be capital intensive. Therefore, in order to design commercial systems it may be beneficial to insulate the production well alone so that the temperature gain in the subsurface through the fractures/loops are preserved.

Four different model frameworks are used to study the effect of number of lateral sections and number of fractures, namely : (1) An analytical solution for wellbore heat transmission (Ramey, 1962); (2) A hybrid numerical-analytical model using Slender Body Theory (SBT); (3) An analytical parallel fracture model (Murphy et al., 1981) and (4) An analytical model to describe thermal performance of an interconnected Discrete Fracture Network (DFN) (Fox et al., 2016). The first and second models are employed in the simulation of U-Loop configurations. The third and fourth models are used for idealized EGS reservoirs with multiple, uniform parallel fractures or interconnections with constant aperture each with uniform one-dimensional flow from inlet to outlet.

Conduction in the direction of fluid flow in both the fracture and the rock formation is neglected. Heat transfer hence occurs only by conduction in the rock in the direction perpendicular to the flow of the fluid and through forced convection along the flow direction in the fracture. These assumptions are reasonable since the magnitude of heat conduction in the direction of flow is several orders of magnitude less than in the perpendicular direction (Fox Dissertation, 2015).

Thermal interference between neighboring fractures/horizontal sections may occur when the thermal penetration length is less than the spacing between them. The thermal penetration length (L_t) can be derived from scaling analysis of the one dimensional heat conduction equation as $L_t = \sqrt{\alpha_r t}$. Where α_r is the thermal diffusivity of the reservoir and t refers to the time period of operation of the reservoir.

For a discretely fractured reservoir operating for 20 years, L_t is around 27 m

and hence to ensure that the fractures are not thermally interacting with each other, a spacing much greater than 27 m is chosen for the simulations i.e. 50 m.

To simulate commercial hydrothermal systems which typically produce fluids at mass flow rates ranging from 30-70 kg/s with very minimal drawdown over a period of 20 years, a simplified linear temperature drawdown of 0.4 °C/year is considered (Snyder et al., 2017).

4.3 Results and Discussions

The thermal performance of idealized fractured EGS reservoirs are compared with a number of CLG and configurations. The performance of the EGS and CLG cases were also compared with a reference commercial hydrothermal system. Because of its importance, the effect of flow rate and contact area of the fluid with the subsurface is explored in detail for both EGS and CLG considering the reservoir block shown in Figure 4.1.

The number of horizontal sections required to equal production from the 4 fractured system is computed. The combined effect of lateral section length and number of laterals is also studied extensively through simulations. Finally, the thermal performance of Discrete Fracture Network (DFN) configurations are also studied and compared with CLG systems.

4.3.1 Effect of Surface Area

For ensuring sustained and acceptable rates of heat extraction from the geothermal system, it is necessary that sufficient heat transfer contact area is established in the subsurface. For CLG systems this can be achieved through drilling multiple horizontal sections at depth. For fractured EGS reservoirs sufficient heat transfer surface area is created using a set of large, non-thermally interacting fractures that were created by stimulation of impermeable rock or by reopening pre existing fractures. As a starting point the thermal performance of a single loop/fracture system was simulated and compared with the reference hydrothermal system.

It is seen that for a single horizontal section that spans about 1 km in length within the reservoir block shown in Figure 4.1, the production well temperatures quickly drop from a peak during the initial few hours of operation to a steady state value which is only around 3-4°C higher than the injection temperature. Better thermal performance can be achieved by reducing the flow rate from 40 kg/s to 10 kg/s through the lateral extension for CLG. However, a reduced flow rate may not necessarily imply a better power output since thermal power depends on both mass flow rate and the temperature difference between the injection and production wells. The production temperature for the single fracture case in the rock initially at 100°C after a period of 20 years was about 71°C which is 46°C higher than the injection temperature of 25°C.

The variation of performance between CLG and EGS primarily lies in the difference in heat transfer contact area of the fluid with the rock. In the case of CLG, the area is equivalent to 785 m^2 (curved surface area of a cylinder) and for the

considered hypothetical EGS case, the area is 1,000,000 m^2. Therefore, it is noted that the contact area of EGS is over 1200 times larger than that of a single loop CLG.

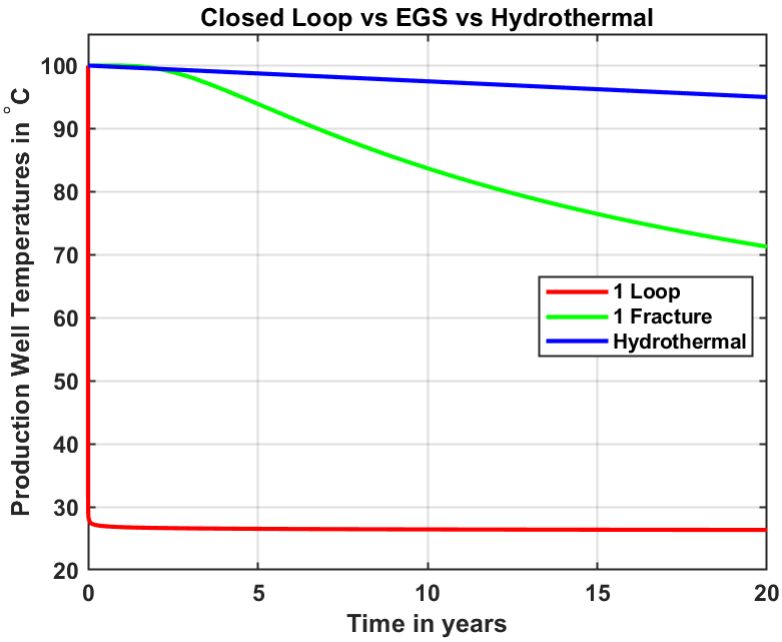

Figure 4.2: Simulated production temperatures over a 20 year period for CLG, EGS and Hydrothermal systems for an initial rock temperature of 100°C. The fluid injection temperature is 25°C and the flow rate is 40 kg/s. In the case of EGS, the fluid is assumed to flow through the entire surface of the fracture of length 1000 m and width 1000 m. For CLG, the lateral section diameter is 0.25 m and the length is 1000 m. A linear temperature decline of 0.4°C/yr is assumed for the Hydrothermal system. It can clearly be seen that to match the performance of EGS, CLG would require multiple horizontal sections to maximize contact area with the rock.

The number of horizontal sections that can be fitted in the considered volume without thermal interaction between the loops is around 80 (20×4). The thermal performance of this configuration is compared with a single fracture system and a 4 fracture system. A hypothetical 80 loop system was needed to show good thermal performance with a production temperature of close to 83°C after a period of 20 years as shown in Figure 4.3. However, when a system with 4 fractures was considered, there is almost no drawdown after a period of 20

years as seen in Figure 4.3 (b).

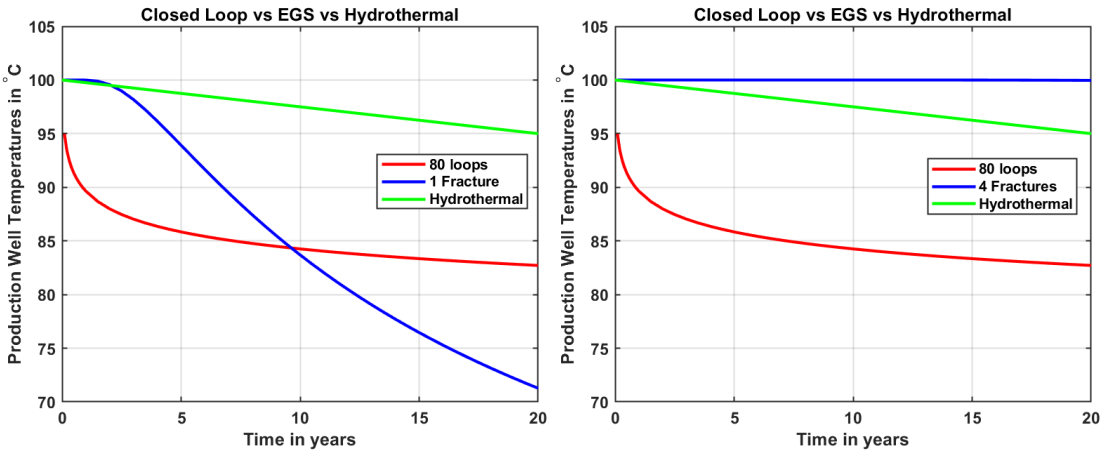

(a) (b)

Figure 4.3: (a) Simulated production temperatures for a CLG with 80 loops, a single fracture system and a Hydrothermal System over a 20 year period. (b) Simulated production temperatures for a CLG with 80 loops, a 4 fracture system and a Hydrothermal System over a period of 20 years. The initial reservoir temperature is 100°C. The fluid injection temperature is 25°C and the total mass flow rate is 40 kg/s. It is assumed that the mass flow rate is equally split into the fractures/loops. In the case of EGS, the fluid is assumed to flow through the entire surface of the fracture of length 1000 m and width 1000 m. For each loop of CLG, the diameter is 0.25 m and the length is 1000 m. A linear temperature decline of 0.4°C/yr is assumed for the Hydrothermal system. It can clearly be seen that to match the performance of EGS, CLG would require multiple horizontal sections to maximize contact area with the rock.

4.3.2 Effect of Number and Length of Horizontal sections

Early time performance of CLG systems are analyzed using the SBT framework and it is seen that the production temperatures are close to the reservoir temperature only during the initial few hrs for both the 1 and 4 loop configuration. A large number of loops are required to show acceptable or significantly low levels of thermal drawdown.

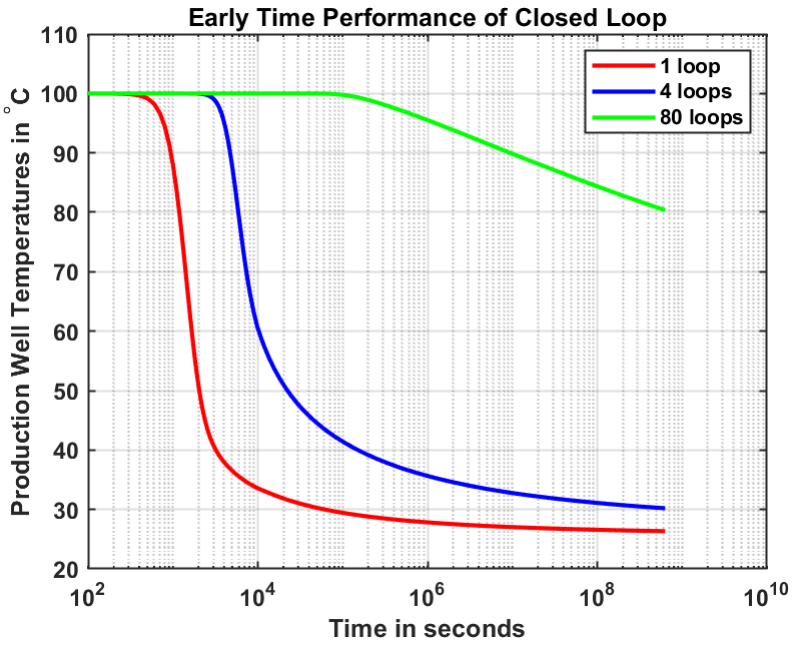

Figure 4.4: Early time performance of CLG with varying number of loops assuming an initial reservoir temperature of 100°C. The fluid injection temperature is 25°C and the total mass flow rate is 40 kg/s. It is assumed that the mass flow rate is equally split into the proposed loops. The diameter of each loop is 0.25 m and the length is 1000 m. The production temperature is close to the reservoir temperature only during the initial few hrs in the case of 1 and 4 loops after which there is a significant drop in the production temperatures. Significant number of loops are needed for these systems to show acceptable levels of drawdown.

For CLG to match the thermal performance of the EGS configuration shown in Figure 4.1, 415 horizontal laterals or loops would be required. Constructing such large number of loops in the selected reservoir volume (1000 m×1000 m×250 m) would not be possible without causing thermal interference between the loops, which in turn, would result in a decrease in the performance of the CLG system. Hence, the volume constraint would have to be relaxed in order to construct 415 loops and the spacing between the adjacent loops must be 50 m.

It was also found that both the length of the loop as well as the number of loops play a crucial role in the thermal performance of CLG systems. The performance

of a single loop system whose length was increased from 1 km to 4km was only marginally better than the former with the 4 km system showing a long term production temperature which is only 2-3°C higher than the 1 km system. The 20 loops system where each loop is 4 km long performed slightly better than the 80 loop system which had 1 km long laterals.

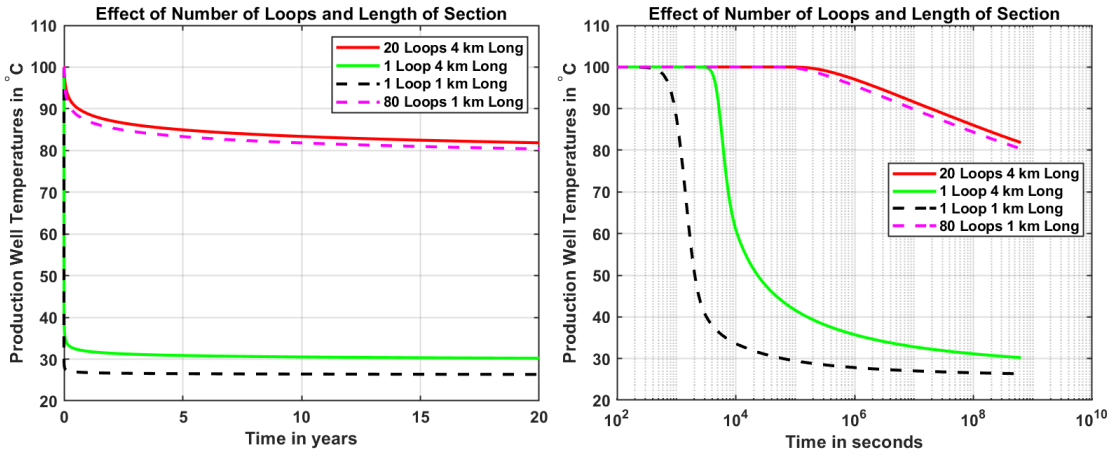

(a) (b)

Figure 4.5: (a) Simulated production temperatures for CLG over a period of 20 years illustrating the combined effect of number of loops and length of section and (b) Early time performance for CLG over a period 20 years illustrating the combined effect of number of loops and length of section. The initial reservoir temperature is 100°C. The fluid injection temperature is 25°C and the total mass flow rate is 40 kg/s. It is assumed that the mass flow rate is equally split into the loops. In the case of EGS, the fluid is assumed to flow through the entire surface of the fracture of length 1000 m and width 1000 m. For each loop of CLG, the diameter is 0.25 m and the length is 1000 m. A linear temperature decline of 0.4°C/yr is assumed for the Hydrothermal system.

4.3.3 Effect of creating fracture networks

Enhanced Geothermal Systems may not necessarily have distinct parallel fractures as assumed in sections 4.3.1 and 4.3.2. Fracture network analysis is pivotal when the geothermal reservoir is developed by stimulation (hydraulic, thermal,

or chemical) of the existing natural fractures to achieve sufficient permeability to produce adequate fluid flow rates of economic success. In low permeability rocks, the process of hydraulic stimulation is conceptualized as a complex network of newly forming fractures and/or natural fractures that slip and open according to the regional stress state (McClure and Horne, 2014). Hence, two DFN configurations (DFN-1 and DFN-2) are chosen to study the effect of a fracture network on the thermal performance of EGS. These configurations are assumed to be contained in the reservoir geometry shown in Figure 3.1. DFN-2 is more branched when compared to DFN-1 and therefore has a greater surface area (2,625,000 m^2 vs 1,833,200 m^2). An analytical technique as prescribed by Fox et al. (2016) is employed to evaluate the thermal performance of DFN. The temperature at the production node is monitored over a 20 year lifetime.

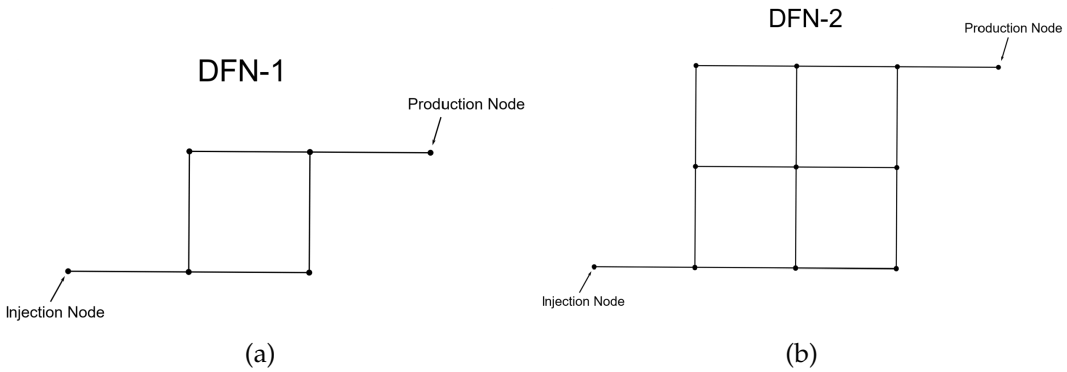

Figure 4.6: (a) DFN-1 configuration with 6 segments/fractures with interconnections. Each horizontal segment has a length of 333.33 m and each vertical segment has a length of 250 m. The width and aperture of all segments are held at constant values of 1000 m and 1 mm. (b) DFN-2 configuration with 14 segments/fractures with interconnections. Each horizontal segment has a length of 250 m and each vertical segment has a length of 125 m. The width and aperture of all segments are held at constant values of 1000 m and 1 mm.

It is found that both DFN-1 and DFN-2 showed a more superior performance when compared to a CLG system with 80 horizontal loops with outlet tempera-

tures that were close to 97°C and 92°C respectively. It is also seen that the fracture network performed better than the single fracture system. DFN-2 showed a lower temperature drop over a period of 20 years when compared to the DFN-1 structure. All these results highlight the importance of creating an extensive fracture network in the geometry to maximize the heat transfer contact area of the fluid with the rock.

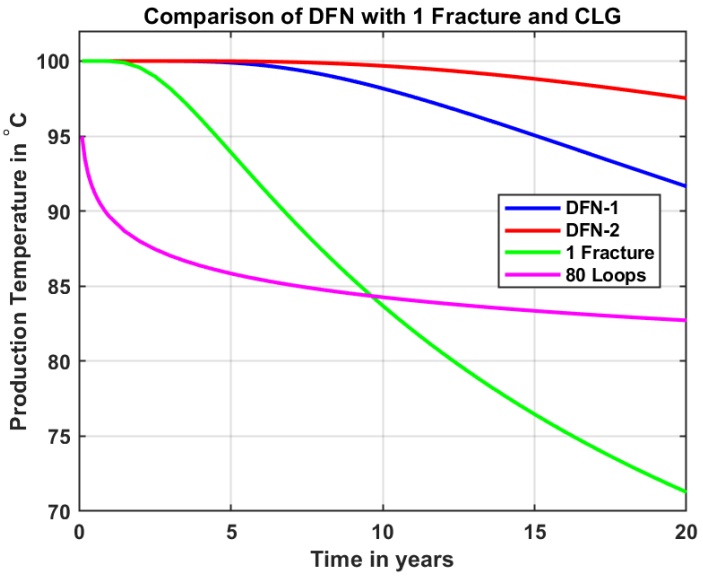

Figure 4.7: Simulated production temperatures for DFN configurations, a single fracture and a 80 loop CLG system. The initial reservoir temperature is 100°C. The fluid injection temperature is 25°C and the total mass flow rate is 40 kg/s. It is assumed that the mass flow rate is equally split into the fractures/loops/networks. In the case of EGS, the fluid is assumed to flow through the entire surface of the fracture. The width of all the discrete fracture networks is held a constant at 1000 m. DFN-1 and DFN-2 show superior thermal performance over the single fracture and 80 loops case. DFN-2 which is more branched shows the best thermal performance. Extensive branching can therefore help increase the production temperatures of EGS.

4.4 Conclusions

A comparative performance analysis over a 20 year life span is performed between idealized CLG systems, EGS and a reference commercial hydrothermal system in a rock mass that is initially at 100°C. Increasing the heat transfer contact area of the fluids with the subsurface at depth is found to play a very important role in maximizing the thermal output of the system. In the case of fractured systems, surface area can be maximized through either through opening pre-existing fractures or by generating new fractures through hydraulic fracturing. In the case of CLG systems, several horizontal extensions would be needed to achieve acceptable heat transfer area. The production well temperature for a single CLG system of horizontal length 1000 m equals the reservoir temperature only during the initial few hours of operation. The outlet temperatures quickly drops and converges to a much lower long term near steady state value. For the geothermal reservoir considered within the 1000 m×1000 m×250 m volume, 415 loops are required to match the thermal power production of a 4 fracture EGS reservoir (each fracture is assumed to have a surface area of 100,000 m^2).

The combined effect of lateral section length and number of laterals can be used to generate heat transfer areas sufficiently large to compensate for the low thermal diffusivity of the rock and low rock thermal conductivity. However, it is noted that drilling costs increase exponentially with total drilled depth (Lukawski et al., 2014) and additional costs may be required to connect the laterals to the injection and production wells to create a leak-tight closed loop system. This process will be very challenging especially with several horizontal loop extensions. The capital costs for CLG are highly dependent on drilling

costs and hence avoiding drilling new wells by repurposing idle or abandoned wells may provide a means to significantly reduce the capital and levelized costs of building such systems (Scherer et al., 2020).

For greenfield sites, EGS reservoirs can supply larger thermal output with less thermal drawdown than comparable CLG systems, only if a fracture/network can be established with sufficient effective heat transfer area. This requirement translates into a need to create a fracture network with well separation distances of 500 to 1000 m where fluid circulating from an injection well to a production well is exposed to rock surface areas approaching 1×10^{6} m^2. In order to be effective, fluid short-circuiting or restricted flow paths need to be avoided as they will dramatically hinder thermal performance.

On the other hand, if a pre-existing reservoir permeability is sufficiently large to achieve economic flow rates through a large enough rock volume, developing a hydrothermal system would likely be the best option. Nonetheless, even in those cases there may be situations where CLG could be a desirable option. For example, when challenging subsurface conditions (e.g., aggressive fluid chemistry or presence of non-condensable gases) may prevent production of brine to the surface. The same is true for extracting heat from formations with low permeability that cannot be stimulated (e.g., because of technical, legal or permitting limitations). In certain developed fields, more brine production could result in a drastic pressure drawdown in the reservoir, or could surpass the production cap as stipulated in the lease. In these situations, CLG could enable the production of more heat from the reservoir without having to drill additional wells to achieve required fluid production rates.

CHAPTER 5

CONCLUSIONS AND FUTURE RECOMMENDATIONS

To help understand and characterize flow channeling in EGS reservoirs, periodic pumping tests were conducted at a meso scale field site located at Altona, NY. An effective width of the channeled section between wells 204 and 304 is computed for a known hydraulic aperture of the fracture. Two storage mechanisms were considered to evaluate the channel width. Firstly, analytical expressions were derived by considering the storage of the fluid to entirely occur in the monitoring wellbores. A constrained optimization framework is then developed using data from all the monitoring wells, different directions of flow and different periods to compute the channel width for a known hydraulic aperture of the fracture. Fast Fourier transformation (FFT) analysis was performed to extract the amplitude of the head oscillations at different periods of pumping.

Secondly, analytical expressions for the steady state channeling behavior at the site considering storage of fluid to occur entirely in the fractured formation were also derived and the channel widths were also evaluated using this approach. For both the approaches it was observed that the width of the channel decreased with increasing period of oscillation for a given hydraulic aperture of the fracture. This can be due to the fact that highly conductive pathways that offer the least resistance to flow are preferred at shorter periods leading to increased width estimates.

In order to separate the influence of fluid storage in the fracture and the storage in the monitoring wells from the results, the effect of monitoring wellbore storage was quantitatively analyzed by expressing the fluid volume stored in

the monitoring wells in a non dimensional fashion. This was then compared with fracture storativity to understand the dominant storage mechanism. It was found that storage in the fracture predominated over storage in the monitoring wells at the Altona field site suggesting the use of the former mechanism to characterize the channeling between wells 204 and 304.

The diffusion length of analysis can be changed by performing the tests at different periods. This resulted in a range of interrogated areas that were sensitive to different distances from the pumping well. Shorter periods can aid in understanding the local heterogeneity in greater detail as compared to larger periods. The period of oscillations considered for testing must be determined using preliminary diffusivity estimates to ensure distances that are well beyond the boundaries of a field site aren't investigated.

It is recommended that future periodic pumping tests at Altona be run at lower periods (0.5 - 2 mins) to understand the channeling and wellbore storage effects in greater detail. Theoretical models may also need to be developed such that the fracture opening behavior is incorporated in the modeling framework.Hence, an effective reservoir compressibility may be required as an input in the expressions. Geomechanical correlations that assess the effective stresses working on the fractures must then be developed for these tests. The combined effect of storage taking place simultaneously in both the fracture as well as the monitoring wells should be developed to help understand the inter well connectivity better.

The thermal performance of CLG systems were simulated for heat production

over a 20 year period. By considering a range of different CLG designs and geometries, reservoir characteristics, operating conditions, the results provide insight into the influence of these parameters and can help guide development decisions. Based on the simulations, for reservoir temperatures ranging between 150 and 300°C at a 2 km depth (which corresponds to relatively high average geothermal gradients, from 65 to 140 °C/km), thermal outputs are expected to be in the range of 0.4 to 0.9 MW_{th} for the 2 km vertical co-axial system.

Heat extraction rates from closed loop systems in conduction-dominated reservoirs are limited because of two underlying reasons: 1) the inherently low thermal conductivity (~1–5 W/m·K) and diffusivity of the rock (~10^{-6} m^2/s of rock), which controls the heat flux through the rock zone surrounding the wellbore, and 2) the restricted contact area in between the fluid and the rock mass as a result of confining the fluid in sealed wells. Larger thermal outputs are obtainable with higher reservoir temperatures, or through more well contact area with the rock, e.g., with a long horizontal extension for a co-axial system. Natural or forced convection increases output but requires relatively high reservoir permeability to have a considerable impact. For in-situ reservoir permeability of $10^{-15}m^2$ (~1 mD), a common natural permeability found at depths of 2 to 4 km, there is only a moderate increase in thermal output.

Future work can focus on simulating Co-Axial Systems with a horizontal extension using a series of 2-D sections wherein, the finite element method could be applied along with finite difference method being employed within each section. In this way the 3-D mesh that is required to simulate the geometry can be reduced to a computationally less expensive 2-D simulation with convection in

the reservoir being captured as well.

For greenfield projects, EGS can supply larger thermal outputs with less thermal drawdown than comparable CLG systems, only if a fracture/network can be established with sufficient effective heat transfer area. In order to be effective, fluid short-circuiting or restricted flow paths need to be avoided as they will dramatically hinder thermal performance. If pre-existing reservoir permeability is sufficiently large to achieve economic flow rates through a large enough rock volume, developing a hydrothermal system would likely be the best option. Nonetheless, even in those cases there may be situations where CLG could be a desirable option. For example, when challenging subsurface conditions (e.g., aggressive fluid chemistry or presence of non-condensable gases) may prevent production of brine to the surface. The same is true for extracting heat from formations with low permeability that cannot be stimulated (e.g., because of technical, legal or permitting limitations). In certain developed fields, more brine production could result in a drastic pressure drawdown in the reservoir, or could surpass the production cap as stipulated in the lease. In these situations, CLG could enable the production of more heat from the reservoir without having to drill additional wells to achieve required fluid production rates.

APPENDIX A

ANALYTICAL MODELING OF WELL HYDRAULICS

The following appendix describes analytical expressions derived for flow channeling in fractures when the bedrock is exposed to periodic pumping tests. Expressions in A.1 assume the fluid storage to entirely occur in the monitoring wellbores. Whereas, expressions in A.2 assume the fluid storage to entirely occur in the fractured bedrock. Appropriate initial and boundary conditions are applied for solving the governing equations in both A.1 and A.2.

A.1 Channel hydraulics with storage in monitoring wells

Considering well 304 as the source well, the head oscillations created at the well vary with time as $h_{304}(t) = h_{304a}\exp(i\omega t)$. The head oscillation at well 204 can be expressed as $h_{204}(t) = \hat{h}_{204}\exp(i\omega t)$. Where, $\hat{h}_{204} = h_{204a}\exp(i\phi_{204})$. Assuming there is no storage taking place in the monitoring well 404, the volume balance around well 204 can be expressed as follows-

$$\frac{dV_{204}}{dt} = \frac{\rho g W b_h^3}{12\mu \times 2L}(h_{304a} - \hat{h}_{204}) - \frac{\rho g W b_h^3}{12\mu L_\infty}(\hat{h}_{204}) \tag{A.1}$$

By not performing a volume balance around the source well, it is assumed that fluid flow may occur through unknown flow paths from the well to an unknown ∞ (Represented by black lines in Figure A.1). Equation A.1 can be rearranged as follows-

$$i\omega\hat{h}_{204} = \frac{\rho g W b_h^3}{12\mu \times 2LA_m}(h_{304a} - \hat{h}_{204}) - \frac{\rho g W b_h^3}{12\mu L_\infty A_m}(\hat{h}_{204}) \tag{A.2}$$

A dimensionless number (B) can then be defined. B can be viewed as a dimensionless resistance to flow at a particular period or frequency since it is directly

proportional to fractured channel properties namely W and b_h^3.

$$B = \frac{\rho g W b_h^3}{12 \mu A_m L \omega} \tag{A.3}$$

The governing equation can then be written in terms of the dimensionless number as follows-

$$\hat{h}_{204}\left[i + \frac{B}{2} + \frac{BL}{L_\infty}\right] = \frac{B}{2} \tag{A.4}$$

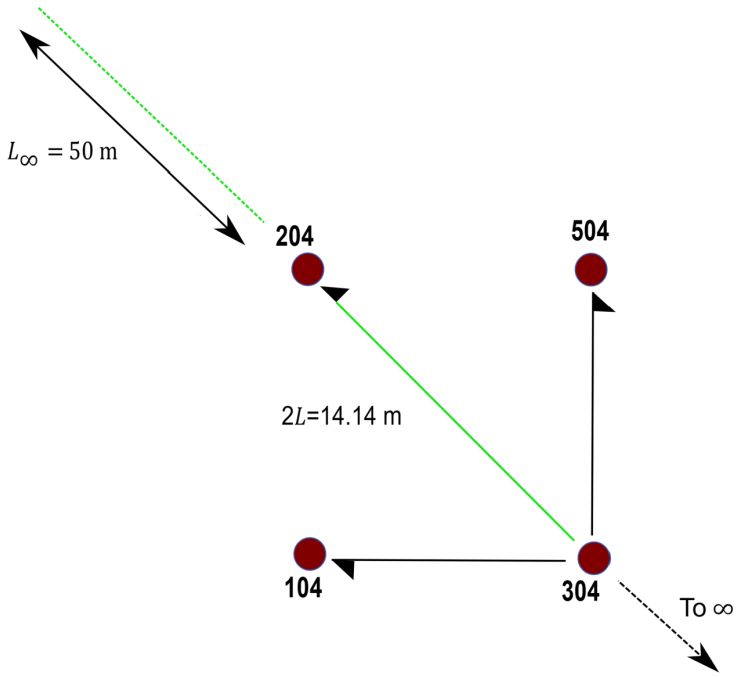

Figure A.1: Using well 304 as the source well to model the storage effects in the monitoring well 204. The geometric properties of the fracture i.e. the width and the aperture are held a constant in the sections denoted by the red color. The sections in black are the possible flow channels that may exist from well 304 and are not considered for the analysis. Since L_∞ is defined before hand the only unknown solved for is the width of the fracture for a given hydraulic fracture aperture.

By substituting L_∞= 50 m and L= 7.07 m, the complex amplitude of h_{204} can then be converted in terms of real amplitude h_{204a} and rearranged to express B in

terms of h_{204a} as follows-

$$B = \sqrt{\frac{h_{204a}^2}{0.25 - 0.409 h_{204a}^2}} \tag{A.5}$$

Expression A.5 provides real results for periods 112.4 s and 224.6 s.

To incorporate the storage effects in all monitoring wells, volume balances are performed around all the monitoring wells. For the case where well 204 is used as a source well, the following equations can be derived from the volume balances around wells 404 and 304.

$$i\omega \hat{h}_{404} = \frac{\rho g W b_h^3}{12\mu L A_m}(h_{204} - \hat{h}_{404}) - \frac{\rho g W b_h^3}{12\mu L A_m}(\hat{h}_{404} - \hat{h}_{304}) \tag{A.6}$$

$$i\omega \hat{h}_{304} = \frac{\rho g W b_h^3}{12\mu L A_m}(\hat{h}_{404} - \hat{h}_{304}) - \frac{\rho g W b_h^3}{12\mu L_{\infty\,204-304} A_m}(\hat{h}_{304}) \tag{A.7}$$

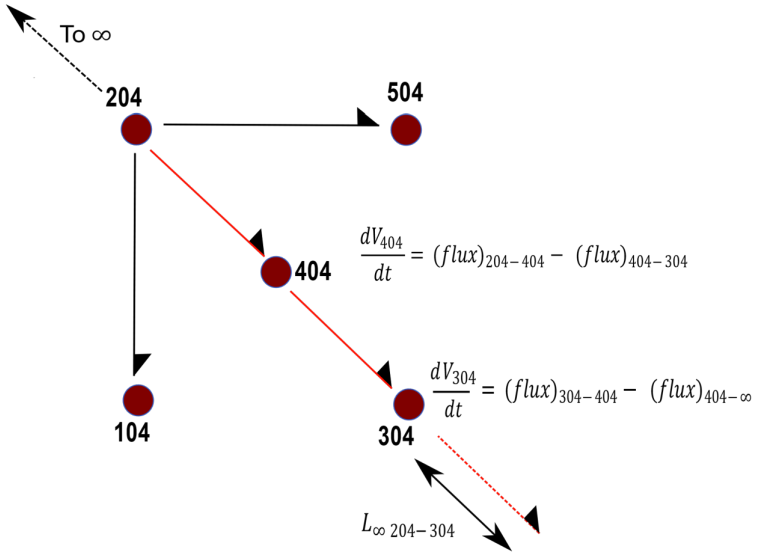

Figure A.2: Using well 204 as the source to model the storage effects in the monitoring wells 404 and 304. The geometric properties of the fracture i.e. the width and the aperture are held a constant in the sections denoted by the red color. The sections in black are the possible flow channels that may exist from well 204 and are not considered for the analysis.

B^* [units s^{-1}] and ℓ [dimensionless] are mathematically expressed as follows-

$$B^* = \frac{\rho g W b_h^3}{12 \mu L A_m} \tag{A.8}$$

$$\ell = \frac{L}{L_{\infty\, 204-304}} \tag{A.9}$$

Therefore, the governing equations can be written in terms of the dimensionless parameters as follows-

$$\hat{h}_{404}\,[i\omega + 2B^*] = B^* + B^* \hat{h}_{304} \tag{A.10}$$

$$\hat{h}_{304}\,[i\omega + B^*(1+\ell)] = B^* \hat{h}_{404} \tag{A.11}$$

From equation A.11, $\hat{h}_{404}$ can be expressed in terms of $\hat{h}_{304}$, B^* and ℓ as follows-

$$\hat{h}_{404} = \hat{h}_{304} \frac{[i\omega + B^*(1+\ell)]}{B^*} \tag{A.12}$$

Incorporating equation A.12 into A.11 and solving for the complex amplitude of h_{304}, the following expression is obtained-

$$\hat{h}_{304} = \frac{B^{*2}}{B^2(2\ell+1) - \omega^2 + (3+\ell)B\omega i} \tag{A.13}$$

To obtain the absolute magnitude of the head signal at h_{304}, complex conjugation is performed and the expression can be rearranged to the following form-

$$h_{304a} = \sqrt{\frac{B^{*4}}{\omega^4 + B^{*2}\omega^2(\ell^2 + 2\ell + 7) + B^{*4}(2\ell+1)^2}} \tag{A.14}$$

A second expression can be obtained from the volume balance from equation A.12. By performing complex conjugation, equation A.12 can also be used to obtain the absolute magnitude of the head signal at h_{304a} in terms of B^*, ℓ and h_{404a} as follows-

$$h_{304a} = \sqrt{\frac{h_{404a}^2}{\frac{\omega^2}{B^{*2}} + (1+\ell)^2}} \tag{A.15}$$

Similarly, using 304 as the source well, volume balances can be made around wells 404 and 204 and two expressions to compute h_{204a} can be derived. The equations have been provided below-

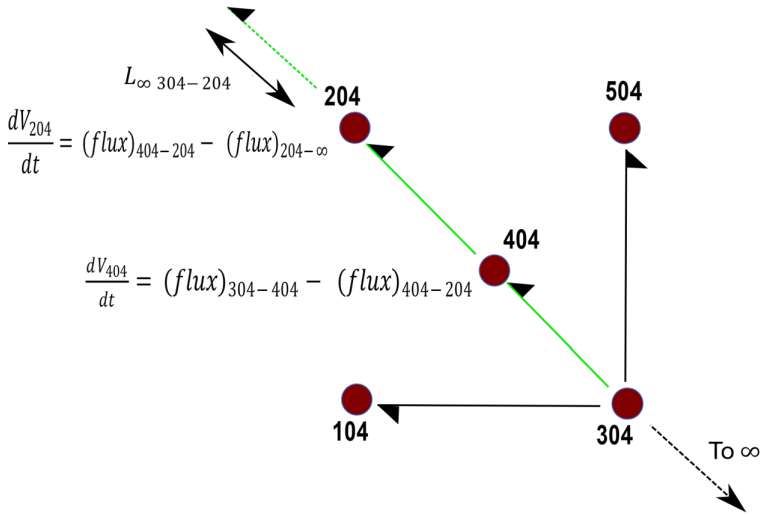

Figure A.3: Using well 204 as the source to model the storage effects in the monitoring wells 404 and 304. The geometric properties of the fracture i.e. the width and the aperture are held a constant in the sections denoted by the red color. The sections in black are the possible flow channels that may exist from well 204 and are not considered for the analysis.

$$h_{204a} = \sqrt{\frac{B^{*4}}{\omega^4 + B^{*2}\omega^2(\ell'^2 + 2\ell' + 7) + B^{*4}(2\ell' + 1)^2}} \tag{A.16}$$

$$h_{204a} = \sqrt{\frac{h_{404a}^2}{\frac{\omega^2}{B^{*2}} + (1 + \ell')^2}} \tag{A.17}$$

where $\ell' = L/L_{\infty\,304-204}$. To obtain the optimal B^*, ℓ and ℓ' that satisfies the data from different wells (204,404 and 304), all periods of operation and two different flow directions (from 304 to 204 and vice versa), a minimization of least squares sum of errors for head amplitudes is conducted (l^2 norm).

$$l^2 = ||h_{mc} - h_m||_2 \tag{A.18}$$

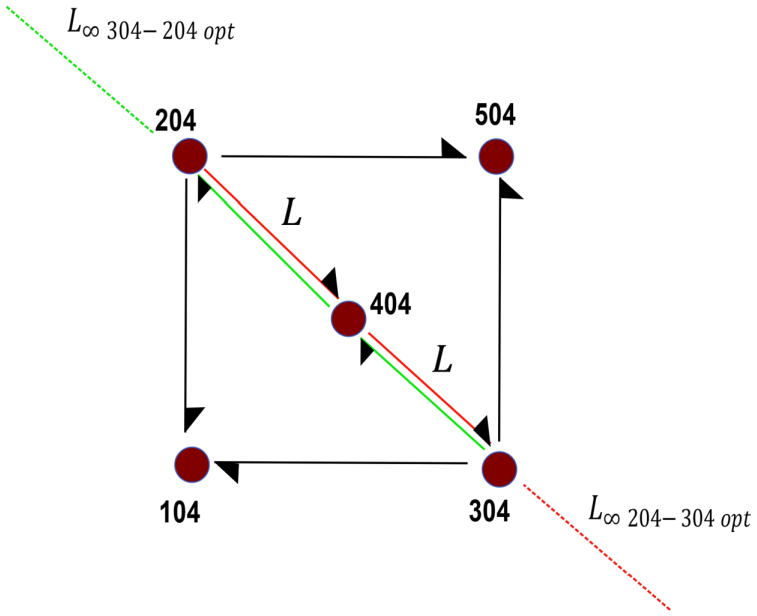

Figure A.4: Constrained optimization problem to model the storage in the monitoring wells by using data across the three different periods for both well 204 and 304 as the source well. The geometric properties of the fracture i.e. the optimal width and the aperture are held a constant in the sections denoted by the red and green color. The sections in black are the possible flow channels that may exist from well 204 and 304 and are not considered for the analysis. The three unknowns in the optimization framework include $L_{\infty\,204-304\,opt}$, $L_{\infty\,304-204\,opt}$ and the the optimal width of the fractured channel (W_{opt}) for a given hydraulic fracture aperture (b_h).

h_{mc} is the vector of calculated head measurements for different periods. B^*, ℓ and ℓ' that match the data are then chosen for the analysis to compute the optimal $L_{\infty\,204-304}$ (i.e. $L_{\infty\,204-304\,opt}$), $L_{\infty\,304-204}$ (i.e. $L_{\infty\,304-204\,opt}$) and optimal width (W_{opt}) of the fracture experiencing channeling between the wells for a given hydraulic fracture aperture.

A.2 Channel hydraulics with storage in the fracture

It is assumed that the fracture is infinitely long and the 1-D diffusion equation for flow from a particular injection source at $x = 0$ is written as-

$$\frac{\partial P^{'}}{\partial t} - D\frac{\partial^2 P^{'}}{\partial x^2} = 0 \tag{A.19}$$

For steady state solution P' is introduced where $P' = P - P_0$. P_0 refers to the reference pressure. The Initial Condition (IC): $P^{'} = 0$ at $t = 0$ and the Boundary Conditions (BC) : $P^{'} = 0$ at $x \to \infty$, $x \to -\infty$ and $P^{'}$=$P_a cos(\omega t)$ at $x = 0$ (Taking only the real part of the oscillations). P_a is the amplitude of the pressure signal.

The Laplace Tranform of this partial differential equation yields-

$$\frac{\partial^2 \overline{P}^{'}}{\partial \overline{x}^2} - \frac{s}{D}\overline{P}^{'} = 0 \tag{A.20}$$

Solving for $\overline{P}^{'}$ we get the following:-

$$\overline{P}^{'} = C_1 \exp\left(\sqrt{\frac{s}{D}}x\right) + C_2 \exp\left(-\sqrt{\frac{s}{D}}x\right) \tag{A.21}$$

Therefore -

$$\overline{P}^{'} = \frac{s\mathcal{H}(s)}{s^2 + \omega^2} \exp\left(-\sqrt{\frac{s}{D}}x\right) + \frac{s\mathcal{H}(-s)}{s^2 + \omega^2} \exp\left(\sqrt{\frac{s}{D}}x\right) \tag{A.22}$$

where $\mathcal{H}$ refers to the Heaviside step function. Inversion of expression A.22 is done analytically using the following expression-

$$P^{'} = \frac{1}{2\pi i}\int_{\gamma - i\infty}^{\gamma + i\infty} \overline{P}^{'} \exp(-st) ds \tag{A.23}$$

Complex Residue theorem is used to solve this definite integral with γ being a real constant whose value is such that the poles are to the left of the line of integration. Since there are two possible poles in the equation (i.e. $s = i\omega$ and $s = -i\omega$) which are imaginary, γ can be a small positive number. The residue at

each of these poles is computed and summed up. The result is then multiplied with $2\pi i$ (Cauchy Integral Theorem).

$$P' = P_a\left(\exp\left(\frac{-x}{\sqrt{2}l_d}\right)\cos\left(\frac{x}{\sqrt{2}l_d}\right)\cos(\omega t) + \exp\left(\frac{-x}{\sqrt{2}l_d}\right)\sin\left(\frac{x}{\sqrt{2}l_d}\right)\sin(\omega t)\right) \quad \text{(A.24)}$$

P' therefore can also be expressed in terms of an amplitude and phase shift as follows -

$$P(x,t) = P' = P_a\exp\left(\frac{-x}{\sqrt{2}l_d}\right)\cos\left(\omega t - \frac{x}{\sqrt{2}l_d}\right) \quad \text{(A.25)}$$

where the amplitude of the pressure signal at a distance x from the source is $P_a\exp(-x/\sqrt{2}l_d)$ and the phase shift is $x/\sqrt{2}l_d$. Incorporating both real and imaginary parts, equation A.25 can be expressed as follows-

$$P(x,t) = P_a\exp\left(\frac{-x}{\sqrt{2}l_d}\right)\exp\left[i\left(\omega t - \frac{x}{\sqrt{2}l_d}\right)\right] \quad \text{(A.26)}$$

In terms of hydraulic head-

$$h(x,t) = h_a\exp\left(\frac{-x}{\sqrt{2}l_d}\right)\exp\left[i\left(\omega t - \frac{x}{\sqrt{2}l_d}\right)\right] \quad \text{(A.27)}$$

where h_a is the amplitude of the slug fluctuation and $h_a\exp(-x/\sqrt{2}l_d)$ is the amplitude of the head signal at a distance x from the source.

APPENDIX B

NUMERICAL MODELING OF CLOSED LOOP GEOTHERMAL SYSTEMS

The following appendix describes the setup of the FEM technique employed on COMSOL for the co-axial closed loop systems, the SBT for transient heat conduction in the reservoir and the validation of the COMSOL model with SBT and the analytical Ramey solution.

B.1 FEM Modeling on COMSOL

A 2-D axisymmetric modeling approach was employed to capture the temperature change with time for the co-axial closed loop systems. Hence, the 3-D problem is reduced to a 2-D problem to increase the computational efficiency. The mesh by the wellbore is of size 0.05 m radially and 50 m axially. A total of 2500 elements were built in the domain which had a fixed width of 100 m. The length of the domain was modified depending on the length of the co-axial system being analyzed. The heat exchange between the pipe and the medium is a function of time and can be expressed as $Q(t)$ in [W/m]. The advective heat transfer due to pipe fluid flow can hence be represented as follows (Bergman et al., 2011):-

$$Q(t) = \frac{T_f(t) - T(t)}{R_t} \tag{B.1}$$

Where, $T_f(t)$ refers to the temperature of the fluid which is dependent on time and $T(t)$ refers to the temperature of the surrounding medium i.e. rock. R_t is the thermal resistance of the pipe in [W^{-1}m.K]. Thermal Resistance and Capacity Models (TRCM) for both the CXA and CXC configurations were adapted from Diersch et al. (2011). The two thermal resistances that exist in the system

include-

$$R_{11} = \frac{1}{2\pi r_0 h_0} \tag{B.2}$$

$$R_{12} = \frac{1}{2\pi r_{ii} h_{fi}} + \frac{1}{2\pi k_{pi}} \ln \frac{r_{io}}{r_{ii}} \tag{B.3}$$

Where R_{11} refers to the thermal resistance of the outer pipe and the borehole wall (assuming open hole production). r_0 refers to the radius of the outer pipe(well radius) in [m], h_{fo} is the heat transfer coefficient for the flow in the annular region of the setup in [W/m^2.K]. R_{12} refers to the thermal resistance between the inner pipe with the insulation coating, r_{ii} refers to the inner radius of the inner pipe and r_{io} refers to the outer radius of the inner pipe and k_{pi} refers to the thermal conductivity of the insulation in [W/m.K] and h_{fi} refers to the heat transfer coefficient for the flow in the inner pipe region.

Both h_{fo} and h_{fi} are calculated using appropriate Nusselts Number correlations (Dittus-Boelter equation). The energy balance of the fluid inside the pipe (neglecting the heat conduction in the fluid) can hence be represented as follows-

$$\rho_f C_{p,f} \frac{\partial T_f(t)}{\partial t} + \rho_f C_{p,f} v \frac{\partial T_f(t)}{\partial s} = \frac{Q(t)}{\pi r_h^2} \tag{B.4}$$

Where, ρ_f is the density of the fluid in [kg/m^3], $C_{p,f}$ is the specific heat capacity of the fluid in [J/kg.K], v refers to the velocity of the fluid in the pipe (the flow in the pipe is assumed to be fully developed) in [m/s]. R_h refers to the hydraulic radius of the pipe which is used to compute the area of the annular region of the setup.

Equations B.1 to B.4 are coupled with the conductive heat transport in the solid matrix -

$$\rho C_p \frac{\partial T(t)}{\partial t} + \rho C_p u.\nabla T + \nabla.q = Q \tag{B.5}$$

Where, ρ is the density of the rock, C_p is the specific heat capacity of the rock, u is the velocity vector of translational motion and Q refers to the additional heat sources in [W/m^2]. q can be expressed from Fouriers Law of heat conduction $q = -k\nabla T$.

The above expressions are assuming the medium is purely conductive in nature. In order to incorporate convective effects in the reservoir, equations B.1 to B.4 are coupled with the following equations following the Darcys Law for porous media flows-

$$\frac{\partial}{\partial t}(\rho\epsilon) + \nabla.(\rho u) = Q_m \tag{B.6}$$

$$u = \frac{-\kappa}{\mu}(\nabla P + \rho g \nabla D) \tag{B.7}$$

$$(\rho C_p)_{eff}\frac{\partial T}{\partial t} + \rho C_p u.\nabla T + \nabla.q = Q \tag{B.8}$$

Where ϵ refers to the porosity of the media, κ refers to the permeability of the media in [m^2], ΔP is the pressure gradient in [Pa], ∇D refers to the effective elevation of the system and Q_m refers to mass source in [kg/m^{3}s] . Since there are solids as well as fluids involved in the media q is defined as $q = -k_{eff}\nabla T$ where $k_{eff} = \theta_p k_p + (1-\theta_p)k_f$. θ_p is the volume fraction of the porous media, k_p is thermal conductivity of the porous media and k_f is the thermal conductivity of the fluid. $\left(\rho C_p\right)_{eff} = \theta_p \rho C_p + (1-\theta_p)\rho_f C_{p,f}$ where ρ_f is the fluid density and $C_{p,f}$ is the specific heat capacity of the fluid.

B.2 Description of SBT Model

The SBT tool is a transient heat transfer simulator for modeling heat extraction with closed-loop geothermal systems in conduction-only or forced-convection

geothermal reservoirs. The tool was originally developed by Beckers et al. (2015) to simulate computationally-fast transient heat transfer of slender bodies (e.g., a geothermal well) in conductive-only media. The theory was derived by asymptotically matching an infinite cylinder as inner solution to a finite line source as outer solution. Heat transfer of the slender body with the medium was coupled to fluid flow inside the slender body to allow simulating heat extraction with heat exchangers such as shallow or deep closed-loop geothermal systems. The SBT model captures curvature and thermal interaction between slender bodies, allows for varying injection temperature and fluid flow rate and can handle both short and long time-scales. An initial rock temperature gradient is allowed but rock properties are required to be constant, isotropic and uniform. Options are available to lift some of these constraints (Beckers et al., 2015), but these are not currently considered.

The SBT model is numerically implemented on MATLAB by discretizing the heat exchanger into a set of straight pipe elements along the center line of the heat exchanger. The heat exchange at each pipe element is further discretized in time as a set of heat pulses that remain constant during each time step. Heat exchange between the fluid inside the heat exchanger and the surrounding rock depends on the temperature difference between the fluid and contacting rock. The SBT model calculates the rock temperature along the heat exchanger using a hybrid approach. The temperature T at each pipe element i at the end of each time step m is the double summation of the temperature change due to all past and current heat pulses n (from 1 to m) from all pipe segments j (from 1 to N with N being the total number of pipe elements):

$$T_{i,m} = \sum_{j=1}^{N} \sum_{n=1}^{m} f_{i,j,m,n} \cdot Q_{j,n} \tag{B.9}$$

with $Q_{j,n}$ the heat pulse at element j during time step n and $f_{i,j,m,n}$ the temperature change at element i at the end of time step m as a result of the heat pulse at element j during time step n. The factors $f_{i,j,m,n}$ are calculated using analytical equations for a cylindrical (infinite or finite), line (infinite or fine) or point source. Decision trees were developed based on non-dimensional numbers reflecting the time and length scales, to calculate $f_{i,j,m,n}$ accurately with the most simple (i.e., computationally-fast) model (Beckers et al., 2015).

The original SBT model assumed heat conduction-only in the reservoir, and water with constant thermo-physical properties as heat transfer fluid in a U-loop type heat exchanger. Updates were made to the SBT model to allow for simulating different heat transfer fluids, variable fluid properties as a function of temperature and pressure, co-axial type heat exchangers, and reservoirs with uniform one-dimensional flow resulting in heat convection in addition to conduction. Following the approach used in several geothermal wellbore simulators (Ortiz-Ramirez, 1983; Bjornsson, 1987; Aunzo and Bjornsson, 1991; Chadha et al., 1993; Hasan and Kabir, 2010), steady-state conservation of mass, momentum and energy is applied to simulate temperature and pressure of the heat transfer/working fluid along the heat exchanger. Single-phase flow and no phase transitions is assumed. Conservation of momentum results in an expression for the pressure gradient as a result of friction, and changes in kinetic and potential energy:

$$-\frac{dP}{dz} = \frac{f\rho v^2}{2d} + \frac{d}{dz}(\rho v^2) + g\rho \sin\theta \tag{B.10}$$

Where P is the fluid pressure in [Pa], z is the local coordinate axially along the heat exchanger in the direction of flow in [m], f is the Darcy friction factor, ρ is the fluid density in [kg/m^3], v is the fluid velocity in [m/s], d is the hydraulic

diameter of the pipe in [m], g is the gravitational acceleration (9.81 m/s^2), θ is the local angle between direction of fluid flow and the horizontal reference (i.e., for flow upwards a vertical well, θ is 90°; for flow downwards a vertical well, θ is -90°). In case of turbulent flow, the Colebrook-White equation is used to calculate f (Fox et al., 2004). Combining conservation of mass and energy yields:

$$\dot{m}\frac{d}{dz}\left(h+\frac{v^2}{2}\right)+\dot{m}g\sin\theta=-Q \tag{B.11}$$

Where $\dot{m}$ is the fluid mass flow rate in [kg/s], h is the specific enthalpy in [J/kg], and Q is the heat exchange with the surroundings in [W/m]. Q is defined as being positive when heat is transferred from the fluid to the rock. For heat exchange between the fluid in a U-loop pipe or in the annulus of a co-axial pipe and the surrounding rock, Q is calculated as:

$$Q=\frac{T_f-T_r}{R_t} \tag{B.12}$$

With T_f being the fluid temperature in [°C], T_r is the rock temperature in contact with the heat exchanger in [°C], and R_t the thermal resistance in [W/m.K]. The heat exchange is assumed positive if heat is transferred from the fluid to the rock, and negative in reverse. For fluid flow in a pipe in direct contact with the rock, R_t is calculated as:

$$R_t=\frac{1}{2\pi r_i h}+\frac{1}{2\pi k}\ln\left(\frac{r_0}{r_i}\right) \tag{B.13}$$

With h is the convective heat transfer coefficient in [W/m^2.K], k is the thermal conductivity of the pipe wall material in [W/m.K], r_i is the inner radius of the pipe in [m] and r_o is the outer radius of the pipe in [m]. Nusselt correlations are used for developed flow through a pipe to calculate h (Cengel, 2003). In case of different layers of thermal resistance (e.g., cement, tubing, vacuum insulation, etc.), additional terms are considered in the equation for R_t, to account for the

thermal resistance in each layer. For a co-axial heat exchanger, similar expressions are used for Q and R_t to account for heat transfer between the fluid in the center pipe and the annulus.

Specific enthalpy and thermo-physical properties (e.g., density, viscosity) of the fluid are calculated as a function of temperature and pressure using the CoolProp open-source libraries (Bell et al., 2014). Fluid temperature, pressure, velocity and properties, as well as rock temperature and heat transfer between the heat exchanger and the rock and, for a co-axial heat exchanger, between the annulus and center-pipe, are coupled and solved iteratively at each time step. Long-term AGS performance in the presence of uniform water flow in the reservoir is simulated by replacing the point source and line source with the moving point and moving line source model (Molina et al., 2011).

B.3 Validation of SBT and COMSOL models with analytical solution

To ensure that the SBT and COMSOL models were yielding accurate results, several validation cases were performed using both simulators. One such validation was a comparison with the wellbore heat transmission model by Ramey (1962). Ramey derived an analytical solution for the fluid temperature over time within a wellbore undergoing heat exchange with the surrounding rock. The solution assumes constant fluid and rock properties and no phase change in the well, and is only valid at long time scales (i.e, the thermal diffusion length must be significantly larger than the well radius). Ramey's solution for the fluid

temperature in a well as a function of time and position is:

$$T(z,t) = T_0 + az - aA + (T_i + aA - T_0)\exp(-z/A) \tag{B.14}$$

where z is the position along the well in the direction of fluid flow (with z = 0 at well inlet) in [m], t is the time in [s], a is the geothermal gradient in [°C/m] (a is positive for injection wells with $z = 0$ at the surface and negative for production wells with $z = 0$ at the bottom of the well, T_o is the rock temperature at the inlet in [°C], T_i is the fluid temperature at the well inlet [°C], and A is a function in [m^{-1}] calculated as:

$$A = \frac{\dot{m}C_{p,f}\left[k_r + r_i U f(t)\right]}{2\pi k_r r_i U} \tag{B.15}$$

where $\dot{m}$ is the mass flow rate of fluid in the well in [kg/s], k_r is the rock thermal conductivity in [W/m·K], r_i is the tubing inner radius in [m], U is the overall heat transfer coefficient between inside of the tubing and outside of the casing in [W/m^{-2}.K], and $f(t)$ is a time function capturing the transient heat conduction in the formation. In certain cases (e.g., water in liquid phase in geothermal wells without insulated tubing), thermal resistance in the wellbore is negligible and A can be simplified to:

$$A = \frac{\dot{m}C_{p,f} f(t)}{2\pi k_r} \tag{B.16}$$

At long enough time scales (i.e., typically after a week), $f(t)$ can be estimated assuming an infinite constant heat flux line source. The corresponding equation for long times is:

$$f(t) = \ln\left(\frac{r_{co}}{\sqrt{4\alpha_r t}}\right) - 0.29 \tag{B.17}$$

with r_{co} being the casing outer radius in [m] and α_r is the rock thermal diffusivity [m^2/s].

A test simulation was constructed for a 7 km long pipe in an infinite medium.

The rock was initially at a uniform temperature of 100°C (i.e., no geothermal gradient). The well was modeled as open-hole with radius of 0.0762 m, thermal conductivity of the rock is 2.83 W/m.K and thermal diffusivity were set at 1.2×10^{-6} m^2/s. Water at 50°C was injected at 10 kg/s. The outlet temperature as a function of time was estimated with the Ramey equation and showed excellent agreement with the results of the SBT and COMSOL models. The SBT model discretized the pipe in 70 elements of 100 m length each. The COMSOL model assumed a 2-D axisymmetric setup with logarithmically spaced mesh in the radial direction (i.e., element size grows in radial direction away from the pipe).

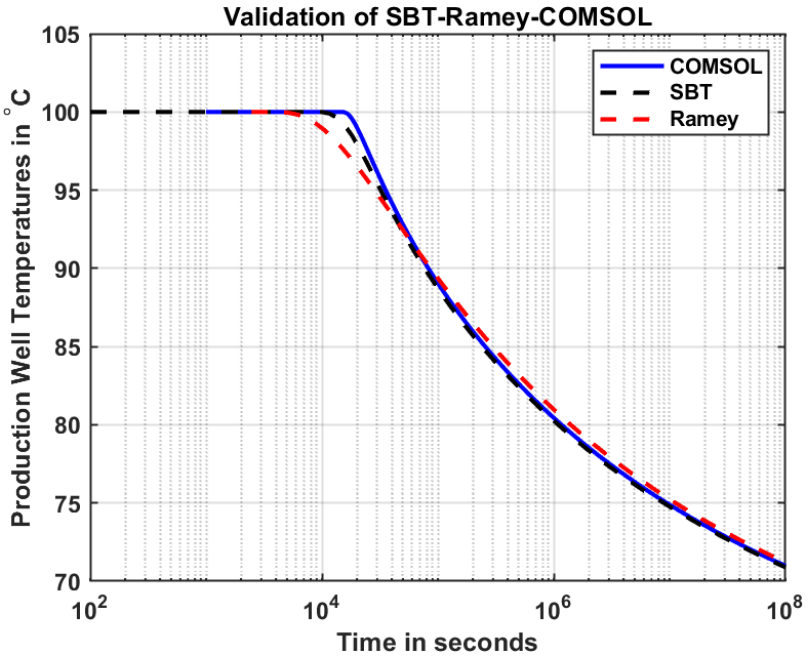

Figure B.1: Outlet temperature for test case calculated with Ramey, SBT model, and COMSOL. Test case considers a 7 km long pipe in rock medium initially at uniform temperature of 100°C, with water injected at 50°C.

B.4 Validation of SBT and COMSOL models for Co-Axial AGS Cases

Several co-axial cases analyzed (heat conduction only) were run both on the SBT and COMSOL models to validate the results. Production temperatures simulated with these models for cases 1 through 3 and cases 7 through 9 are shown below indicating excellent agreement.

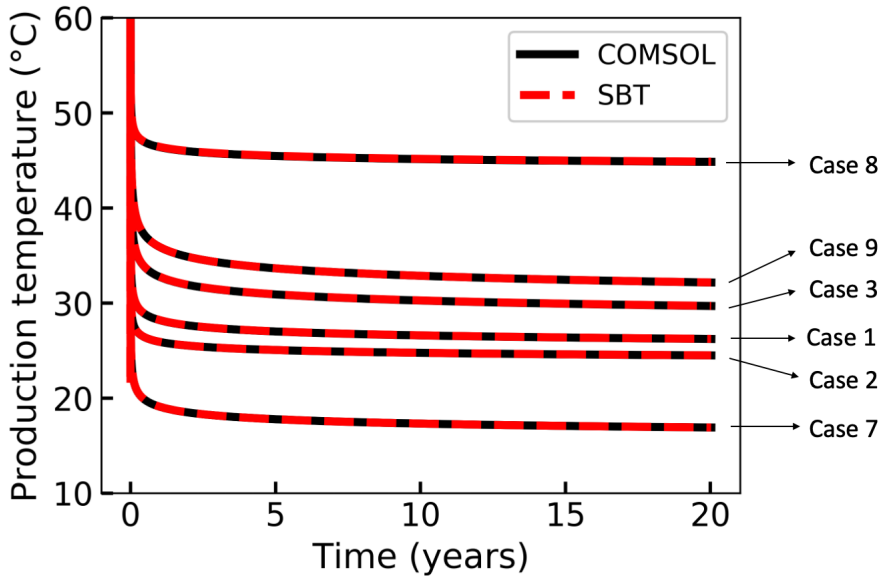

Figure B.2: Comparison of production temperature simulated with COMSOL and SBT model for co-axial AGS Cases 1 through 3 and 7 through 9, indicating excellent agreement in results.

B.5 Co-Axial with Horizontal Extension with SBT and COMSOL

The 2-D axisymmetric model employed on COMSOL was also used to simulate a CXA Co-axial system with a horizontal extension. The model was simulated

by constructing an extra section with a constant temperature gradient along with the appropriate boundary conditions to capture the thermal performance of the horizontal section. Case 13 is considered as the test case (2 km vertical, 2km horizontal extension, 20°C injection temperature and 20 kg/s mass flow rate with water as the working fluid). It is found that as shown in Figure B.3 the long term production temperatures predicted from the axisymmetric COMSOL model is around 1.5°C higher than the predictions from SBT. The reason lies in the fact that the effect of the 90° bend or curvature that occurs at a depth of 2 km from the surface cannot be captured by the model. The thermal penetration length increases with increase in production time which implies the temperature of the fluid in the vertical section of the configuration influences the temperature in the horizontal section. This effect of thermal interference between the two sections should lead to a decrease in the production temperature which is not captured by the COMSOL Model.

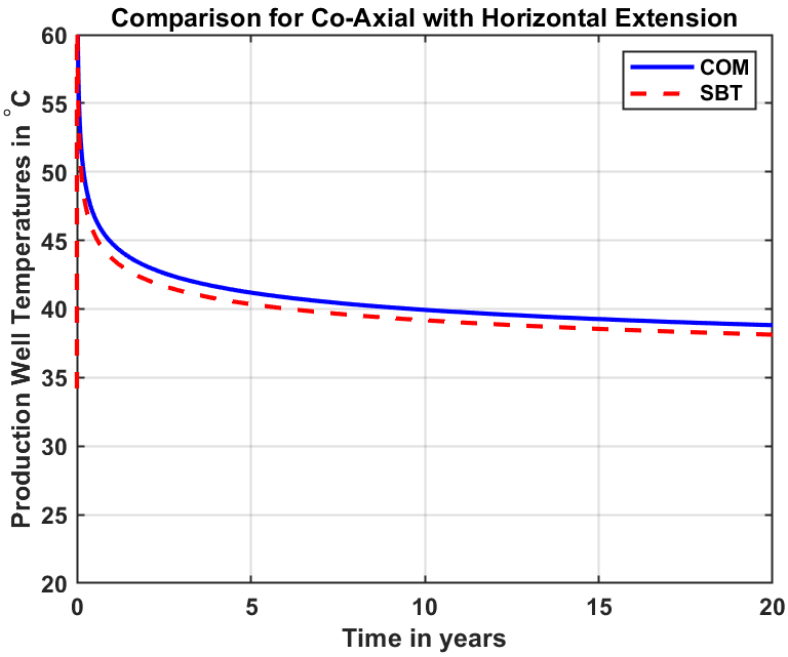

Figure B.3: Variation of production temperatures in °C with time for a Co-axial system with a horizontal extension using the COMSOL and SBT Models. The COMSOL model predicts a slightly higher production temperature since the effect of thermal interference at the 90° bend in configuration is not captured by COMSOL.

The SBT Model on the other hand is specifically designed to simulate curved slender bodies and hence efficiently captures the effect of the bend involved in the configuration.

Bibliography

Ahn, Sanghui, and Roland N. Horne. "The use of attenuation and phase shift to estimate permeability distributions from pulse tests", SPE Annual Technical Conference and Exhibition. OnePetro, (2011).

Amaya, A., Scherer, J., Muir, J., Patel, M., and Higgins, B. (2020). "GreenFire Energy Closed-Loop Geothermal Demonstration using Supercritical Carbon Dioxide as Working Fluid. Proceedings", 45th Workshop on Geothermal Reservoir Engineering, Stanford University, Stanford California, February, pp10-12, (2019).

Armstead, H. CH, and Jefferson W. Tester. "Heat mining". (1986).

Aunzo, Zosimo P., G. Bjornsson, and G. S. Bodvarsson. "Wellbore models GWELL, GWNACL, and HOLA user's guide", No. LBL-31428. Lawrence Berkeley National Lab.(LBNL), Berkeley, CA, (United States), (1991).

Baker, M."Ground-penetrating radar imaging of fluid flow through a discrete fracture", M.S. Thesis, University of Kansas, (2014).

Becker, Matthew W., and Eric Guiltinan. "Cross-hole periodic hydraulic testing of interwell connectivity", Proceedings, Thirty-Fifth Workshop on Geothermal Reservoir Engineering Stanford University, vol. 35, pp. 292-297, (2010).

Becker, Matthew W., and Georgios P. Tsoflias. "Comparing flux-averaged and resident concentration in a fractured bedrock using ground penetrating radar", Water Resources Research 46, no. 9 (2010).

Beckers, Koenraad F., Donald L. Koch, and Jefferson W. Tester. "Slender-body theory for transient heat conduction: theoretical basis, numerical implementation and case studies", Proceedings of the Royal Society A: Mathematical, Physical and Engineering Sciences 471, no. 2184 (2015): 20150494.

Bell, Ian H., Jorrit Wronski, Sylvain Quoilin, and Vincent Lemort. "Pure and pseudo-pure fluid thermophysical property evaluation and the open-source thermophysical property library CoolProp", Industrial engineering chemistry research 53, no. 6 (2014): 2498-2508.

Bergman, Theodore L., Frank P. Incropera, David P. DeWitt, and Adrienne S. Lavine. "Fundamentals of heat and mass transfer", John Wiley Sons, 2011

Beyrle, N. K. "Using polarized ground penetrating radar to improve subsurface imaging of bedrock fractures", M.S. Thesis, State University of New York, Buffalo, (2005).

Bjornsson, Grimur. "A multi-feedzone geothermal wellbore simulator", M.S. Thesis, Lawrence Berkeley Laboratory, University of California, (1987).

Blackwell, David, Maria Richards, Zachary Frone, Joe Batir, Andrés Ruzo, Ryan Dingwall, and Mitchell Williams. "Temperature-at-depth maps for the conterminous US and geothermal resource estimates", No. GRC1029452. Southern Methodist University Geothermal Laboratory, Dallas, TX (United States), (2011).

Bobok E., Tóth, A., and Turzó, Z. "Sustainable Production of a Closed Loop Geothermal Well". GRC Transactions, Vol. 31, (2007). Available at: http://pubs.geothermal-library.org/lib/grc/1025219.pdf

Bodvarsson, G., and J. M. Hanson. "Forced Geoheat Extraction from Sheet-like Fluid

Conductors", Proceedings of the Second NATO-CCMS Information Meeting on Dry Hot Rock Geothermal Energy. Los Alamos Scientific Laboratory report, LA-7021:85, 1977

Boussinesq, Joseph. "Mémoire sur l'influence des frottements dans les mouvements réguliers des fluids", Journal de mathématiques pures et appliquées 13, no. 2 (1868): 377-424.

Brown, Donald, Robert DuTeaux, Paul Kruger, Daniel Swenson, and Tsutomu Yamaguchi. "Fluid circulation and heat extraction from engineered geothermal reservoirs", Geothermics 28, no. 4-5 (1999): 553-572.

Breede, Katrin, Khatia Dzebisashvili, Xiaolei Liu, and Gioia Falcone. "A systematic review of enhanced (or engineered) geothermal systems: past, present and future", Geothermal Energy 1, no. 1 (2013): 1-27.

Cardiff, M., T. Bakhos, P. K. Kitanidis, and W. Barrash. "Aquifer heterogeneity characterization with oscillatory pumping: Sensitivity analysis and imaging potential", Water Resources Research 49, no. 9 (2013): 5395-5410.

Castagna, Marta, Matthew W. Becker, and Alberto Bellin. "Joint estimation of transmissivity and storativity in a bedrock fracture", Water Resources Research 47, no. 9 (2011).

Cengel, Y. "Heat Transfer: A practical approach", New York, NY, USA: McGraw-Hill, (2003).

Chadha, P. K., M. R. Malin, and A. Palacio-Perez. "Modelling of two-phase flow inside geothermal wells", Applied mathematical modelling 17, no. 5 (1993): 236-245.

Cole, Matthew C. "Periodic Hydraulic Tests in a Fractured Crystalline Bedrock", M.S. Thesis, California State University, Long Beach, (2018).

COMSOL. "COMSOL Multiphysics Reference Manual", Comsol, Inc., Burlington, MA, United States, (2019). Available at `https://doc.comsol.com/5.5/doc/com.comsol.help.comsol/COMSOL_ReferenceManual.pdf`

Cummings RG, Morris GE. "Economic modeling of electricity production from Hot Dry Rock geothermal reservoirs: methodology and analysis", EA-630, Research Project 1017 LASL (LA-7888-HDR). OSTI Information Bridge. (1979).

Diersch, H-JG, D. Bauer, W. Heidemann, Wolfram Rühaak, and Peter Schätzl. "Finite element modeling of borehole heat exchanger systems: Part 1. Fundamentals", Computers Geosciences 37, no. 8 (2011): 1122-1135.

Esmaeilpour, M., Korzani, M. G., and Kohl, T. "Performance Analyses of Deep Closed-loop U-shaped Heat Exchanger System with a Long Horizontal Extension", Proceedings, 46th Workshop on Geothermal Reservoir Engineering, Stanford University, Stanford, California, February 15-17, (2021).

Fokker, P.A., Renner, J., Verga, F. "Numerical modeling of periodic pumping tests in wells penetrating a heterogeneous aquifer". Am. J. Environ. Sci. 9 (1), (2013)

Fox, Don. "Thermal Hydraulic Modeling of Discretely Fractured Geothermal Reservoirs", Doctoral dissertation. Cornell University, Ithaca, New York, (2015).

Fox, Don B., Donald L. Koch, and Jefferson W. Tester. "An analytical thermohydraulic model for discretely fractured geothermal reservoirs", Water Resources Research 52, no.

9 (2016): 6792-6817.

Fox, Don B., Donald L. Koch, and Jefferson W. Tester. "The effect of spatial aperture variations on the thermal performance of discretely fractured geothermal reservoirs", Geothermal Energy, no. 1 (2015): 1-29.

Fox, Don, Brian Higgins. "The Effect of Well Density on Resource Depletion for a Vertical Closed-Loop sCO2 Geothermal Well System", Geothermal Resource Council Transactions 40 (2016).

Fox, Robert W., Alan T. McDonald, and P. J. Pritchard. "Introduction to Fluid Mechanics", (2004).

Frigo, M., and S. G. Johnson. "FFTW: An Adaptive Software Architecture for the FFT", Proceedings of the International Conference on Acoustics, Speech, and Signal Processing. Vol. 3, (1998), pp. 1381-1384.

Guiltinan, Eric, and Matthew W. Becker. "Measuring well hydraulic connectivity in fractured bedrock using periodic slug tests", Journal of Hydrology 521 (2015): 100-107.

Gustafson, J.O., Smith, J.D., Beyers, S.M., Al Aswad, J.A., Jordan, T.E., Tester, J.W. and Khan, T.M. "Risk Reduction in Geothermal Deep Direct-Use Development for District Heating: A Cornell University Case Study", Proceedings: 44th Workshop on Geothermal Reservoir Engineering, Stanford University, Stanford, California, February 11-13, 2019, SGP-TR-214. (2019).

Greengard, L., and Rokhlin, V. "A fast algorithm for particle simulations", Journal of computational physics, (1997)

Haborak, Kevin George. "Analytical solutions to flow in aquifers during sinusoidal aquifer pumping tests", Doctoral dissertation, University of Georgia, (1999).

Hasan, A. Rashid, and C. Shah Kabir. "Modeling two-phase fluid and heat flows in geothermal wells", Journal of Petroleum Science and Engineering 71, no. 1-2 (2010): 77-86.

Hawkins, Adam J., Matthew W. Becker, and Jefferson W. Tester. "Inert and Adsorptive Tracer Tests for Field Measurement of Flow-Wetted Surface Area." Water Resources Research 54.8 (2018): 5341-5358.

Hawkins, Adam J., Matthew W. Becker, and Georgios P. Tsoflias. "Evaluation of inert tracers in a bedrock fracture using ground penetrating radar and thermal sensors." Geothermics 67 (2017): 86-94.

Hawkins, Adam J., Don B. Fox, Donald L. Koch, Matthew W. Becker, and Jefferson W. Tester. "Predictive Inverse Model for Advective Heat Transfer in a Short-Circuited Fracture: Dimensional Analysis, Machine Learning, and Field Demonstration", Water Resources Research 56, no. 11 , (2020).

Hodgson, J. L. "Examination of the problem of utilizing the Earth's internal heat", Proceedings in Section G of the British Association for the Advancement of Science at its Leeds Meeting, September 2, (1927).

Hogarth, Robert, and Heinz-Gerd Holl. "Lessons learned from the Habanero EGS Project", Transactions, Geothermal Resources Council 41, (2017).

Horne, R. N. "Reservoir engineering aspects of reinjection", Geothermics, 14.2-3 , (1985): 449-457.

Horne, R. N. "Design considerations of a down-hole coaxial geothermal heat exchanger", Trans.-Geotherm. Resour. Counc.;(United States) 4, no. CONF-800920-(1980).

Huttrer, G. W. "Geothermal power generation in the world 2015-2020 update report", Proceedings World Geothermal Congress 2020, Reykjavik, Iceland, April 26 –May 2, (2020).

Higgins, B., Muir, J., Scherer, J., and Amaya, A. "GreenFire Energy Closed-Loop Geothermal Demonstration at the Coso Geothermal Field", GRC Transactions, Vol. 43, (2019).

IEA - International Energy Agency (2021). Data and Statistics. Available at https://www.iea.org/data-and-statistics

Ingebritsen, Steven E., and C. E. Manning. "Permeability of the continental crust: dynamic variations inferred from seismicity and metamorphism", Geofluids 10, no. 1-2 (2010): 193-205.

Iwai, Katsuhiko. "Fundamental studies of fluid flow through a single fracture", University of California, Berkeley, (1976).

Klimczak, Christian, Richard A. Schultz, Rishi Parashar, and Donald M. Reeves. "Cubic law with aperture-length correlation: implications for network scale fluid flow", Hydrogeology journal 18, no. 4 (2010): 851-862.

Knudby, C., and Carrera, J. "On the use of apparent hydraulic diffusivity as an indicator of connectivity", Journal of Hydrology, (2006), v. 329, p. 377–389.

Liu, Enru. "Effects of fracture aperture and roughness on hydraulic and mechanical properties of rocks: implication of seismic characterization of fractured reservoirs." Journal of Geophysics and Engineering 2, no. 1 (2005): 38-47.

Lu SM. "A global review of enhanced geothermal system (EGS)", Renewable and Sustainable Energy Reviews, (2018), 81, 2902-2921.

Lund, J. W., and Toth A. N. Direct Utilization of Geothermal Energy 2020 Worldwide Review. In Proceedings World Geothermal Congress 2020, Reykjavik, Iceland, April 26 –May 2, (2020). Available at: https://www.geothermal-energy.org/pdf/IGAstandard/WGC/2020/01018.pdf.

Lukawski, Maciej Z., Brian J. Anderson, Chad Augustine, Louis E. Capuano Jr, Koenraad F. Beckers, Bill Livesay, and Jefferson W. Tester. "Cost analysis of oil, gas, and geothermal well drilling", Journal of Petroleum Science and Engineering 118 (2014): 1-14.

Malek, A. E., Adams, B., Rossi, E., Schiegg, H. O., and Saar, M. O. Electric Power Generation, Specific Capital Cost, and Specific Power for Advanced Geothermal Systems (AGS). In 46th Workshop on Geothermal Reservoir Engineering, Stanford University, Stanford, California, February 15-17, (2021).

McClure, M.W., and Horne, R.N. "An investigation of stimulation mechanisms in Enhanced Geothermal Systems", International Journal of Rock Mechanics Mining Sciences, 72, (2014), 242-260.

Molina-Giraldo, Nelson, Philipp Blum, Ke Zhu, Peter Bayer, and Zhaohong Fang. "A moving finite line source model to simulate borehole heat exchangers with groundwa-

ter advection", International Journal of Thermal Sciences 50, no. 12 (2011): 2506-2513.

Morita, K., and Tago, M. (1995). Development of the downhole coaxial heat exchanger system: potential for fully utilizing geothermal resources. GRC Bulletin, March 1995, 83-92. Available at: http://pubs.geothermal-library.org/lib/grc/7002528.pdf

Morita, K., Tago, M., and Ehara, S. (2005). Case studies on small-scale power generation with the downhole coaxial heat exchanger. Proceedings, World Geothermal Congress, Antalya, Turkey, 24-29 April, 2005. Available at: https://www.geothermal-energy.org/pdf/IGAstandard/WGC/2005/1622.pdf.

Mouchot, J., Genter, A., Cuenot, N., Scheiber, J., Seibel, O., Bosia, C., Ravier, G., Mouchot, J., Genter, A., Cuenot, N. and Scheiber, J. (2018). First year of operation from EGS geothermal plants in Alsace, France: scaling issues. In Proceedings of the 43rd Workshop on Geothermal Reservoir Engineering Stanford University, Stanford, California. Available at: https://pangea.stanford.edu/ERE/pdf/IGAstandard/SGW/2018/Mouchot.pdf

Murphy, Hugh D., Jefferson W. Tester, Charles O. Grigsby, and Robert M. Potter. "Energy extraction from fractured geothermal reservoirs in low-permeability crystalline rock", Journal of Geophysical Research: Solid Earth 86, no. B8 (1981): 7145-7158.

Nalla, G., Shook, G. M., Mines, G. L., and Bloomfield, K. K. "Parametric sensitivity study of operating and design variables in wellbore heat exchangers", Geothermics, (2005), 34(3), 330-346. Available at: https://doi.org/10.1016/j.geothermics.2005.02.001.

Neuzil, C. E., and James V. Tracy. "Flow through fractures" Water Resources Research 17, no. 1 (1981): 191-199.

Okoroafora, Esuru Rita, Michael J. Williamsb, Jean Gossuinb, Olalekan Jimoh-Kenshirob, and Roland N. Hornea. "Comparison of EGS Thermal Performance with CO2 and Water as Working Fluids."

Ortiz-Ramirez, J. "Two-Phase Flow in Geothermal Wells: Development and Uses of a Good Computer Code (No. SGP-TR-66)". Stanford University, Stanford, CA, (1983).

Olasolo, P., M. C. Juárez, M. P. Morales, and I. A. Liarte. "Enhanced geothermal systems (EGS): A review." Renewable and Sustainable Energy Reviews 56 (2016): 133-144.

Pinder, George F., and Michael A. Celia. "Subsurface hydrology", John Wiley Sons, 2006.

Rasmussen, T.C., Haborak, K.G., and Young, M.H, "Estimating aquifer hydraulic properties using sinusoidal pumping at the Savannah River site", South Carolina, USA: Hydrogeology Journal, (2003), v. 11, p. 466-482.

Riahi, A., Moncarz, P., Kolbe, W., and Damjanac, B. "Innovative closed-loop geothermal well designs using water and super critical carbon dioxide as working fluids". Proceedings, 41st workshop on geothermal reservoir engineering, Stanford University, Stanford, California, February 13-15, (2017).

Rabinovich, Avinoam, Warren Barrash, Michael Cardiff, David L. Hochstetler, Tania Bakhos, Gedeon Dagan, and Peter K. Kitanidis. "Frequency dependent hydraulic properties estimated from oscillatory pumping tests in an unconfined aquifer." Journal of Hydrology 531 (2015): 2-16.

Ramey Jr, H. J. “Wellbore heat transmission”, Journal of Petroleum Technology, (1962), 14(04), 427-435.

Renner, Jörg, and Mareike Messar. “Periodic pumping tests.”, Geophysical Journal International 167, no. 1 (2006): 479-493.

Rybach, L., Megel, T., and Eugster, W. “At what time scale are geothermal resources renewable?”, Proceedings World Geothermal Congress 2000, Kyushu - Tohoku, Japan, May 28 - June 10, (2000), volume 2, pages 867–873.

Robinson, Bruce A., and Jefferson W. Tester. “Dispersed fluid flow in fractured reservoirs: An analysis of tracer-determined residence time distributions”, Journal of Geophysical Research: Solid Earth 89.B12 (1984): 10374-10384.

Robertson, E. C. Thermal Properties of Rocks. United States Geological Survey (USGS), Reston, VA. Available from `http://pubs.er.usgs.gov/publications/ofr88441`.

Rosa, A.J. “Reservoir Description by Well Test Analysis Using Cyclic Flow Rate Variation”. Doctoral dissertation, Stanford U., Stanford, C.A, (1991).

Sayler, C., Cardiff, M., and Fort, M.D, “Understanding the Geometry of Connected Fracture Flow with Multiperiod Oscillatory Hydraulic Tests”, Groundwater, p. 1–12, (2017).

Scherer, J., Higgins, B., Muir, J., and Amaya, A. “Closed-Loop Geothermal Demonstration Project”. California Energy Commission. Publication Number: CEC-300-2020-007, (2020).

Snyder, D. M., Beckers, K. F., Young, K. R., and Johnston, B. “Analysis of geothermal reservoir and well operational conditions using monthly production reports from Nevada and California”, GRC Trans, (2017), 41, 2844-2856.

Talley, Jennifer, Gregory S. Baker, Matthew W. Becker, and Nicholas Beyrle. “Four dimensional mapping of tracer channelization in subhorizontal bedrock fractures using surface ground penetrating radar”, Geophysical Research Letters 32, no. 4 (2005).

Tsoflias, Georgios P., and Matthew W. Becker. “Ground-penetrating-radar response to fracture-fluid salinity: Why lower frequencies are favorable for resolving salinity changes”, Geophysics 73, no. 5 (2008): J25-J30.

Tsang, C.F., and I. Neretnieks, “Flow channeling in heterogeneous fractured rocks”, Reviews of Geophysics, (1998), 36, 275-298.

Tester, Jefferson W., Elisabeth M. Drake, Michael J. Driscoll, Michael W. Golay, and William A. Peters. “Sustainable energy: choosing among options”, MIT press, (2012).

Tester, J. W., and Smith, M. C. “Energy Extraction Characteristics of Hot Dry Rock Geothermal Systems”, Proceedings of the Twelfth Intersociety Energy Conversion Engineering Conference, 1:816. Washington, DC: American Nuclear Society, (1997).

Tester, J. W., Anderson, B., Batchelor, A., Blackwell, D., DiPippo, R., Drake, E., Garnish, J., Livesay, B., Moore, M. C., Nichols, K., Petty, S., Toksz, M. N., and Veatch, Jr. R. W. “The future of geothermal energy: impact of Enhanced Geothermal Systems (EGS) on the United States in the 21st Century”. Massachusetts Institute of Technology, (2006), DOE contract DE-AC07-05ID14517 Final Report.

Tester, J. W., Brown, D. W., and Potter, R. M. “Hot Dry Rock Geothermal Energy —

A New Energy Agenda for the Twenty-first Century". Los Alamos National Laboratory, LA-11514-MS, (1989).

Tester, J.W., Beyers, S., Gustafson, J.O., Jordan, T.E., Smith, J.D., Aswad, J.A., Beckers, K.F., Allmendinger, R., Brown, L., Horowitz, F. and May, D. "District geothermal heating using EGS technology to meet carbon neutrality goals: a case study of earth source heat for the Cornell University campus", Proceedings of the World Geothermal Congress (2020).

Tsang, Y.W. and Witherspoon, P.A. "Hydromechanical behavior of a deformable rock fracture subject to normal stress." Journal of Geophysical Research: Solid Earth 86, no. B10 (1981), pp.9287-9298.

Tsang, Y. W., and Paul A. Witherspoon. "The dependence of fracture mechanical and fluid flow properties on fracture roughness and sample size." Journal of Geophysical Research: Solid Earth 88, no. B3 (1983): 2359-2366.

Uchida, M., T. Doe, W. Dershowitz, A. Thomas, P. Wallmann, and A. Sawada. "Discrete-fracture modeling of the Aspo LPT-2, large-scale pumping and tracer test, SKB International Cooperation report ICR 94-09." Swedish Nuclear Fuel and Waste Management Co., Stockholm, Sweden (1994).

Van Oort, E., Chen, D., Ashok, P., and Fallah, H. "Constructing Deep Closed-Loop Geothermal Wells for Globally Scalable Energy Production by Leveraging Oil and Gas ERD and HPHT Well Construction Expertise", Paper presented at the SPE/IADC International Drilling Conference and Exhibition, Virtual, (2021). https://doi.org/10.2118/204097-MS

Witherspoon, Paul Adams, Joseph SY Wang, K. Iwai, and John E. Gale. "Validity of cubic law for fluid flow in a deformable rock fracture", Water resources research 16, no. 6 (1980): 1016-1024.

Xu, Tianfu, Zixu Hu, Bo Feng, Guanhong Feng, Fengyu Li, and Zhenjiao Jiang. "Numerical evaluation of building heating potential from a co-axial closed-loop geothermal system using wellbore–reservoir coupling numerical model", Energy Exploration Exploitation 38, no. 3 (2020): 733-754.

Zhang, Lianyang. "Engineering properties of rocks", Butterworth-Heinemann, (2016).